Studies of high energy pp collisions

Glover, Edward William Nigel

STUDIES OF HIGH ENERGY $\bar{p}p$ COLLISIONS.

Edward William Nigel Glover

Hatfield College

Durham

A thesis submitted for the Degree of Doctor of Philosophy

in the Department of Physics,

University of Durham.

June 1985

STUDIES OF HIGH ENERGY $p\bar{p}$ COLLISIONS

E.W.N. Glover

ABSTRACT

The Standard Model of particle physics is examined in the context of high energy proton-antiproton collider experiments. The large energies available offer the possibility of producing new particles which may then be observed via their decay.

Heavy quark production is examined through the production of unlike-sign lepton pairs. Methods for isolating several dilepton production mechanisms are given, including an $e\mu$ signal for the top quark. Moreover, ψ production is shown to serve as a particularly clean tag for the production of particles containing b quarks.

The possibility of observing a fourth generation heavy lepton via W decay is investigated. The hadronic decay mode leads to a promising signature of large missing p_T accompanied by two hadronic jets and has a very healthy event rate.

The monojet events found by the UA1 experiment are reviewed. Various extensions of the Standard Model are examined as possible explanations of these events. The first interpretation involves the production of SUSY particles. These are found to be compatible with the data if two squarks exist with mass O(30GeV) and the gluino has mass $>$ O(60GeV). Secondly, interpretations based on four point effective interactions of the form $q\bar{q}Zg$ are investigated, and are shown to be unable to account for the observed monojet rate. Finally, the production and decay of new heavy states (for example excited quarks) could account for the monojet data, but are found to predict large numbers of W + jet and γ + jet events which have not been seen.

ACKNOWLEDGEMENTS

I would like to thank Alan Martin for his collaboration, advice and support throughout the period in which this research was undertaken and for reading the manuscript.

I also thank Anthony Allan, Howie Baer, Vernon Barger, Stuart Grayson, Francis Halzen, Franz Herzog, Mike Pennington and Roger Phillips for many enjoyable and fruitful collaborations.

I thank the members of the particle physics group at Durham - Alan Martin, Peter Collins, Fred Gault, Mike Pennington, Chris Maxwell, John Wheater, Mike Whalley, Stuart Grayson, Tim Spiller, James Webb, Anthony Worrall, Anthony Allan, Neil Speirs, King Lun Au, Martin Carter, Tony Peacock, Simon Webb and Yanos Michopoulos - for providing the friendly and stimulating atmosphere in which this work was carried out.

I would also like to thank Richard Ansorge who first introduced me to particle physics.

I am grateful to the Science and Engineering Research Council for financing this research.

Finally, I would like to thank my family for continual support and encouragement. This thesis is dedicated to my parents.

CONTENTS

Chapter One

Introduction to Particle Physics

1.1 Preamble

In recent years there has been significant progress towards the understanding of the basic interactions of nature. In particular, at current limits of resolution, all matter appears to be constructed of point-like, spin-1/2 quarks and leptons. Moreover the interactions amongst these particles - the strong, weak and electromagnetic forces (neglecting gravity which is a small perturbation at current energies) - appear to be described by gauge theories and are mediated by spin-1 gauge bosons.

The known leptons form three families,

$$\begin{pmatrix} \nu_e \\ e \end{pmatrix} \quad \begin{pmatrix} \nu_\mu \\ \mu \end{pmatrix} \quad \begin{pmatrix} \nu_\tau \\ \tau \end{pmatrix} \tag{1.1}$$

and interact through the electromagnetic and weak forces. The leptons are directly observable in the laboratory and are well known. The quarks, however, interact strongly as well and have not been studied in isolation since it is thought that they are permanently confined within the hadrons, such as the proton. Five quark flavours are well established suggesting the existence of a sixth, the top quark t,

$$\begin{pmatrix} u \\ d \end{pmatrix} \quad \begin{pmatrix} c \\ s \end{pmatrix} \quad \begin{pmatrix} t \\ b \end{pmatrix}. \tag{1.2}$$

At present, there is no conclusive proof of the existence of the top

quark, although there is some evidence [1] for the top quark to exist in the mass range 30GeV $< m_t <$ 50GeV.

The gauge bosons of the Standard Model of $SU(3)_C \times SU(2)_L \times U(1)_Y$ have now all been observed [2-7] (albeit indirectly in the case of the strong force mediating gluon) thus lending support to the theoretical prejudice in favour of gauge theories. The main supports for gauge theories are (a) theoretical, in that gauge theories are renormalisable i.e. the divergences in higher order calculations can be removed in a well defined way, and (b) experimental, for example, the predictions of QED for the anomalous magnetic moment of the muon agree with experiment to better than 1 part in 10^5. The next three sections briefly describe the ideas behind the gauge principle and how the weak and electromagnetic forces are thought to unify. Some problems within the Standard Model are discussed in Section 1.5 whilst Section 1.6 contains a brief description of the possibilities of finding new physics in proton-antiproton collisions.

1.2 Gauge theories and electromagnetism

The basis of the gauge principle is the invariance of the fundamental Lagrangian under various field transformations. These "symmetries" lead to conserved currents and thus to conserved charges, for example, electric charge. Consider the Lagrangian for a non-interacting spin-1/2 fermion ψ with mass m,

$$L = i\bar{\psi}\gamma_\mu\partial^\mu\psi - m\bar{\psi}\psi. \qquad (1.3)$$

The Euler-Lagrange equations for this Lagrangian lead to the familiar Dirac equation,

$$i\gamma_\mu \partial^\mu \psi - m\psi = 0. \tag{1.4}$$

This Lagrangian is invariant under the global phase transformation,

$$\psi \rightarrow \exp(i\alpha)\psi, \ \bar{\psi} \rightarrow \exp(-i\alpha)\bar{\psi} \tag{1.5}$$

which leads to the conserved current,

$$j_\mu = \bar{\psi}\gamma_\mu \psi. \tag{1.6}$$

In practise, the invariance under such a global phase transformation means that the phase α is unmeasurable and can be specified arbitrarily. A more general invariance occurs if the phase is space-time dependent, i.e. $\alpha \rightarrow \alpha(x)$. Lagrangians invariant under the space-time dependent transformation are said to be locally gauge (or phase) invariant.

The Lagrangian for Quantum Electrodynamics (QED) [8] is given by,

$$L_{QED} = \bar{\psi}(i\gamma_\mu \partial^\mu - m)\psi + e\bar{\psi}\gamma_\mu A^\mu \psi - (1/4)F_{\mu\nu}F^{\mu\nu} \tag{1.7}$$

where ψ is the fermion field, A_μ the photon field and $F_{\mu\nu}$ the electromagnetic field strength tensor defined by,

$$F_{\mu\nu} = \partial_\nu A_\mu - \partial_\mu A_\nu. \tag{1.8}$$

e is the electric charge of the fermion. This Lagrangian is invariant under the local transformation,

$$\psi \rightarrow \exp(i\alpha(x))\psi \tag{1.9}$$

if A_μ transforms as,

$$A_\mu \rightarrow A_\mu + (1/e)\partial_\mu \alpha(x) \tag{1.10}$$

which is the usual gauge transformation for the electromagnetic potential. The fermion-photon coupling term is required to cancel off the unwanted terms generated by the local gauge transformations, and is restricted to be of this form. The $F_{\mu\nu}F^{\mu\nu}$ term represents the kinetic energy of the photon. One consequence of requiring local

gauge invariance is that a mass term of the type $m^2 A_\mu A^\mu$ is not allowed - i.e. the photon is massless. The success of QED and the "natural" way in which both the photon-fermion coupling and the masslessness of the photon arise suggest that local gauge invariance is an important property and so attempts have been made to describe the strong and weak forces in the same way.

1.3 The Strong interaction

The gauge transformations $\exp(i\alpha(x))$ of QED form a unitary Abelian group - U(1). Quantum Chromodynamics (QCD) (" the theory of the strong interaction") [9,10] is based on the unitary non-abelian group SU(3) called "colour". In contrast to the single U(1) generator, there are eight SU(3) generators and consequently eight vector fields (gluons) which mediate the interaction. The quarks lie in the fundamental triplet representation and the gluons in the adjoint octet representation. The eight generators T^a (a=1,8) form the Lie algebra,

$$[T^a, T^b] = if^{abc}T^c \qquad (1.11)$$

where the f^{abc} are the structure constants of the algebra. In the adjoint representation, the T^a are traceless 3 x 3 matrices.

In analogy with QED, the QCD Lagrangian is,

$$L_{QCD} = \bar{q}(i\gamma_\mu\partial^\mu - m)q - g(\bar{q}\gamma_\mu T^a q)G^{\mu a} - (1/4)G_{\mu\nu}{}^a G^{\mu\nu a} \qquad (1.12)$$

where q is a quark of mass m, $G_\mu{}^a$ (with colour label a=1,8) the octet of gauge fields, $G_{\mu\nu}{}^a$ the gluon field strength tensor and g the strong coupling constant. Each term in the Lagrangian is a colour singlet.

This Lagrangian must be invariant under the local gauge transformation,

$$q \rightarrow \exp(i\alpha^a(x)T^a)q, \tag{1.13}$$

which, for infinitesimal α^a lead to the following requirements,

$$G_\mu{}^a \rightarrow G_\mu{}^a - (1/g)\partial_\mu\alpha^a - f^{abc}\alpha^b G_\mu{}^c \tag{1.14}$$

if,

$$G_{\mu\nu}{}^a = \partial_\nu G_\mu{}^a - \partial_\mu G_\nu{}^a - gf^{abc}G_\mu{}^b G_\nu{}^c. \tag{1.15}$$

The non-abelian nature of the group (i.e. $f^{abc} \neq 0$) leads to triple and quartic gluon interactions in the kinetic energy term. Another way of expressing this fact is that in QCD, the gluons carry the "colour" charge to which they couple, whereas in QED the photon is chargeless. One consequence of these self interactions is that the one loop beta function has the opposite sign to the QED case provided there are less than 17 flavours of quarks [10]. This means that for $Q^2 > \mu^2$, $g(Q^2) < g(\mu^2)$ and $g(Q^2) \rightarrow 0$ as $Q^2 \rightarrow \infty$ and "asymptotic freedom" is achieved [11]. In other words, at very small distances coloured objects appear to be free. Furthermore as $g(Q^2)$ is small at large Q^2, sensible perturbation expansions are permitted and the theory may be tested [12]. At large distances $g(Q^2)$ is not small and the non-perturbative region of hadronic physics is entered. Presently it is thought that this increase in the strong coupling constant as Q^2 decreases may lead to the "confinement" of coloured objects within hadrons [13]. This has made direct tests of QCD difficult, though many predictions (e.g. hadronic jets) have been tested [10].

1.4 Electroweak unification.

The impressive success of QED and QCD leads one to hope that the weak interaction may also be described by a gauge theory. However, the short range nature of the interaction suggests that the mediating particles have large mass O(100GeV) whereas gauge invariance forbids mass terms of the form $m^2 A_\mu A^\mu$. Nevertheless, the Glashow-Weinberg-Salam model was proposed in an attempt both to get round this stumbling block and to unify the weak and electromagnetic interactions.

Since the weak vector bosons are massive, the gauge symmetry must be broken. In giving mass to the vector bosons, care has to be taken to preserve the renormalisability of the theory and not to break unitarity requirements. The trick to do this is "spontaneous symmetry breaking" in which one constructs a gauge invariant theory with a non-invariant ground state. The particular structure of the ground state leads to well defined symmetry breaking effects that preserve the important features of the theory.

The Standard Model of electroweak unification [14-16] uses the Higgs mechanism [17-19] and has been shown to be renormalisable [20]. It is based on a SU(2)xU(1) gauge theory with the four gauge bosons coupled to a SU(2) doublet of complex scalar fields φ. The Lagrangian is,

$$L_{GWS} = (\partial_\mu \varphi - igT^a W_\mu{}^a \varphi - ig'YB_\mu \varphi)^+ (\partial^\mu \varphi - igT^a W^{\mu a} \varphi - ig'YB^\mu \varphi) \quad (1.16)$$

$$+ V(\varphi^+ \varphi) - (1/4) W_{\mu\nu}{}^a W^{\mu\nu a} - (1/4) B_{\mu\nu} B^{\mu\nu}$$

where $W_\mu{}^a$ (with weak isospin label a=1,3) and B_μ are the gauge fields

of the SU(2) and U(1) groups respectively and $W_{\mu\nu}{}^{a}$ and $B_{\mu\nu}$ their field strength tensors. The couplings of the SU(2) and U(1) groups are g and g′ and their generators T^{a} (a=1,3) and Y. The scalar potential V is,

$$V(\varphi^{+}\varphi) = \mu^{2}\varphi^{+}\varphi + \lambda(\varphi^{+}\varphi)^{2} \tag{1.17}$$

where $\lambda > 0$ so V is bounded below. If $\mu^{2} > 0$ then V has a minimum at $\varphi^{+}\varphi = 0$ and the ground state is gauge invariant. On the other hand, if $\mu^{2} < 0$, V has a minimum at $\varphi^{+}\varphi = v^{2}/2$ where $v^{2} = \mu^{2}/\lambda$. When the fields are expressed as perturbations from this ground state the theory is no longer gauge invariant. Furthermore three of the scalars have become the longitudinal components of the gauge bosons which are now massive. Expanding about one of the minima,

$$\varphi(x) = \frac{1}{\sqrt{2}}\begin{bmatrix} 0 \\ v + h(x) \end{bmatrix} \tag{1.18}$$

where $\varphi_{vacuum} = v/\sqrt{2}$. The first term in the Lagrangian (1.16) becomes,

$$L_{GWS}(1) = 1/2(\partial_{\mu}h)(\partial^{\mu}h) + 1/2(gv/2)^{2}(W_{\mu}{}^{1}W^{\mu 1} + W_{\mu}{}^{2}W^{\mu 2}) \tag{1.19}$$

$$+ 1/2(v/2)^{2}((gW_{\mu}{}^{3} - g'B_{\mu})(gW^{\mu 3} - B^{\mu})) + h.o.t.$$

which can be rewritten,

$$L_{GWS}(1) = 1/2(\partial_{\mu}h)(\partial^{\mu}h) + M_{W}{}^{2}(W_{\mu}{}^{+}W^{\mu +} + W_{\mu}{}^{-}W^{\mu -}) \tag{1.20}$$

$$+ M_{Z}{}^{2}(Z_{\mu}Z^{\mu}) + h.o.t.$$

where,

$$\begin{aligned} W_{\mu}{}^{\pm} &= 1/\sqrt{2}(W_{\mu}{}^{1} \mp iW_{\mu}{}^{2}) \\ Z_{\mu} &= \cos\theta_{W}W_{\mu}{}^{3} - \sin\theta_{W}B_{\mu} \\ A_{\mu} &= \sin\theta_{W}W_{\mu}{}^{3} + \cos\theta_{W}B_{\mu}, \end{aligned} \tag{1.21}$$

and,

$$\tan\theta_W = g'/g. \qquad (1.22)$$

Comparing (1.19) and (1.20) it can be seen that three ($W^{\pm}$ and Z) of the gauge bosons have acquired a mass,

$$M_W{}^{\pm} = gv/2,\ M_Z = M_W/\cos\theta_W \qquad (1.23)$$

whilst the fourth remains massless and, when identified as the photon, gives the relation,

$$e = g\sin\theta_W = g'\cos\theta_W. \qquad (1.24)$$

Since the photon is massless, there exists an unbroken U(1) symmetry as required by QED.

To account for the V-A structure of the weak interaction, the fermions are introduced in left-handed doublets and right-handed singlets of SU(2).

e.g.
$$\begin{bmatrix} \nu_e \\ e \end{bmatrix}_L ,\ e_R \qquad (1.25)$$

where $f_L^R = 1/2\ (1 \pm \gamma_5)f$. Because of this the SU(2) group is commonly labelled with a subscript L. The fermions are singlets under the original U(1) group and possess a weak hypercharge Y. After symmetry breaking this is related to the electric charge by,

$$Q = T^3 + Y. \qquad (1.26)$$

The $SU(2)_L \times U(1)_Y$ Lagrangian for fermion-gauge boson interactions is,

$$L_{int} = -\bar{L}\gamma_\mu(gT^a W^{\mu a} + g'YB^\mu)L - \bar{R}\gamma_\mu(g'YB^\mu)R \qquad (1.27)$$

where L(R) denotes a left-(right-)handed fermion doublet(singlet). In terms of the $U(1)_Q$ theory,

$$L_{int} = -e\bar{L}\gamma_\mu QA^\mu L - e\bar{R}\gamma_\mu QA^\mu R$$
$$- (g/\sqrt{2})\bar{L}\gamma_\mu T^{\pm}W^{\mu\pm}L$$

$$- (g/\cos\theta_W)\bar{L}\gamma_\mu(T^3 - \sin^2\theta_W Q)Z^\mu L$$

$$- (g/\cos\theta_W)\bar{R}\gamma_\mu(- \sin^2\theta_W Q)Z^\mu R. \quad (1.28)$$

The photon and Z couple to both right- and left-handed fermions, while the $W^\pm$ couple only to left-handed fermions.

Since the right- and left-handed fermions transform differently under $SU(2)_L$, a fermion mass term of the form,

$$m(\bar{\psi}_L\psi_R + \bar{\psi}_R\psi_L) \quad (1.29)$$

is forbidden. An attractive feature of the introduction of the Higgs field in the Standard Model is that the fermions acquire a mass through a Yukawa coupling to the Higgs doublet. This is achieved by introducing terms of the form,

$$L = - G_e(\bar{L}_e\varphi R_e + \bar{R}_e\varphi^+ L_e) \quad (1.30)$$

which is gauge invariant (the subscript e refers to the multiplets containing the electron). After spontaneous symmetry breakdown, the redefinition of the Higgs field (1.18) one obtains,

$$L = - G_e v/\sqrt{2}(\bar{e}_L e_R + \bar{e}_R e_L) - G_e/\sqrt{2}(\bar{e}_L e_R + \bar{e}_R e_L)h(x). \quad (1.31)$$

Providing G_e is chosen such that $m_e = G_e v/\sqrt{2}$,

$$L = - m_e\bar{e}e - (m_e/v)\bar{e}eh \quad (1.32)$$

so the electron has gained a mass. Since $v \backsim 250GeV$, the remaining Higgs-fermion coupling is small. Moreover as G_e is arbitrary, the electron mass is not predicted. Each fermion that has a mass has a free coupling parameter in the theory. Note that the form of the Higgs field (1.18) prevents the neutrino from acquiring a mass. The quark masses are generated by the Higgs doublet,

$$\varphi_c = -2iT^2\varphi^* \quad (1.33)$$

which does allow the charge 2/3 quarks to acquire a mass.

1.5 Some successes and failures of the Standard Model

The Standard Model prediction for the decay $\mu^- \rightarrow e^- \bar{\nu}_e \nu_\mu$ corresponds with the V-A theory if,

$$G_F/\sqrt{2} = g^2/8M_W^2. \tag{1.34}$$

Using this and equation (1.24) gives an expression for the W boson mass,

$$M_W = (\pi\alpha/\sqrt{2}G_F)^{1/2}/\sin\theta_W = 37.3\text{GeV}/\sin\theta_W \tag{1.35}$$

and hence,

$$M_Z = M_W/\cos\theta_W = 74.6\text{GeV}/\sin 2\theta_W. \tag{1.36}$$

The world average of $\sin^2\theta_W$ is [21],

$$\sin^2\theta_W = 0.219 \pm 0.006 \tag{1.37}$$

which leads to $M_W \backsim 80$GeV and $M_Z \backsim 90$GeV. Radiative corrections [22] modify these estimates to give,

$$M_W = 82.6 \pm 1.2\text{GeV}, \tag{1.38}$$

and,

$$M_Z = 93.4 \pm 1.6\text{GeV}. \tag{1.39}$$

These gauge bosons have been seen at the CERN $\bar{p}p$ collider with average masses [21],

$$\begin{aligned} M_W &= 82.2 \pm 1.8\text{GeV}, \\ M_Z &= 93.2 \pm 1.5\text{GeV}. \end{aligned} \tag{1.40}$$

There is impressive agreement between the theoretical predictions and the experimental measurements.

A validation of the SU(3) part of the Standard Model in high energy $\bar{p}p$ collisions has been the observation of large transverse

momentum hadron jets [6,7] as predicted by QCD [12]. This lends strong support to the idea that hard two-body scattering of quarks and gluons is actually taking place.

Nevertheless, the theory contains some rather unsatisfactory features. For example,

(a) the Higgs sector of the theory is rather unsatisfactory and the Higgs particle has interactions put in in a rather ad hoc way. The mass of the Higgs is unconstrained by the theory and may be unstable against radiative corrections;

(b) there is no limit to the number of quark and lepton generations - indeed with the growing number of "elementary" particles one may question whether quarks and leptons are really elementary;

(c) the masses of both the quarks and leptons and the mixing [23] between the charge -1/3 quarks are not explained;

(d) the observed parity violation of the weak current is put in by hand since the left- and right-handed fermions transform differently under the SU(2) gauge group;

(e) CP violation is not explained;

(f) gravity is not included.

These problems have inspired much theoretical work beyond the Standard Model. For example, grand unified theories [24], supersymmetry [25], supergravity [26], left-right symmetric models [27], technicolour [28] or compositeness [29]. In all of these, the Standard Model is recovered in the low energy limit and, because of this, there has been no direct evidence for such theoretical extensions from low-energy experiments.

1.6 New physics from $\bar{p}p$ collisions

The CERN proton-antiproton collider was designed to enable high energy parton-parton collisions to occur in a laboratory environment at energies up to O(0.5TeV). This is a large increase on the centre-of-mass energy of e^+e^- experiments at DESY ($\sim$ 0.04TeV) and so opens up the possibility of observing new particles and new interactions if they occur at such energies. Since the proton is composed of several partons, much of this energy is wasted and carried off by the proton debris left by the hard scattering sub-process. Nevertheless the possibility of making more detailed studies of the particle spectrum and of the various Standard Model predictions is a real one.

Having been presented with the opportunity of confronting the current theoretical paradigm in such an experimental set-up, Chapter 2 is devoted to describing the framework for calculations of proton-antiproton collisions. The proton is described as a bag of coloured partons with given momentum distributions, thus enabling elementary sub-process interactions to be calculated. Chapter 3 contains an analysis of unlike-sign dilepton signatures at $\sqrt{s}$ = 540GeV [30,31]. It is possible that the sixth quark flavour (top) may be confirmed through this channel. Information on the gluon structure function and the Drell-Yan process may also be extracted. If a fourth generation of leptons exists, then there is a possibility that they may be produced from W decay. The CERN collider provides a source of W bosons and offers the chance of seeing a fourth generation charged lepton if it is light enough. Chapter 4 examines the feasability of such a signal [32].

During the 1983 run of the CERN $\bar{p}p$ collider several "monojet" events were produced which did not appear to be of Standard Model origin. These events are described in Chapter 5. In Chapter 6 a supersymmetric extension to the Standard Model which is examined as a possible explanation of the "monojet" events [33,34]. The large degree of freedom in such supersymmetric models makes it very hard to distinguish amongst them and such hypotheses are therefore rather unsatisfactory. The same "monojet" events are considered from a different viewpoint in Chapter 7. The possibility of a new sort of effective interaction (similar to the Fermi four point interaction) between bosons and fermions as a source of "monojet" events is examined [35]. As an example the production of very heavy quarks (with up or down flavour) as intermediate states is evaluated.

The conclusions of these studies are presented in Chapter 8.

References

(1) G.Arnison et al., UA1 collab., Phys. Lett. 147B, 493, (1984)

(2) G.Arnison et al., UA1 collab., Phys. Lett. 122B, 103, (1983)

(3) M.Banner et al., UA2 collab., Phys. Lett. 122B, 476, (1983)

(4) G.Arnison et al., UA1 collab., Phys. Lett. 126B, 398, (1983)

(5) P.Bagnaia et al., UA2 collab., Phys. Lett. 129B, 130, (1983)

(6) G.Arnison et al., UA1 collab., Phys. Lett. 123B, 115, (1983)

(7) P.Bagnaia et al., UA2 collab., Z.Phys. C20, 117, (1983)

(8) R.P.Feynman, Quantum Electrodynamics (Benjamin) (1961)

(9) H.D.Politzer, Phys. Rep. 14C, 129, (1974)

(10) M.R.Pennington, Rep. on Prog. in Phys. 46, 393, (1983)

(11) H.D.Politzer, Phys. Rev. Lett. 30, 1346, (1973)

(12) E.Reya, Phys. Rep. 69C, 195, (1981)

(13) R.P.Feynman, Photon-Hadron Interactions (Benjamin) (1972)

(14) S.L.Glashow, Nucl.Phys. 22, 579, (1967)

(15) S.Weinberg, Phys. Rev. Lett. 19, 1264, (1967)

(16) A.Salam, Proc. 8th Nobel Symp. ed. N.Svartholm (Amqvist and Wiksell) (1968)

(17) P.W.Higgs, Phys. Rev. Lett. 12, 132, (1964); ibid 13, 508, (1964)

(18) F.Englert and R.Brout, Phys. Rev. Lett. 13, 321, (1964)

(19) G.S.Guralnik, C.R.Hagen and T.W.B.Kibble, Phys. Rev. Lett. 13, 585, (1964)

(20) G.t'Hooft, Nucl. Phys. B33, 173, (1971); ibid B35, 167, (1971)

(21) W.J.Marciano, Proc. of 4th Topical Workshop on $\bar{p}p$ Collider Physics, BERNE, (1984)

(22) C.H.Llewellyn-Smith and J.F.Wheater, Phys. Lett. 105B, 486, (1981)

(23) M.Kobayashi and T.Maskawa, Prog. Theor. Phys. 49, 652, (1973)

(24) P.Langacker, Phys. Rep. 72C, 185, (1981)

(25) P.Fayet and S.Ferrara, Phys. Rep. 32C, 249, (1977)

(26) P.van Nieuwenhuizen, Phys. Rep. 68C, 191, (1981)

(27) J.C.Pati and A.Salam, Phys. Rev. Lett. 31, 661, (1973)

(28) L.Susskind, Phys. Rev. D20, 2619, (1979)

(29) L.Lyons, Prog. Part. Nucl. Phys. 10, 227, (1983)

(30) E.W.N.Glover, F.Halzen and A.D.Martin, Phys. Lett. 141B, 429, (1984)

(31) F.Halzen, F.Herzog, E.W.N.Glover and A.D.Martin, Phys. Rev. D30, 700, (1984)

(32) V.Barger, H.Baer, A.D.Martin, E.W.N.Glover and R.J.N.Phillips, Phys. Lett. 133B, 449, (1983); Phys. Rev. D29, 2020, (1984)

(33) A.R.Allan, E.W.N.Glover and A.D.Martin, Phys. Lett. 146B, 247, (1984)

(34) A.R.Allan, E.W.N.Glover and S.L.Grayson, Durham report DTP/84/28 (1984)

(35) E.W.N.Glover, A.D.Martin and M.R.Pennington, Phys. Lett. 153B, 330, (1984)

Chapter Two

Introduction to Collider Physics

2.1 Introduction

The so called "deep inelastic scattering" experiments, in which the structure of nucleons was probed with high energy leptons, have given rise to the idea that the nucleon consists of point-like constituents [1-3]. The extremely successful parton model [4] arose to describe these constituent partons as quasi free particles. Subsequently these partons have been identified as the quarks and gluons of the Standard Model.

The main assumptions of the parton model are,

(1) at short distances hadrons look as though they are made of almost free (α_s(large Q^2) is small) partons (that is quarks and gluons). This a consequence of "asymptotic freedom".

(2) at larger distances, quarks and gluons are "confined" by colour forces. Hence struck partons must fragment into colour singlet hadrons, at a scale μ such that $\alpha_s(\mu^2) \sim 1$.

(3) if the scattering process is characterised by sufficiently high energy (i.e. very short distances) the scattering of the quasi free partons occurs at times much less than the time for hadronisation to occur. This means that the scattering and hadronisation processes may be considered independent.

In the parton model, the cross section for the hadronic reaction,

$$a + b \rightarrow c + \text{anything} \qquad (2.1)$$

is given schematically by (see Fig. 1.),

$$d\sigma(a + b \rightarrow c + X) = \Sigma\, f_i^{(a)} f_j^{(b)} d\hat{\sigma}(i + j \rightarrow c + X') \qquad (2.2)$$

where the summation is over all the parton constituents i and j of a and b. $f_i^{(a)}$ is the probability of finding parton i in hadron a and $\hat{\sigma}(i + j \rightarrow c + X')$ is the cross section for the elementary subprocess leading to the required final state. Proton-antiproton collisions fit naturally into this form and consequently these basic parton ideas underpin the whole of this work.

To compute cross sections and experimental distributions, two ingredients are necessary,

(1) subprocess cross sections calculated using perturbation theory,

(2) parton distributions, measured in deep inelastic lepton-hadron scattering and evolved to higher momentum scales using a perturbative QCD approach.

This chapter is organsied into six parts. Firstly, the parton model is discussed and the parton kinematics described. This will provide the framework for subsequent calculations. Scaling violations due to the coloured nature of the partons lead to the QCD improved parton model of section 2.3. In section 2.4 the parton distributions and their evolution in Q^2 are discussed; and several parameterisations of the structure functions are compared. The differential luminosity is introduced in section 2.5 and used in section 2.6 to calculate weak boson production as an example of 2 to 1 scattering. Finally 2 to 2 scattering kinematics are given which again form the basis of many of

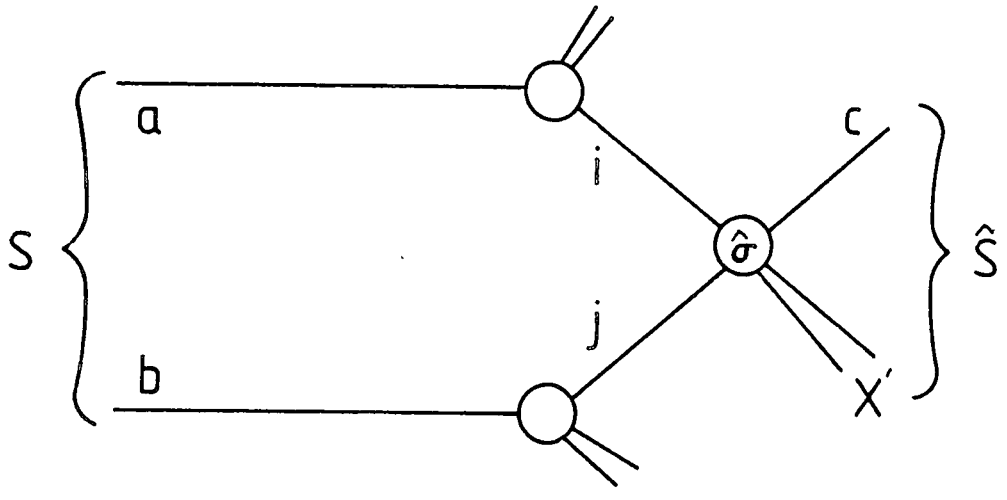

Figure 1

The hadronic interaction a + b → c + X in terms of the parton subprocess i + j → c + X´.

the subsequent calculations.

2.2 Parton model kinematics

In the parton model [4] the hadron is regarded as a collection of quasi free partons which share its momentum. Each parton i carries a longitudinal momentum fraction x_i of the parents momentum. That is, for a parent momentum P, the parton has momentum $x_i P$. Clearly to conserve longitudinal momentum, these momentum fractions x_i satisfy,

$$0 < x_i < 1 \tag{2.3}$$

and,

$$\sum_i x_i = 1. \tag{2.4}$$

Since the partons are confined to a small spatial region, they possess a Fermi motion and this allows a certain degree of transverse motion of O(0.4GeV). Since most of the work presented here is for large mass objects at large p_T, this transverse motion is generally neglected.

Consider the reaction (2.1) shown in Fig. 1. The cross section is given by,

$$\sigma(a + b \to c + X) = \int \sum_{ij} f_i^{(a)}(x_a) f_j^{(b)}(x_b) \hat{\sigma}(i + j \to c + X') dx_a dx_b. \tag{2.5}$$

The summation runs over all the contributing parton configurations, and the integral in x_a, x_b space extends only over the kinematically allowed region, $x_a x_b s = \hat{s} \geq (m_c + m_{X'})^2$. $\sqrt{s}$ is the hadron centre-of-mass energy and m_c, $m_{X'}$ the masses of the produced particles.

An alternative pair of variables are τ and x_F where,

$$\begin{aligned} \tau &= x_a x_b = \hat{s}/s \\ x_F &= x_a - x_b \end{aligned} \tag{2.6}$$

so that,

$$x_{a,b} = ((x_F^2 + 4\tau)^{1/2} \pm x_F)/2 \tag{2.7}$$

and,

$$dx_a dx_b = dx_F d\tau/(x_F^2 + 4\tau)^{1/2}. \tag{2.8}$$

If the threshold s for some process is M^2 at some hadron centre-of-mass energy $\sqrt{s}$ then the limits on τ and x_F are,

$$\begin{aligned} M^2/s < \tau < 1 \\ -(1 - \tau) < x_F < (1 - \tau) \end{aligned} \tag{2.9}$$

The corresponding limits on x_a and x_b are,

$$\begin{aligned} M^2/s < x_a < 1 \\ M^2/(x_a s) < x_b < 1. \end{aligned} \tag{2.10}$$

Hence, typically for a process a + b $\rightarrow$ c + d the cross section is given by,

$$\begin{aligned} \sigma(a + b \rightarrow c + d) &= \int\int dx_a dx_b (..) \hat{\sigma}(i + j \rightarrow c + d) \\ &= \int\int d\tau dx_F/(x_F^2 + 4\tau)^{1/2} (..) \hat{\sigma}(i + j \rightarrow c + d) \end{aligned} \tag{2.11}$$

where,

$$(..) = \Sigma(f_i^{(a)}(x_a) f_j^{(b)}(x_b) + i \leftrightarrow j).$$

2.3 Scale violation and an improved parton model

Since the partons are coloured, they may radiate other partons, see Fig. 2., and this introduces a correction to the naive parton model described above. In the leading logarithm approximation [5] these modifications are independent of the subprocess i + j $\rightarrow$ c + d and are incorporated into the structure functions,

$$f_i^{(a)}(x_a) \rightarrow f_i^{(a)}(x_a, Q^2), \tag{2.12}$$

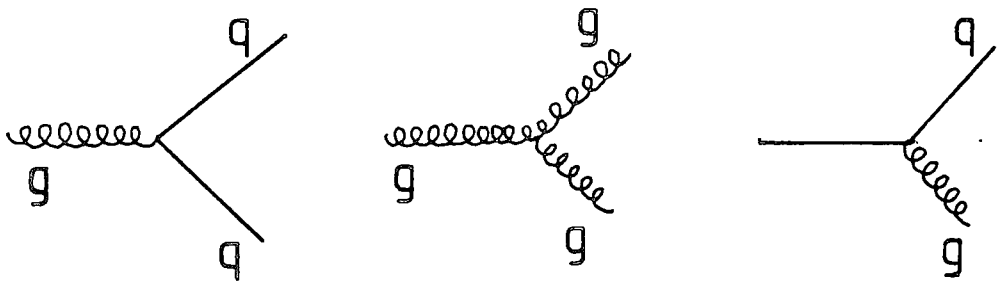

Figure 2

Basic parton subprocesses for radiation of coloured partons. These processes are described by the splitting functions of reference 12.

where Q^2 is some scale of the interaction.

Similarly the correction to the strong coupling constant from higher order Feynman graphs can be summed to give a running coupling constant,

$$\alpha_s(Q^2) = 4\pi/(\beta_o \ln(Q^2/\Lambda^2)) \qquad (2.13)$$

where β_o is the coefficient of the logarithms generated by the one loop graphs shown in Fig. 3., and is given by,

$$\beta_o = 11 - 2N_F/3 \qquad (2.14)$$

where N_F is the number of active quark flavours - i.e. those that go round the fermion loop. Λ is the QCD scale and may be extracted from data on deep inelastic scattering experiments [6,7] and is in the range,

$$0.1\text{GeV} \lesssim \Lambda \lesssim 0.5\text{GeV}. \qquad (2.15)$$

There is an uncertainty as to the actual choice of Q^2, Λ^2 and N_F and these choices affect the overall normalisations of the cross sections. For example, either increasing N_F, Λ^2 or decreasing Q^2 causes α_s to rise while decreasing N_F, Λ^2 or increasing Q^2 causes α_s to fall. The actual choices are stated in the relevant sections.

By making the approximation that higher order contributions may be factored off into α_s, structure functions etc. then the use of lowest order hard scattering subprocesses is on a sound footing. Higher order corrections lead to the so called "K factor" [8,9] that may be as large as 2 at low $\sqrt{\hat{s}}$ and multiplies the cross section. This K factor is subprocess dependent and also Q^2 and p_T^2 dependent and will be set equal to 1 unless otherwise specified. The $O(\alpha_s)$ contributions to this enhancement have been calculated in some cases, for example, vector boson production [10,11]. Typically these

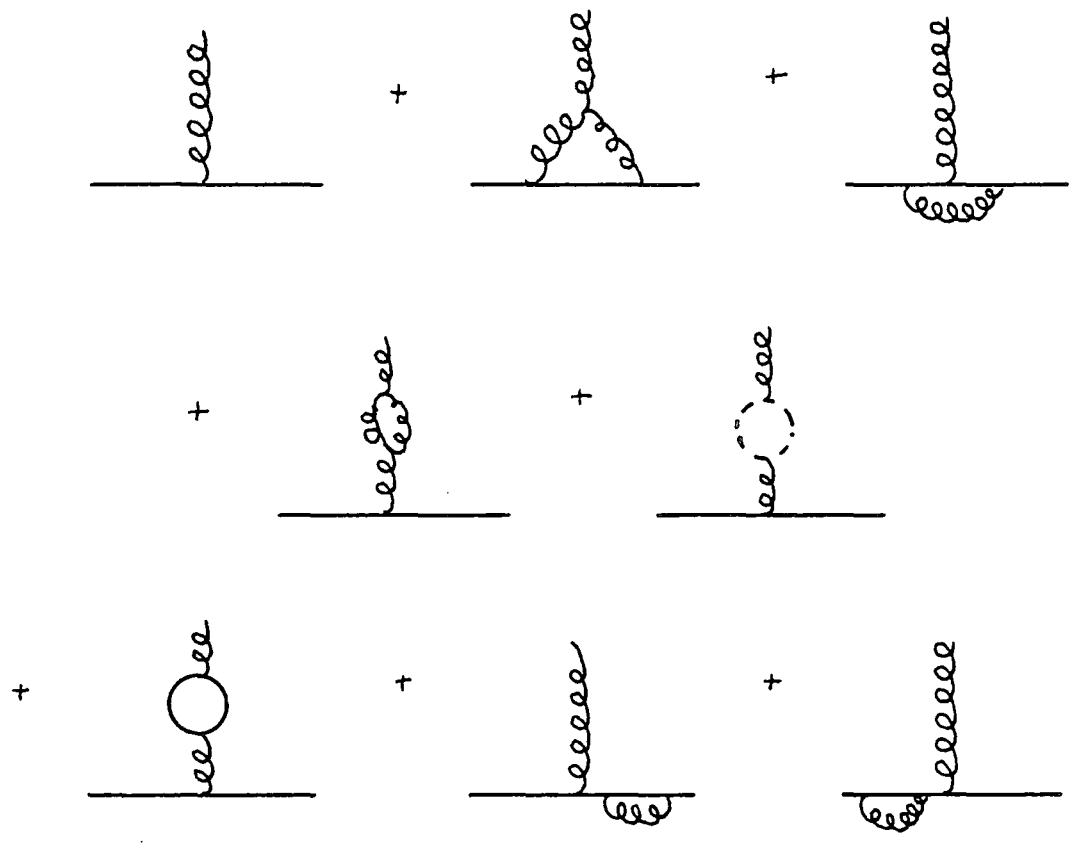

Figure 3

The one loop contributions to the quark-gluon coupling. All physically indistinguishable diagrams need to be included to give a finite answer.

corrections to the total cross section are O(30%) at $\sqrt{s}$ = 540GeV. The transverse momentum distributions are much harder to calculate since the corrections are p_T dependent and both low p_T and large p_T effects must be included [12].

2.4 Scale violating parton densities

Many sets of scale violating parton densities have been proposed in the literature [13-16]. The data from deep inelastic scattering experiments have been used to generate structure functions at some Q_o^2 and these are then evolved in Q^2 using QCD in the form of the Altarelli-Parisi equations [17]. Typically structure functions are measured at $Q_o^2 \sim 4GeV^2$ and then a parameterisation is extracted that follows the predicted evolution. Small errors in the input distribution lead to large errors at large Q^2. Furthermore, the very low x values are not well determined at low Q_o^2 so that the region in which particular parameterisations are valid must not be overstepped.

For a $p\bar{p}$ collider operating at $\sqrt{s}$ = 540GeV and producing centre-of-mass energies from, say $4m_b^2$ (corresponding to $\bar{b}b$ production threshold) to M^2, where M is the mass of a heavy object $\sim$ O(100GeV) the required region in x is approximately,

$$(4m_b^2/s)^{1/2} < x < (M^2/s)^{1/2}, \qquad (2.16)$$

or,

$$0.02 < x < 0.2, \qquad (2.17)$$

for,

$$10^2GeV^2 < Q^2 < 10^4GeV^2. \qquad (2.18)$$

Several parameterisations exist which are valid in this region, for example, Owens and Reya [13] (OR), Gluck et al. [14] (GHR) and Duke and Owens [15] (DO1 and DO2). Figs. 4-7 show the gluon, valence up, valence down and sea structure functions for these four parameterisations evaluated at (a) $Q^2 = 4GeV^2$ and (b) $Q^2 = M_W^2$. All show a decrease in the mean value of x as Q^2 increases. This is a reflection of the fact that as each quark is probed deeper and deeper the cloud of coloured objects screening its colour charge is resolved and the number of partons sharing the momentum increases. Since the sum of the momentum fractions is 1, the probability of finding a particular parton having a particular x is increased for low x. In other words, there is an increased probability of finding a parton at small x and a decreased chance of finding one at large x because the high momentum partons lose momentum by radiating other partons.

Although the structure functions are quite different at low Q^2, the evolution is such that these differences tend to decrease as Q^2 increases. This is because, at a given $\sqrt{s} \sim 0.5TeV$, large Q^2 values correspond to the region in x which is well measured at small $\sqrt{s}$ values.

The Owens-Reya distributions are evolved from the rather low value of $Q_o^2 = 1.8GeV^2$. This invites complications from higher-twist effects (which decrease like $1/Q_o^n$, $n > 1$) and can distort the structure function. This parameterisation has been superseded by the more recent work of Duke and Owens.

The choice of Λ influences the hardness of the gluon density. The larger Λ, the harder the distribution at relatively low Q^2. As Q^2 increases this effect is gradually washed out.

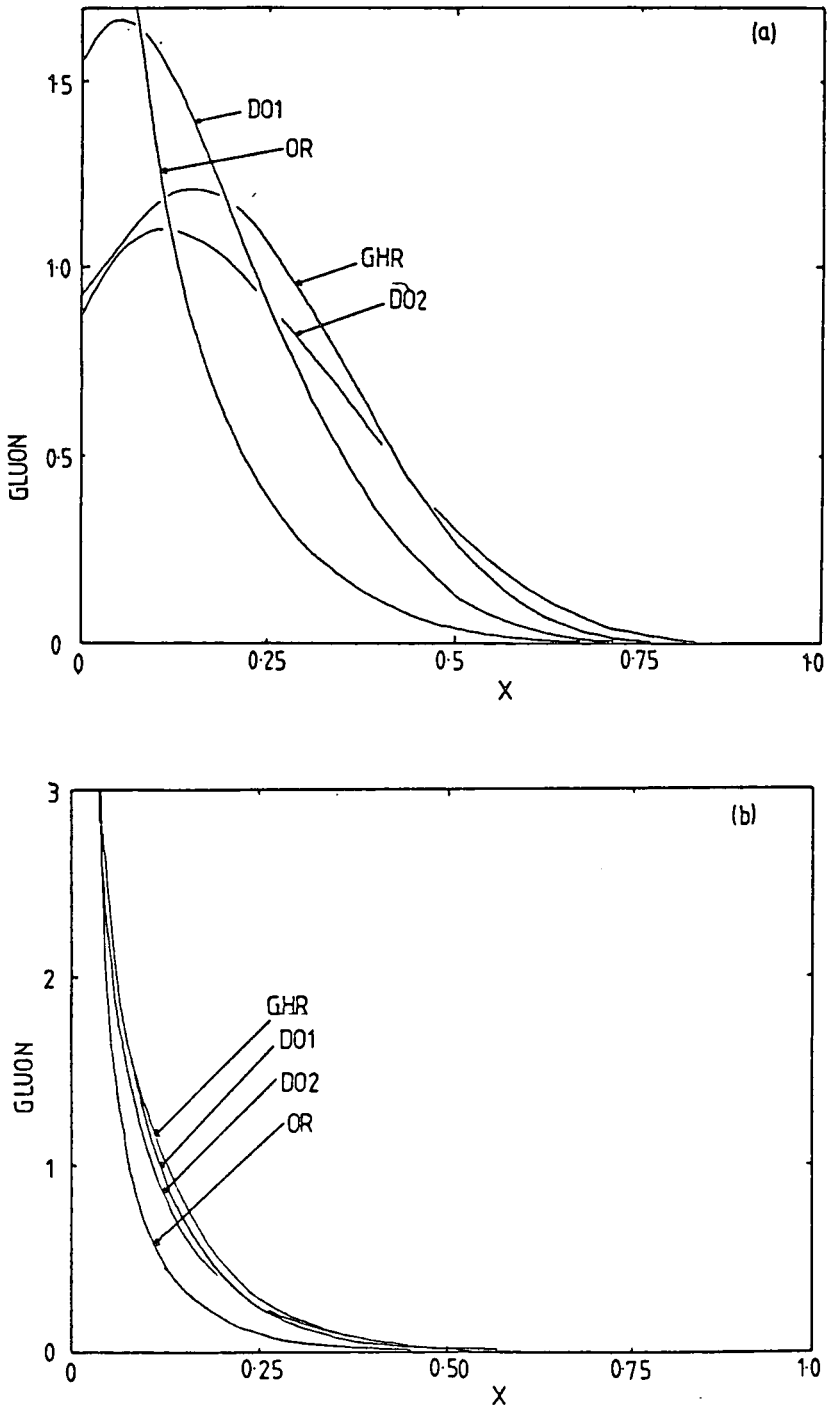

Figure 4

The gluon distribution for the four representative sets of parton densities (OR, GHR, DO1, DO2) evaluated at (a) $Q^2 = 4GeV^2$ and (b) $Q^2 = M_W^2$.

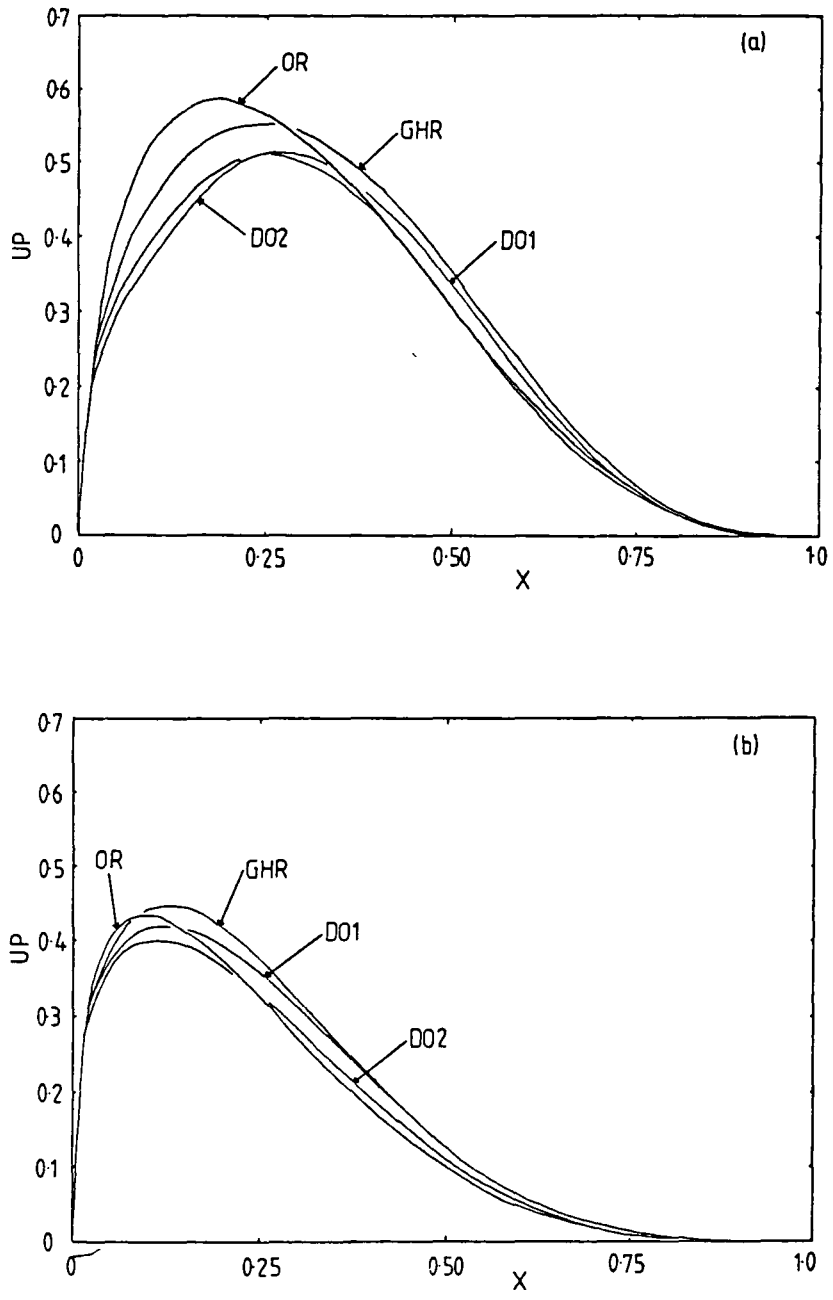

Figure 5

The up quark valence distribution for the four representative sets of parton densities (OR, GHR, DO1, DO2) evaluated at (a) $Q^2 = 4GeV^2$ and (b) $Q^2 = M_W^2$.

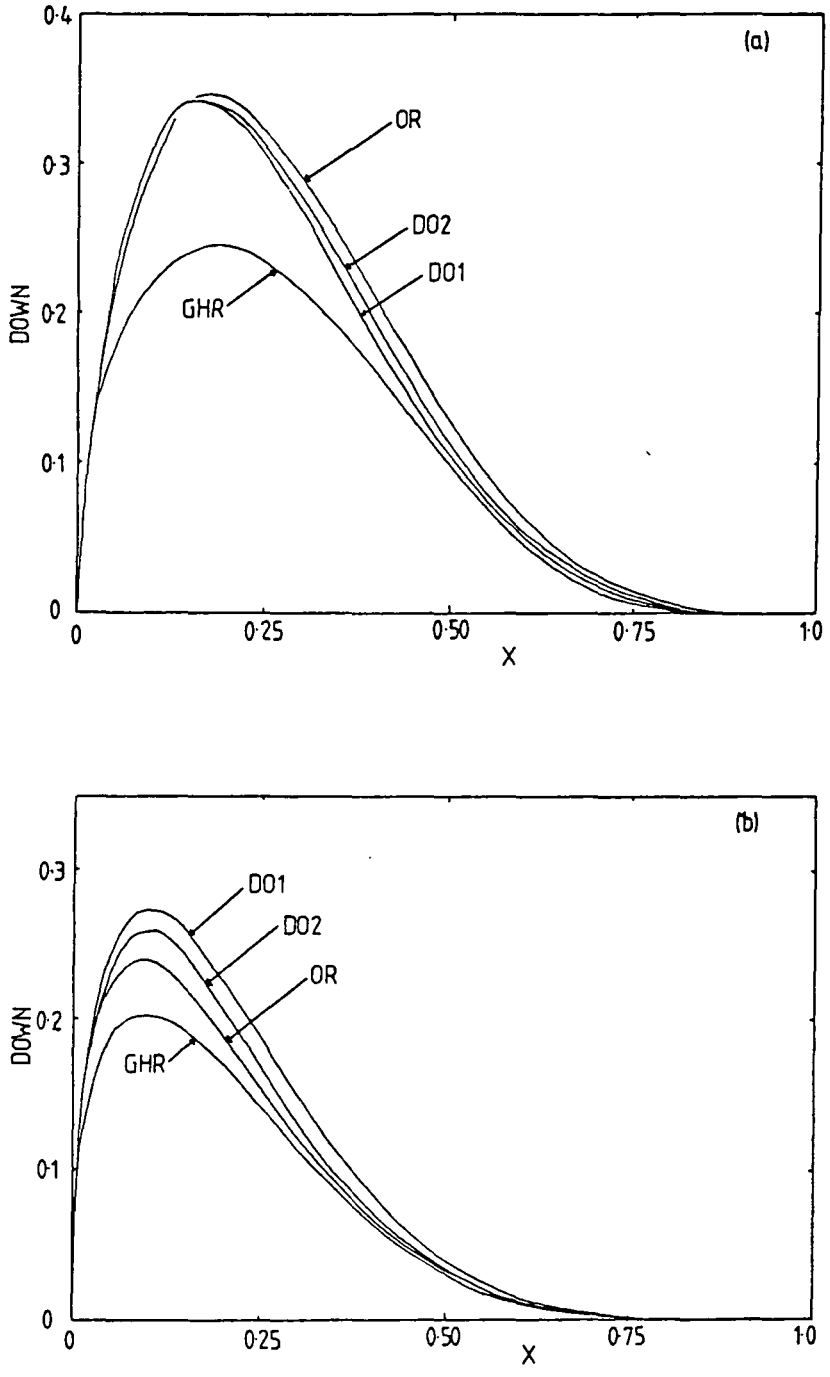

Figure 6

The down quark valence distribution for the four representative sets of parton densities (OR, GHR, DO1, DO2) evaluated at (a) $Q^2 = 4GeV^2$ and (b) $Q^2 = M_W^2$.

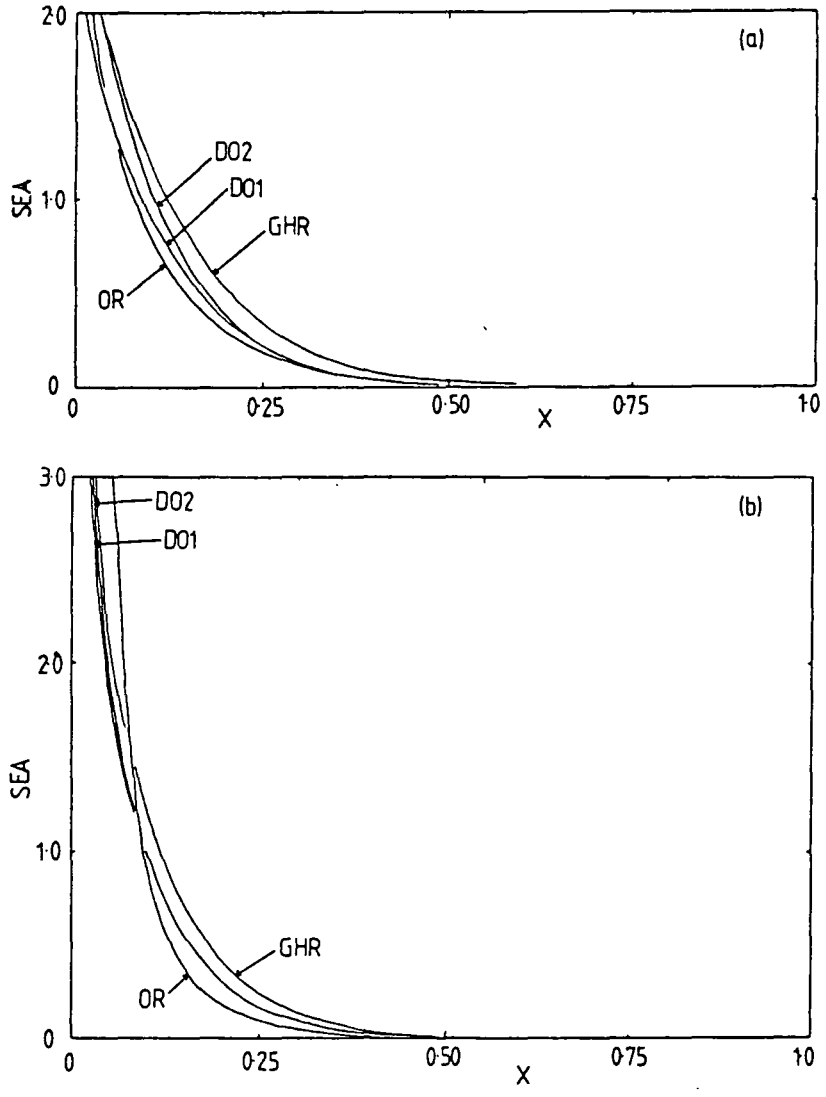

Figure 7

The sea quark distribution for the four representative sets of parton densities (OR, GHR, DO1, DO2) evaluated at (a) $Q^2 = 4GeV^2$ and (b) $Q^2 = M_W^2$.

2.5 Differential luminosities

The differential cross section for the process, $a + b \rightarrow c + X$, can be written,

$$\frac{d\sigma(ab \rightarrow c)}{d\tau} = \sum_{ij} \frac{dL_{ij}}{d\tau} \hat{\sigma}(ij \rightarrow c). \qquad (2.19)$$

where $dL_{ij}/d\tau$ is the differential luminosity. The x_a, x_b integrations in the inclusive counterpart of (2.11) have been replaced by an integration over τ and an integration over x at fixed τ. The differential luminosity is defined as,

$$\frac{dL_{ij}}{d\tau} = \frac{1}{1 + \delta_{ij}} \int_{\tau}^{1} \frac{dx}{x} (f_i^{(a)}(x,Q^2) f_j^{(b)}(\tau/x,Q^2) + i \leftrightarrow j) \qquad (2.20)$$

and gives the probability of finding incident partons (i and j) to give a particular value of τ within the colliding beams. The differential luminosities are fixed functions at particular values of $\sqrt{s}$ and are common to many $\bar{p}p$ calculations.

The differential luminosities for the six main combinations of partons ($u\bar{u}$, $d\bar{d}$, $u\bar{d}$, gg, ug and dg) for $p\bar{p}$ collisions at $\sqrt{s}$ = 540GeV are shown in Fig. 8 (9) as a function of M (= $\sqrt{(s\tau)}$) for the GHR (DO1) structure functions evolved in Q^2 to $Q^2 = M^2$. For small M values the subprocesses involving gluons dominate. As the $x_a x_b$ value increases, the rapid fall away of the gluon structure function allows the quark subprocesses to become relatively more important. At large M the gluon subprocesses are the weakest channels. The two sets of parton densities are very similar over most of the range of M. The differences tend to occur at either very low M or very large M since

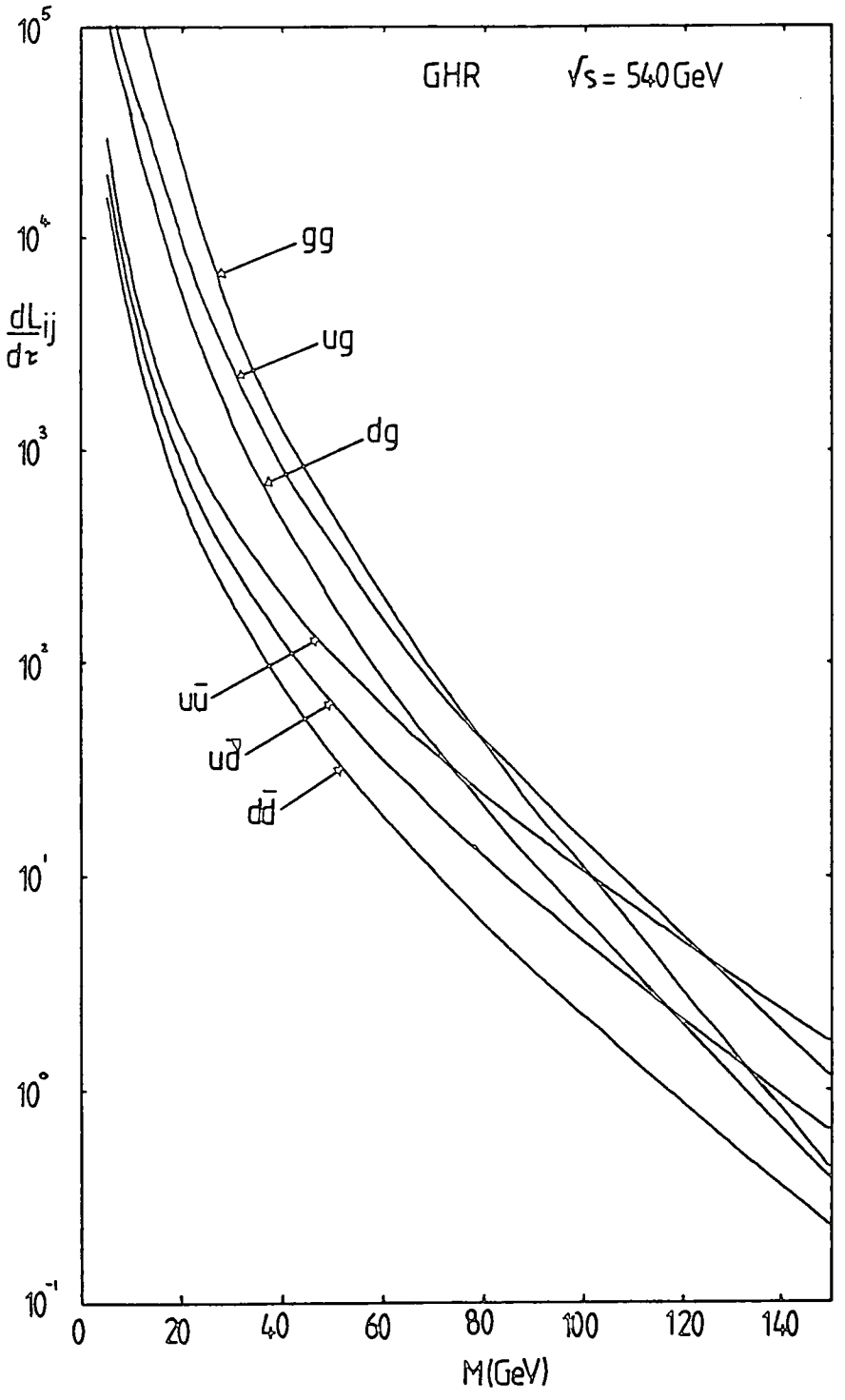

Figure 8

The differential luminosities ($dL_{ij}/d\tau$) as a function of M at $\sqrt{s}$ = 540GeV for the GHR structure functions evaluated at $Q^2 = M^2$ and where $\tau = M^2/s$. All six main parton channels are shown.

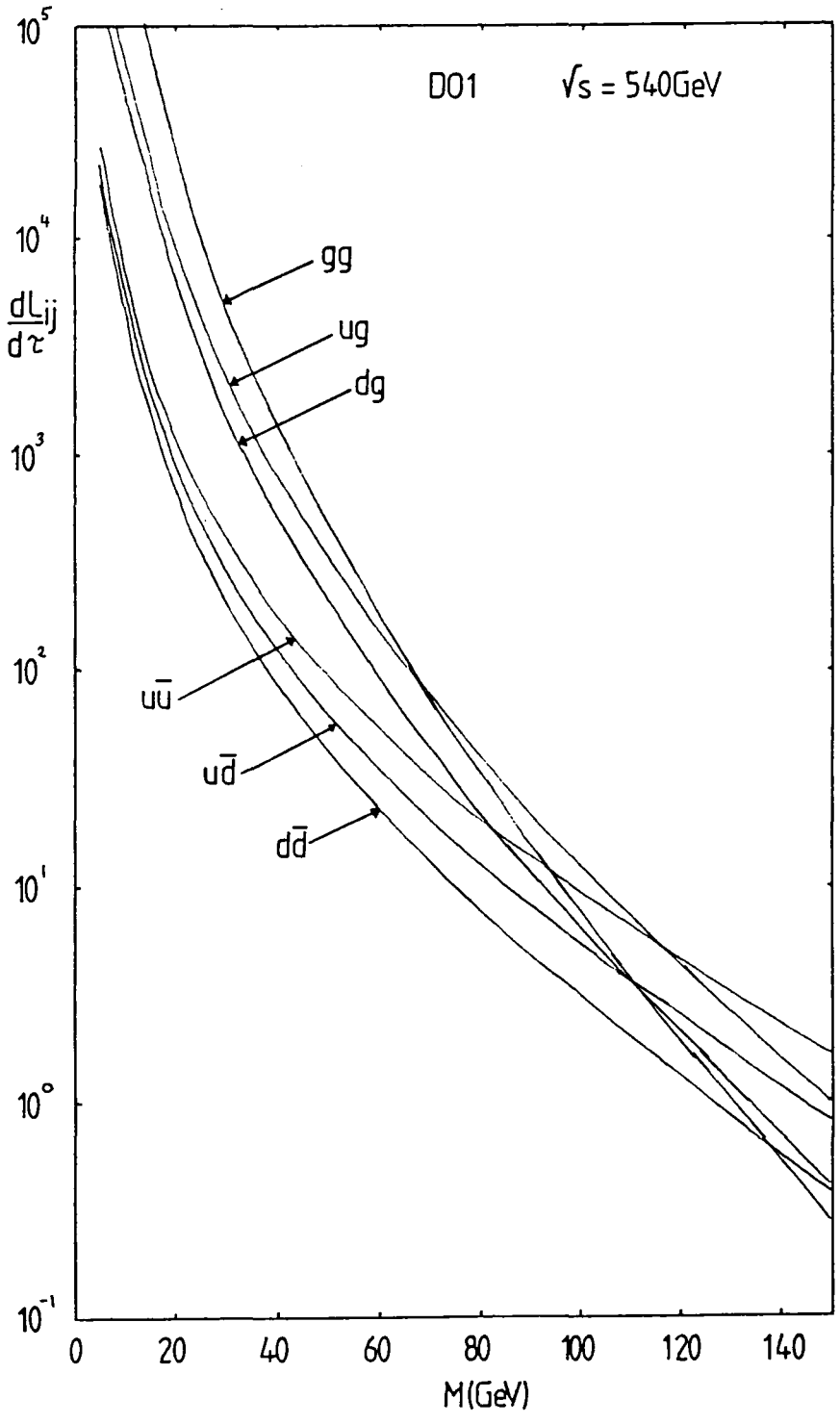

Figure 9

The differential luminosities ($dL_{ij}/d\tau$) as a function of M at $\sqrt{s}$ = 540GeV for the DO1 structure functions evaluated at $Q^2 = M^2$ and where $\tau = M^2/s$. All six main parton channels are shown.

this is where the structure functions are least well determined.

Equation (2.19) is generally true, though for $2 \rightarrow 1$ processes the τ integration may be performed and the total cross section written in terms of the decay width of the particle c. The next section utilises this fact to calculate W and Z production cross sections.

2.6 2 to 1 processes and weak boson production

For $2 \rightarrow 1$ processes, the subprocess cross section $\hat{\sigma}(ij \rightarrow c)$ can be written [18] in the narrow width approximation,

$$\hat{\sigma}(ij \rightarrow c) = \frac{S(2J_c + 1)n_c}{(2J_i + 1)n_i(2J_j + 1)n_j}\Gamma(c \rightarrow ij)\frac{16\pi^2}{M^3}\tau\delta(\tau - M^2/s) \quad (2.21)$$

and hence,

$$\sigma(ab \rightarrow cX) = \frac{S(2J_c + 1)n_c}{(2J_i + 1)n_i(2J_j + 1)n_j}\Gamma(c \rightarrow ij)\frac{16\pi^2}{M^3}\tau\frac{dL_{ij}}{d\tau} \quad (2.22)$$

where $dL_{ij}/d\tau$ is evaluated at $\tau = M^2/s$. J_c, J_i, J_j (n_c, n_i, n_j) are the spins (colours) of c, i and j respectively. S is a symmetry factor equal to 2 for indistinguishable bosons i,j and 1 otherwise.

Using equation (2.22) and Figs. 8 and 9, estimates of weak boson production cross sections can be obtained. For example, consider W^+ production from $u\bar{d}$. $J_W = 1$, $J_u = J_{\bar{d}} = 1/2$, $n_W = 1$, $n_u = n_{\bar{d}} = 3$ and $S = 1$ so,

$$\sigma(p\bar{p} \rightarrow W^+X) = \frac{4\pi^2}{3M_W^3}\Gamma(W^+ \rightarrow u\bar{d})\tau\frac{dL_{u\bar{d}}}{d\tau} \quad (2.23)$$

The total W^+ width is,

$$\Gamma_W = \sqrt{2}M_W^3 G_F/\pi \quad (2.24)$$

and the partial width to $u\bar{d}$ is 3/11 of this (neglecting Cabbibbo

mixing). From Fig. 8 or 9, at M = 81GeV, $dL_{u\bar{d}}/d\tau$ = 12 so at $\sqrt{s}$ = 540GeV,

$$\sigma(p\bar{p} \rightarrow W^{+}X) = 1.95\text{nb}$$

and,

$$\sigma(p\bar{p} \rightarrow W^{\pm}X \rightarrow e^{\pm}\nu X) = 0.36\text{nb}.$$

which may be compared with the experimental values at $\sqrt{s}$ = 540GeV,

$$\sigma(p\bar{p} \rightarrow W^{\pm}X \rightarrow e^{\pm}\nu X) = 0.53 \pm 0.08 \pm 0.09\text{nb UA1 [19]},$$

$$= 0.53 \pm 0.10 \pm 0.10\text{nb UA2 [20]}.$$

Similarly the Z cross section may be calculated. The partial width to massless colour triplet fermion-antifermion pair is,

$$\Gamma(Z \rightarrow f\bar{f}) = (a^2 + b^2)G_F M_Z^{\,3}\sqrt{2}/\pi \qquad (2.25)$$

where $a = (T_3 - 2Q\sin^2\theta_W)/2$ and $b = T_3/2$. So for a Z of mass 95GeV and $\sin^2\theta_W = 0.22$,

$$\Gamma(Z \rightarrow u\bar{u}) = 0.32\text{GeV}$$

$$\Gamma(Z \rightarrow d\bar{d}) = 0.42\text{GeV}.$$

From Fig. 8, $dL_{u\bar{u}}/d\tau$ = 11 and $dL_{d\bar{d}}/d\tau$ = 3.8 at M = 95GeV so,

$$\sigma(p\bar{p} \rightarrow ZX) = 0.95\text{nb}$$

and,

$$\sigma(p\bar{p} \rightarrow ZX \rightarrow e^{+}e^{-}X) = 0.03\text{nb}.$$

which may be compared with the experimental values at $\sqrt{s}$ = 540GeV,

$$\sigma(p\bar{p} \rightarrow ZX \rightarrow e^{+}e^{-}X) = 0.071 \pm 0.024 \pm 0.013\text{nb UA1 [21]},$$

$$= 0.110 \pm 0.040 \pm 0.020\text{nb UA2 [20]}.$$

These rough estimates could be improved by including the strange sea contribution. They do, however, give a quick rough estimate to the production cross sections. Including higher order corrections [22] gives cross sections,

$$\sigma(p\bar{p} \rightarrow W^{\pm}X \rightarrow e^{\pm}\nu) = 0.370 + 0.110 - 0.060\text{ nb},$$

$$\sigma(p\bar{p} \rightarrow ZX \rightarrow e^+e^-) = 0.042 + 0.012 - 0.006 \text{ nb},$$

where the errors represent the theoretical uncertainties. These cross sections are larger than the rough calculations by about a factor of 1.4.

2.7 2 to 2 Scattering kinematics

Although $2 \rightarrow 1$ scattering is an important feature of proton-antiproton collisions, $2 \rightarrow 2$ scattering is also important. For example, the production of a pair of hadronic jets via the subprocess $q\bar{q} \rightarrow gg$.

In general $2 \rightarrow 2$ processes $ij \rightarrow cd$ will involve a 3-dimensional integral (2x3 - 4 from the Lorentz invariant two particle phase space - 1 from cylindrical symmetry + 2 from the parton momentum fraction integrals). There are several ways to express the total cross section. Two of the most common (and useful) forms are given below. Both involve the subprocess differential cross section $d\sigma/dt$.

Firstly the most obvious form is,

$$\sigma(ab \rightarrow cdX) = \int\int\int dx_a dx_b d\cos\theta (...) d\hat{t}/d\cos\theta \qquad (2.26)$$

where,

$$(...) = (f_i^{(a)}(x_a) f_j^{(b)}(x_b) + i \leftrightarrow j) d\hat{\sigma}(ij \rightarrow cd)/d\hat{t}. \qquad (2.27)$$

θ is the angle between c and the a beam direction and $\hat{t}$ is the momentum transfer in the process $= (p_i - p_c)^2$.

In cases where there is a singularity in the subprocess differential cross section when one of the final state particles is parallel with one of the initial state particles it is convenient to

make a change of variables. In doing this the rapidity, y, is defined,

$$y = 0.5\ \ln((E + p_L)/(E - p_L)) \tag{2.28}$$

where E is the particle energy and p_L the longitudinal momentum. In the lab frame, y = 0 for particles emitted at 90^o to the beam axis. The three integration variables are y_c, y_d and p_T, where p_T is the transverse momentum of one of the final state particle. The total cross section is given by [23],

$$\sigma(ab \rightarrow cdX) = \int\int\int dp_T^2 dy_c dy_d x_a x_b (\ldots) \tag{2.29}$$

with limits given by,

$$\ln(\bar{x}_{Tc}/(2 - \bar{x}_{Td}\exp(-y_d))) \leq y_c \leq \ln((2 - \bar{x}_{Td}\exp(y_d))/\bar{x}_{Tc}),$$

$$\ln((a - \sqrt{(a^2 - \bar{x}_{Td}^2)})/\bar{x}_{Td}) \leq y_d \leq \ln((a + \sqrt{(a^2 - \bar{x}_{Td}^2)})/\bar{x}_{Td}),$$

$$0 \leq p_T^2 \leq s((1 - (m_c^2 + m_d^2)/s)^2 - 4m_c^2 m_d^2/s^2)/4, \tag{2.30}$$

where,

$$\bar{x}_{Ti} = 2\sqrt{((m_i^2 + p_T^2)/s)}, \quad i=c,d$$

$$a = 1 + (m_d^2 - m_c^2)/s, \tag{2.31}$$

and the usual momentum fractions x_a and x_b are given by,

$$x_a = \sum_{i=c,d} \bar{x}_{Ti}\exp(y_i)/2,$$

$$x_b = \sum_{i=c,d} \bar{x}_{Ti}\exp(-y_i)/2. \tag{2.32}$$

The Mandelstam subprocess invariants are given by,

$$\hat{t} = - x_b x_T \exp(y_c) s/2,$$

$$\hat{u} = - x_a x_T \exp(-y_c) s/2, \tag{2.33}$$

with $x_T = 2p_T/\sqrt{s}$.

The divergences arising from parallel initial and final state particles may be eliminated by imposing a minimum p_T cut.

$$p_T(\min)^2 \leq p_T^2 \qquad (2.34)$$

This is a convenient procedure since in practise particles require a non-zero p_T to be identified.

2.8 Summary

In this chapter the main ingredients for making studies of hadron-hadron collisions have been discussed. In the leading log approximation, the interaction ab $\rightarrow$ cX may be described in terms of the parton model with non-scaling parton densities and non-scaling strong coupling constant. The kinematics for 2 $\rightarrow$ 1 and 2 $\rightarrow$ 2 processes have been given in detail. The Monte Carlo techniques required to perform the integrations and simulate experimental cuts and triggers are described in the Appendix.

References

(1) J.D.Bjorken, Proc. 3rd Int. Symp. on Electron + Photon Interactions, Stanford

(2) R.P.Feynman, Phys. Rev. Lett. 23, 1415, (1969)

(3) J.D.Bjorken and E.A.Paschos, Phys. Rev. D10, 2973, (1969)

(4) R.P.Feynman, Photon-Hadron Interactions (Benjamin),(1972)

(5) V.N.Gribov and L.N.Lipatov, Yad. Fiz. 15, 781, (1972); ibid 15, 1218, (1972)

(6) R.M.Barnett and D.Schlatter, Phys. Lett. 112B, 475, (1982)

(7) R.M.Barnett, Phys. Rev. Lett. 48, 1657, (1982)

(8) G.Altarelli, R.K.Ellis and G.Martinelli, Nucl. Phys. B157, 461, (1979)

(9) G.Parisi, Phys. Lett. 90B, 295, (1980)

(10) G.Altarelli, R.K.Ellis and G.Martinelli, Nucl. Phys. B157, 461, (1979)

(11) J.Kubar-Andre and F.E.Paige, Phys. Rev. D19, 221, (1979)

(12) G.Altarelli, R.K.Ellis and G.Martinelli, CERN report CERN-TH-4015 (1984)

(13) J.F.Owens and E.Reya, Phys. Rev. D17, 3003, (1978)

(14) M.Gluck, E.Hoffmann and E.Reya, Z.Phys. C13, 119, (1982)

(15) D.W.Duke and J.F.Owens, Phys. Rev. D27, 508, (1984)

(16) E.Eichten, I.Hinchliffe, K.Lane and C.Quigg, Rev. Mod. Phys. 56, (1984)

(17) G.Altarelli and G.Parisi, Nucl. Phys. B126, 298, (1977)

(18) V.Barger, H.Baer and K.Hagiwara, Phys. Lett. 146B, 257, (1984)

(19) G.Arnison et al., UA1 collab., Phys. Lett. 129B, 273, (1983)

(20) J.Schacher, UA2 collab., Proc. 4th Topical Workshop on $p\bar{p}$ Collider Physics, Berne, (1984)

(21) C.Rubbia, UA1 collab., Proc. 4th Topical Workshop on $p\bar{p}$ Collider Physics, Berne (1984)

(22) G.Altarelli, R.K.Ellis, M.Greco and G.Martinelli, Nucl. Phys. B246, 12, (1984)

(23) D.M.Scott, Proc. Workshop on Lepton-Pair Production in Hadron-Hadron Collisions, Bielefeld (1978)

Chapter Three

Dileptons: The key to heavy quarks.

3.1 Introduction

One of the major successes of the CERN $\bar{p}p$ collider has been the discovery of the W and Z bosons [1,2]. The W was first observed in 1982 via its decay into a high p_T electron accompanied by large missing transverse momentum ($\not{p}_T$), whilst the Z was first seen in 1983 as an e^+e^- pair with each lepton having large p_T. These observations demonstrate the resolving power of the UA1 and UA2 detectors in the case of high p_T charged leptons and, especially for UA1, large missing $\not{p}_T$. Other particles with lepton signals can therefore be looked for with confidence.

The heavy quark semileptonic branching ratios are known to be O(10%) for the b and c quarks [3,4], and expected to be similar in the case of the top quark [5], hence heavy quark decays may lead to final states containing leptons. Indeed lepton + jet(s) topologies, for example,

$$q\bar{q} \rightarrow W \rightarrow t\bar{b} \text{ with } t \rightarrow be\nu, \qquad (3.1)$$

have been proposed [6-14] as possible heavy quark signals and there is evidence for the top quark in this channel [15]. Cuts to identify the top quark reduce the predicted lepton + 2 jet signal to O(10) events in close agreement with the 6 "lepton + 2 jet" events found by UA1 in

1983. Difficulties in measuring the jet E_T accurately lead to the rather poor bound on the top quark mass,

$$30 < m_t < 50\text{GeV}. \qquad (3.2)$$

In contrast multi-charged-lepton signals are not associated with difficulties in reconstructing jets and may offer cleaner signatures of the underlying mechanisms.

Cascade decays of naked heavy quarks, for example, $t \rightarrow b \rightarrow c \rightarrow s$ can lead to multi-charged-lepton final states. Indeed it has been known for some time that heavy quarks may be looked for in the multi-charged -lepton channel [16-21]. Fig. 1 shows schematically the various origins of leptons in cascade decays of $Q\bar{Q}$ (Q = c, b, t) and $t\bar{b}$ systems. Although the leptonic branching ratio is O(20%) for both e and μ channels, the large number of possible decays means that it is relatively unlikely that there is no charged lepton in the final state. However, there are experimental difficulties in recognising leptons (a) with low transverse momentum e.g., $p_{\mu T} < 5\text{GeV}$, $p_{eT} < 15\text{GeV}$, and (b) where there is hadronic debris close by i.e., the lepton is in or near a jet. This means that leptons from a secondary or tertiary decay are less likely to be seen than those from primary decays, where the lepton generally has a larger p_T and is more separated from the associated jet. Leptons may be separated into isolated (those not accompanied by hadronic debris) and not-isolated (those that are). This leads to the concept of isolation cuts where, for example [13], leptons are "isolated" if the total hadronic debris within a cone of 30^o from the lepton momentum vector has a scalar E_T less than 3GeV. Primary decay leptons from large mass quarks tend to be isolated and so isolation cuts may lead to an enriched heavy quark

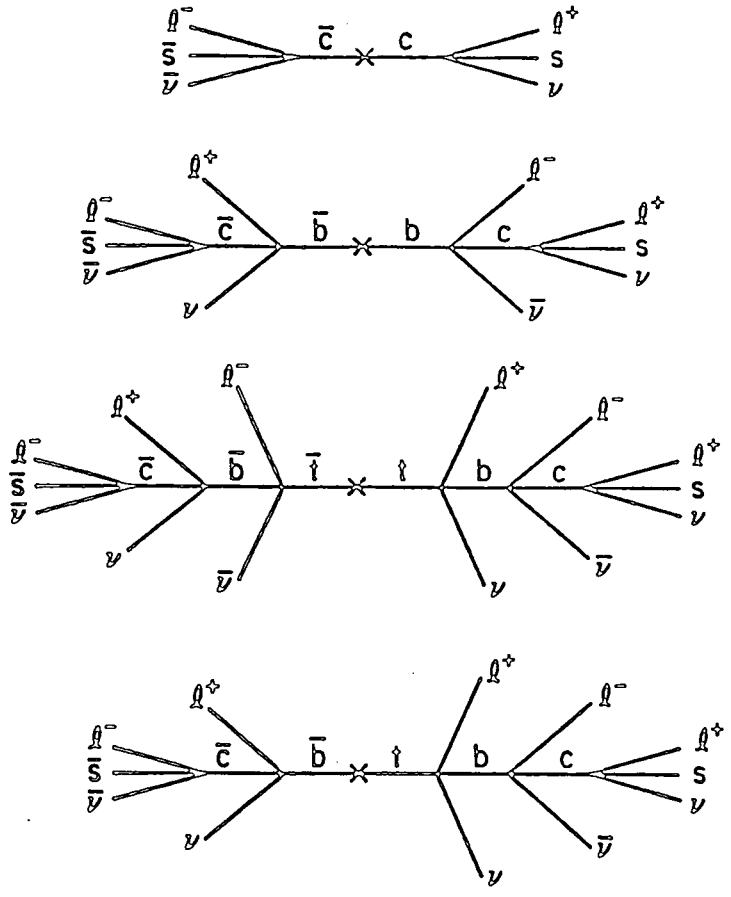

Figure 1

Multilepton possibilities in $c\bar{c}$, $b\bar{b}$, $t\bar{t}$ and $t\bar{b}$ cascade decays; at each vertex the leptons $l\bar{\nu}$ can be replaced by the quarks $q\bar{q}'$.

sample.

Throughout this chapter, only dileptons from primary heavy quark decays will be studied (since they are most easily recognised in the detector). Dileptons separate into like-sign and unlike-sign pairs, which are either isolated or not-isolated.

Heavy quark sources of primary decay dileptons are,

$$q\bar{q},\ gg \rightarrow Q\bar{Q} \rightarrow (q\bar{l}\nu)(\bar{q}l\bar{\nu}), \tag{3.3}$$

$$q\bar{q} \rightarrow Z \rightarrow Q\bar{Q} \rightarrow (q\bar{l}\nu)(\bar{q}l\bar{\nu}), \tag{3.4}$$

where Q = c, b, t, and,

$$q'\bar{q} \rightarrow W \rightarrow t\bar{b} \rightarrow (b\bar{l}\nu)(c\bar{l}\nu). \tag{3.5}$$

The lepton pairs may be of mixed flavour. Note that, in the case of $b\bar{b}$ production, if a B^0 meson is formed from the b quark fragmentation it may mix to form a $\bar{B}^0$ meson [22] which can then decay to give a lepton of the same sign as that produced by the $\bar{b}$ quark on the opposite side.

There is a contribution to dilepton production from the decays of "hidden" flavour states, e.g., $\psi \rightarrow l\bar{l}$, which are always unlike sign. Since leptons from hidden flavour decays have small momentum in the parent rest frame, the parent must have a significant transverse momentum in the lab frame to enable the leptons to have sufficient p_T to be recognised. Quarkonium production at large p_T, e.g.,

$$gg \rightarrow Yg \rightarrow \mu^+\mu^-g, \tag{3.6}$$

satisfies this requirement.

Another source of dilepton events is the Drell-Yan process [23],

$$q\bar{q} \rightarrow Z,\ \gamma \rightarrow l^+l^-. \tag{3.7}$$

The leptons from this source are isolated and approximately back to back in the transverse plane.

These different dilepton production mechanisms are categorised as follows,

origin	description
$b\bar{b}$, $c\bar{c}$	unlike sign, not isolated
$t\bar{t}$	unlike sign, isolated
$t\bar{b}$	like sign, isolated
"hidden flavour"	unlike sign, isolated
Drell-Yan	unlike sign, isolated
$b\bar{b}$ (B^0-$\bar{B}^0$ mixing)	like sign, not isolated

It should be emphasised that the like sign dimuon signal from $W \rightarrow t\bar{b} \rightarrow \mu^+\mu^+$, where one of the muons is isolated and the other is close to a jet [16] is an excellent signature for the top quark.

This chapter is organised as follows. Section 3.2 contains a description of heavy quark production (a) via QCD fusion and (b) via electroweak production. The heavy quarks, Q, are pair produced and then allowed to fragment into unpolarised heavy mesons $Q\bar{q}$ which then decay semileptonically. The fragmentation and decay steps are also described.

Section 3.3 briefly discusses the dileptons from the Drell-Yan process (3.7). Section 3.4 compares unlike sign dileptons from heavy quark production and the Drell-Yan process. The $b\bar{b}$ and $c\bar{c}$ backgrounds are removed by requiring that the leptons are isolated leaving a Drell-Yan dominated sample with some $t\bar{t}$ contamination. By specialising to $e\mu$ pairs a "clean" $t\bar{t}$ signal can be found.

Hidden flavour production at high p_T is discussed in section 3.5.

Two different mechanisms for ψ production at high p_T are considered and methods for direct measurement of the $b\bar{b}$ production cross section and small x gluon structure function proposed.

The results are summarised in section 3.6.

3.2 Naked flavour production

Heavy quarks may be produced (a) via QCD fusion,

$$q\bar{q},\ gg \rightarrow Q\bar{Q}, \tag{3.8}$$

or (b) through electroweak production,

$$q\bar{q} \rightarrow Z \rightarrow Q\bar{Q}, \tag{3.9}$$

$$q'\bar{q} \rightarrow W \rightarrow t\bar{b}, \tag{3.10}$$

where Q = c, b, t.

The subprocess differential cross sections for (3.8) (see Fig. 2) are [24],

$$\frac{d\hat{\sigma}(q\bar{q} \rightarrow Q\bar{Q})}{d\hat{t}} = \frac{4\pi\alpha_s^2}{9}\,\frac{(m^2 - \hat{t})^2 + (m^2 - \hat{u})^2 + 2m^2\hat{s}}{\hat{s}^4}, \tag{3.11}$$

and,

$$\frac{d\hat{\sigma}(gg \rightarrow Q\bar{Q})}{d\hat{t}} = \frac{\pi\alpha_s^2}{16\hat{s}^2}\left[\frac{6(m^2-\hat{t})(m^2-\hat{u})}{\hat{s}^2} + \frac{8(m^2 - \hat{t})(m^2 - \hat{u}) - 16m^2(m^2 + \hat{t})}{3(m^2 - \hat{t})^2}\right. \tag{3.12}$$

$$\left. - \frac{m^2(\hat{s} - 4m^2)}{3(m^2 - \hat{t})(m^2 - \hat{u})} - \frac{6((m^2 - \hat{t})(m^2 - \hat{u}) + m^2(\hat{u} - \hat{t}))}{\hat{s}(m^2 - \hat{t})} + (\hat{u} \leftrightarrow \hat{t})\right]$$

where m is the mass of quark Q and α_s is the strong coupling constant evaluated at some Q^2,

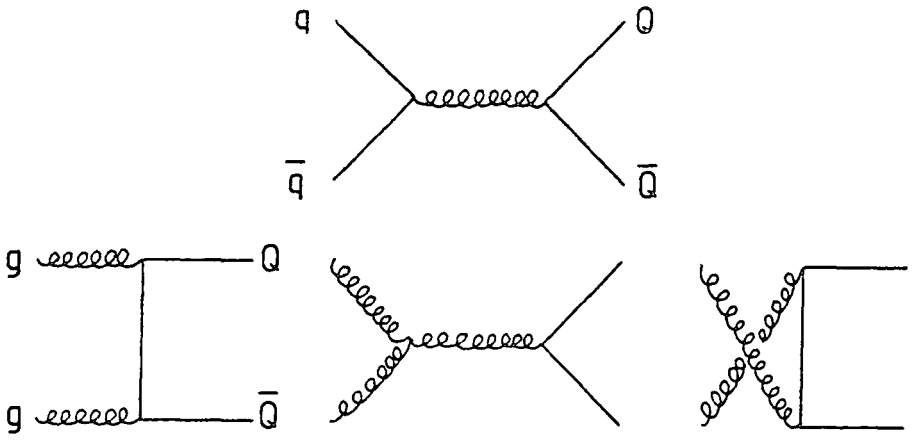

Figure 2

Lowest order QCD diagrams for the "flavour-creation" processes $q\bar{q} \rightarrow Q\bar{Q}$ and $gg \rightarrow Q\bar{Q}$.

$$\alpha_s(Q^2) = \frac{12\pi}{(33 - 2N_F)\ln(Q^2/\Lambda^2)} \qquad (3.13)$$

where N_F is the number of quark flavours and Λ the QCD scale. The cross sections for heavy quark production from these subprocesses for a range of collider energies are shown in Figure 3 (using the parton densities of Gluck et al.[25] evaluated at $Q^2 = \hat{s}$). The cross sections die very rapidly with increasing quark mass. The total fusion cross sections for $q\bar{q}$, $gg \rightarrow Q\bar{Q}$ at $\sqrt{s}$ = 540GeV for particular quark masses are listed below,

Mass (GeV)	σ (nb)
1.5	2×10^5
4.6	6.6×10^3
25	5
35	0.8
45	0.2

with Λ = 0.4GeV, N_F = 4(5) for the b and c (t) quarks. By making different choices of Λ and N_F these cross sections can be altered by O(30%). As Λ and N_F increase so does α_s and hence the cross section rises, while if Λ and N_F decrease the cross section drops. Different structure functions also lead to different cross sections. For example, the Owens-Reya [26] parameterisation of the gluon distribution is much softer and therefore enhances the low mass region while the Gluck et al. set has a hard gluon distribution and is larger at higher mass values.

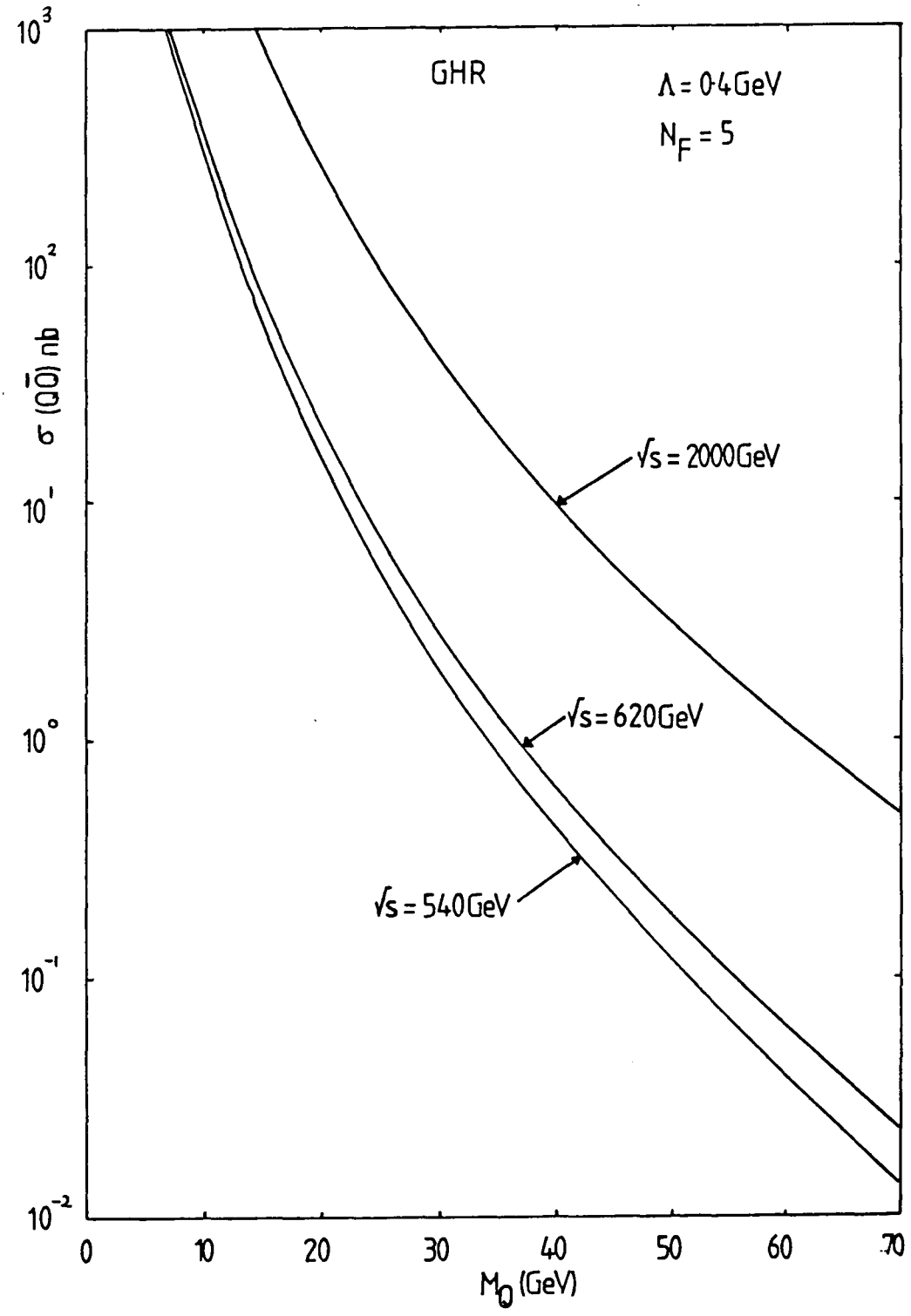

Figure 3

Heavy quark production in $p\bar{p}$ collisions at centre-of-mass energy $\sqrt{s}$ through the $O(\alpha_s^2)$ diagrams of Fig. 2. The structure functions used are those of Gluck et al. with Λ = 0.4GeV and $Q^2 = \hat{s}$. N_F has been set equal to 5 corresponding to five active quark flavours.

The subprocess differential cross section for electroweak production of heavy quarks (see Fig. 4) are,

$$\frac{d\hat{\sigma}(q\bar{q} \rightarrow Z \rightarrow Q\bar{Q})}{d\hat{t}} = \frac{2\pi\alpha^2}{\sin^4\theta_W \cos^4\theta_W \hat{s}^2((\hat{s} - M_Z^2)^2 + \Gamma_Z^2 M_Z^2)} \tag{3.14}$$

$$\times \quad [((m^2 - \hat{u})^2 + (m^2 - \hat{t})^2)(a^2 + b^2)(a'^2 + b'^2)$$

$$+ 2\hat{s}m^2(a^2 + b^2)(a'^2 - b'^2) + 4aa'bb'((m^2 - \hat{u})^2 - (m^2 - \hat{t})^2)]$$

where $a(a') = (T^3 - 2Q\sin^2\theta_W)/2$ and $b(b') = T^3/2$ for the $q(Q)$ quarks, and,

$$\frac{d\hat{\sigma}(q\bar{q}' \rightarrow W \rightarrow Q\bar{Q}')}{d\hat{t}} = \frac{\pi\alpha^2}{4\sin^4\theta_W} \frac{|U_{qq'}|^2 |U_{QQ'}|^2}{\hat{s}^2} \frac{(\hat{u} - m_Q^2)(\hat{u} - m_{Q'}^2)}{((\hat{s} - M_W^2)^2 + \Gamma_W^2 M_W^2)} \tag{3.15}$$

The initial quarks q and q′ have been taken to be massless. $\hat{s}$, $\hat{t}$, $\hat{u}$ are the usual Mandelstam invariants.

Cross sections for top quark production via the W and Z at $\sqrt{s}$ = 540GeV are,

m_t	$\sigma(p\bar{p} \rightarrow ZX \rightarrow t\bar{t}X)$	$\sigma(p\bar{p} \rightarrow W^{\pm}X \rightarrow (t\bar{b}$ or $\bar{t}b)X)$
25GeV	0.097nb	0.96nb
35GeV	0.057nb	0.80nb
45GeV	0.014nb	0.71nb

where the bottom quark mass is taken to be 4.6GeV. The overall normalisations correspond to $\sigma(p\bar{p} \rightarrow ZX \rightarrow e^+e^-) = 0.042$nb and $\sigma(p\bar{p} \rightarrow W^{\pm}X \rightarrow e^{\pm}\nu X) = 0.37$nb [27].

Once the t quarks are produced in the parton subprocess the

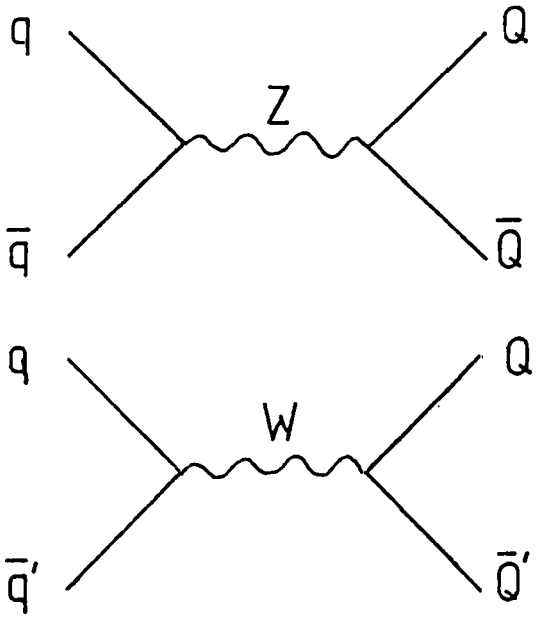

Figure 4

The Feynman diagrams for the production of heavy quarks Q,Q′ from $q\bar{q}$ annihilation via weak bosons.

sequence of events is taken to be that shown in Figure 5. That is, the t quark fragments into a T meson with a time scale $O(10^{-23}s)$ and then decays weakly at times $O(10^{-11}s)$. Peterson et al. [28] have proposed a simple model for fragmentation based on the standard quantum-mechanical parton model approach to calculate transition amplitudes. Consider a heavy quark Q moving with momentum P that fragments into a heavy meson $H = (Q\bar{q})$ with momentum zP and a light quark $\bar{q}$ with momentum (1-z)P (see Fig.6). The transition amplitude is roughly given by $1/(E_H+E_q-E_Q)$ which can be rewritten as,

$$M \propto (1 - 1/z - \varepsilon_Q/(1 - z))^{-1} \qquad (3.16)$$

where $\varepsilon_Q = m_q^2/m_Q^2$. Allowing a factor 1/z for longitudinal phase space yields the form of the fragmentation function,

$$D_Q^H(z) = \frac{N}{z(1 - 1/z - \varepsilon_Q/(1 - z))^2} \qquad (3.17)$$

where N is fixed by requiring,

$$\int_0^1 D_Q^H(z)\, dz = 1 \qquad (3.18)$$

This function is illustrated in Figure 7 for Q = c, b and t (m_t = 35GeV) with $\varepsilon_c = 0.15$ and $\varepsilon_Q = (m_c/m_Q)^2\varepsilon_c$. The fragmentation function peaks at $z \sim 1 - 2\varepsilon_Q$ with a width $\sim \varepsilon_Q$, hence for more and more massive quarks the meson H takes more and more of the parent quark momentum. This parameterisation appears to be consistent with experimental measurements - see Ref. 28.

The semileptonic decay (Fig. 8) has the invariant matrix element,

$$-iM = \bar{u}(q)(-i(g/\sqrt{2})U_{Qq}\gamma_\mu((1-\gamma_5)/2))u(Q)$$
$$\times \frac{i}{(W^2 - M_W^2)}\left[-g^{\mu\nu} + \frac{W^\mu W^\nu}{M_W^2} \right] \qquad (3.19)$$
$$\times \bar{u}(\nu)(-i(g/\sqrt{2})\gamma_\nu((1-\gamma_5)/2))v(l).$$

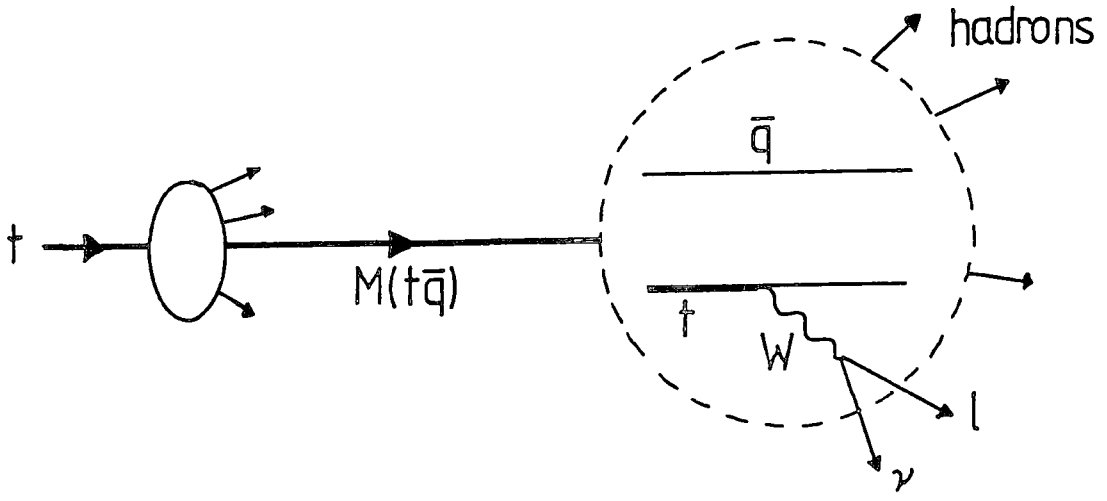

Figure 5

A t quark fragmenting into a meson M which decays semileptonically.

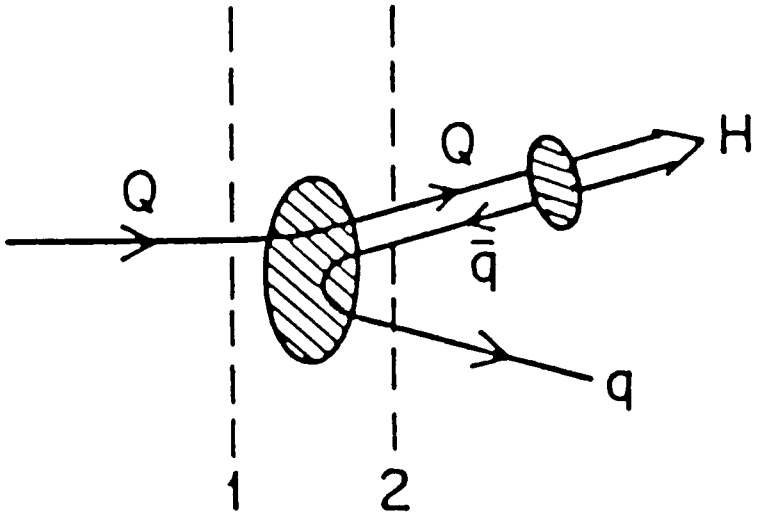

Figure 6

The fragmentation of a heavy quark Q into a meson H($Q\bar{q}$) with momentum fraction z.

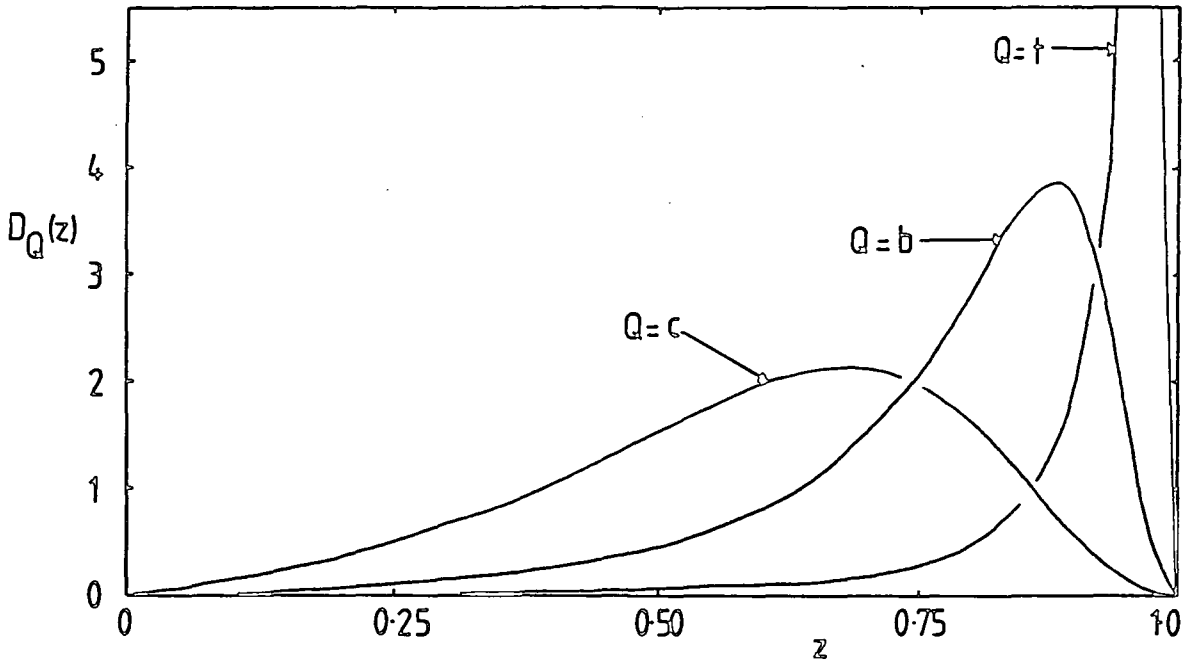

Figure 7

The fragmentation functions $D_c(z)$, $D_b(z)$ and $D_t(z)$ from 3.17 using $\varepsilon_c = 0.15$ and $\varepsilon_Q = \varepsilon_c(m_c^2/m_Q^2)$ with a top quark mass of 35GeV.

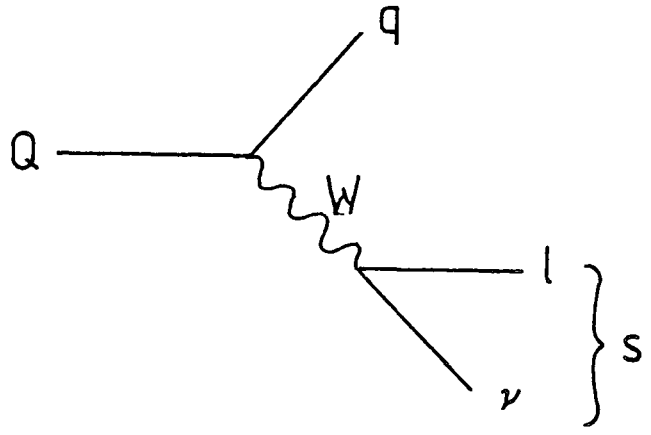

Figure 8

The semileptonic decay of heavy quark Q at the quark level. The invariant mass of the lepton pair is $\sqrt{s}$.

Since the helicity is conserved, the $W^{\mu}W^{\nu}$ term does not contribute and the spin averaged matrix element squared is,

$$\Sigma|M|^2 = \frac{2g^4 \ |U_{Qq}|^2}{(\hat{s} - M_W^2)^2} \ Q.l \ q.\nu, \qquad (3.20)$$

where particle labels represent their momenta and $\sqrt{\hat{s}}$ is the invariant mass of the lepton pair. Note that the heavy quark has been taken to be unpolarised - although the top quark is produced in a given helicity state the fragmentation into a heavy spin-0 T meson is assumed to "wash out" the quark polarisation. This is not always the case [28] since there will be some spin-1 T^* production and preserving the quark polarisation may lead to slightly harder lepton spectra. Nevertheless, this assumption is physically reasonable and is made throughout this chapter.

3.3 Dileptons from the Drell-Yan mechanism

The pair production of leptons from the neutral bosons (the Drell-Yan mechanism) is well established [23]. Both the γ and Z mediated diagrams (see Fig. 9) must be considered. The differential cross section is,

$$\frac{d\hat{\sigma}(q\bar{q} \rightarrow l\bar{l})}{d\hat{t}} = \frac{2\pi\alpha^2}{3\hat{s}^2}\left[\frac{e_q^2(\hat{u}^2+\hat{t}^2)}{\hat{s}^2} - \frac{2e_q(\hat{s}-M_Z^2)[(\hat{u}^2+\hat{t}^2)aa' + (\hat{u}^2-\hat{t}^2)bb']}{x(1-x)\,\hat{s}((\hat{s}-M_Z^2)^2 + \Gamma_Z^2 M_Z^2)}\right.$$

$$\left. + \frac{(a^2+b^2)(a'^2+b'^2)(\hat{u}^2+\hat{t}^2) + 4aba'b'(\hat{u}^2-\hat{t}^2)}{x^2(1-x)^2\,((\hat{s}-M_Z^2)^2 + \Gamma_Z^2 M_Z^2)}\right] \qquad (3.21)$$

where $a(a') = (T^3 - 2Qx)/2$ and $b(b') = T^3/2$ for the quark q (lepton l) and $x = \sin^2\theta_W$. e_q is the quark charge and $\hat{s}$, $\hat{t}$, $\hat{u}$ the Mandelstam

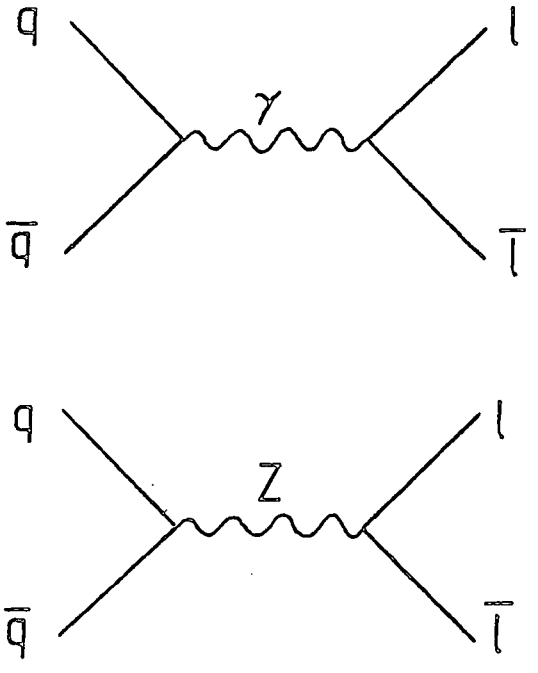

Figure 9

The $O(\alpha^2)$ Feynman graphs contributing to the Drell-Yan process.

invariants. The quarks and leptons have been taken to be massless.

Fig. 10 shows the l^+l^- invariant mass distribution of Drell-Yan pairs for $p\bar{p}$ collisions at $\sqrt{s}$ = 540GeV.

3.4 A top quark signal from lepton pairs.

It has been anticipated for some time [17,30] that lepton pairs with invariant mass $M < M_Z$ will originate from two competitive sources (A) the Drell-Yan mechanism [23],

$$q\bar{q} \rightarrow \gamma, Z \rightarrow l^+l^-, \tag{3.22}$$

and,

(B) the associated production of a heavy quark pair $\bar{Q}Q$ followed by semileptonic decays $Q \rightarrow q\bar{l}\nu$, $\bar{Q} \rightarrow \bar{q}l\bar{\nu}$.

In case (B) the invariant mass of the two charged leptons $M(l^+l^-)$ can exceed $2M_Q$ as a result of the relative transverse momentum of the Q and $\bar{Q}$. Figure 10 compares the l^+l^- invariant mass distribution of Drell-Yan pairs with that from the QCD fusion subprocesses as described in section 3.2. For low M values, $b\bar{b}$ and $c\bar{c}$ initiated lepton pairs have larger cross sections. It is impossible to precisely predict the relative rate of the two sources of lepton pairs due to the large ambiguities in computing the cross sections - see section 3.2. Since diffractive production is ignored, estimates of heavy quark production based on QCD fusion alone should be regarded as conservative.

It has long been thought [17,30] that for small M(ll) the Drell-Yan l^+l^- production would have a smaller rate than that for lepton pairs from heavy quark decays. (These previous calculations used the

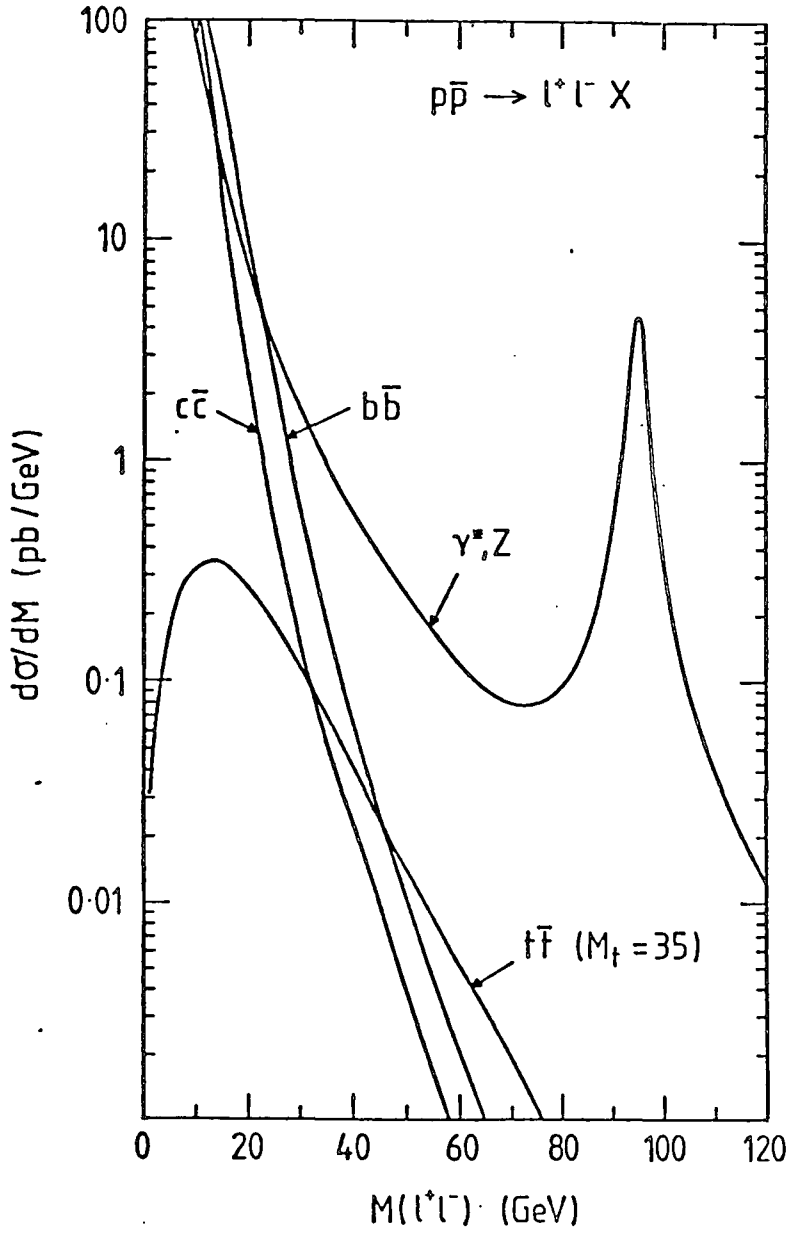

Figure 10

The invariant mass distributions of l^+l^- pairs originating from Drell-Yan and $Q\bar{Q}$ production (Q = c, b, t) in $p\bar{p}$ collisions at $\sqrt{s}$ = 540GeV. No K factor is included. The mass of the top quark is taken to be 35GeV. The electroweak parameters used are; M_Z = 95GeV, Γ_Z = 3GeV and $\sin^2\theta_W$ = 0.21.

collinear approximation for quark decays which enhances the lepton p_T leading to events with higher invariant mass.) In practise this is not the case. Dileptons from $c\bar{c}$ and $b\bar{b}$ events are preferentially suppressed in a realistic experiment as a result of the minimum p_T cuts on the lepton tracks, which are required for lepton/hadron separation in the detector. Moreover isolation cuts on the leptons can be imposed to remove these events and so leave a clean Drell-Yan data sample together with a $t\bar{t}$ initiated "background". These $t\bar{t}$ events may then be separated from this sample.

Firstly, consider the effects of the minimum p_T cut. At present the UA1 detector, for example, can identify muons with $p_T > 5$GeV and electrons with $p_T > 15$GeV. Fig. 11 shows the expected l^+l^- invariant mass distributions of Figure 10 but with these cuts imposed on the lepton p_T. The p_T cut greatly suppresses the $c\bar{c}$ and $b\bar{b}$ initiated events in the region $M(l^+l^-) \backsim 2p_T(\text{min})$, since the requirement of a minimum p_T on each of the decay leptons pushes the other decay products into unfavoured regions of phase space. The suppression is clearly less severe in the $\gamma^* \rightarrow \mu^+\mu^-$ decay. Indeed, Figure 11 shows that there is a relatively mild suppression of the Drell-Yan and $t\bar{t}$ initiated events in the region just above $M(l^+l^-) = 2p_T(\text{min})$; the latter largely survive, even at low $M(l^+l^-)$, since, on average, the lepton acquires considerable p_T from the large mass of the t quark.

Secondly, consider the effects of the isolation cut, which requires the lepton track to have minimal accompanying hadronic debris [13,14,31-33]. Large-mass lepton pairs from $c\bar{c}$ and $b\bar{b}$ production have a characteristic property. They are generated by c, $\bar{c}$ or b, $\bar{b}$ quarks of large p_T (which are approximately back-to-back in the transverse

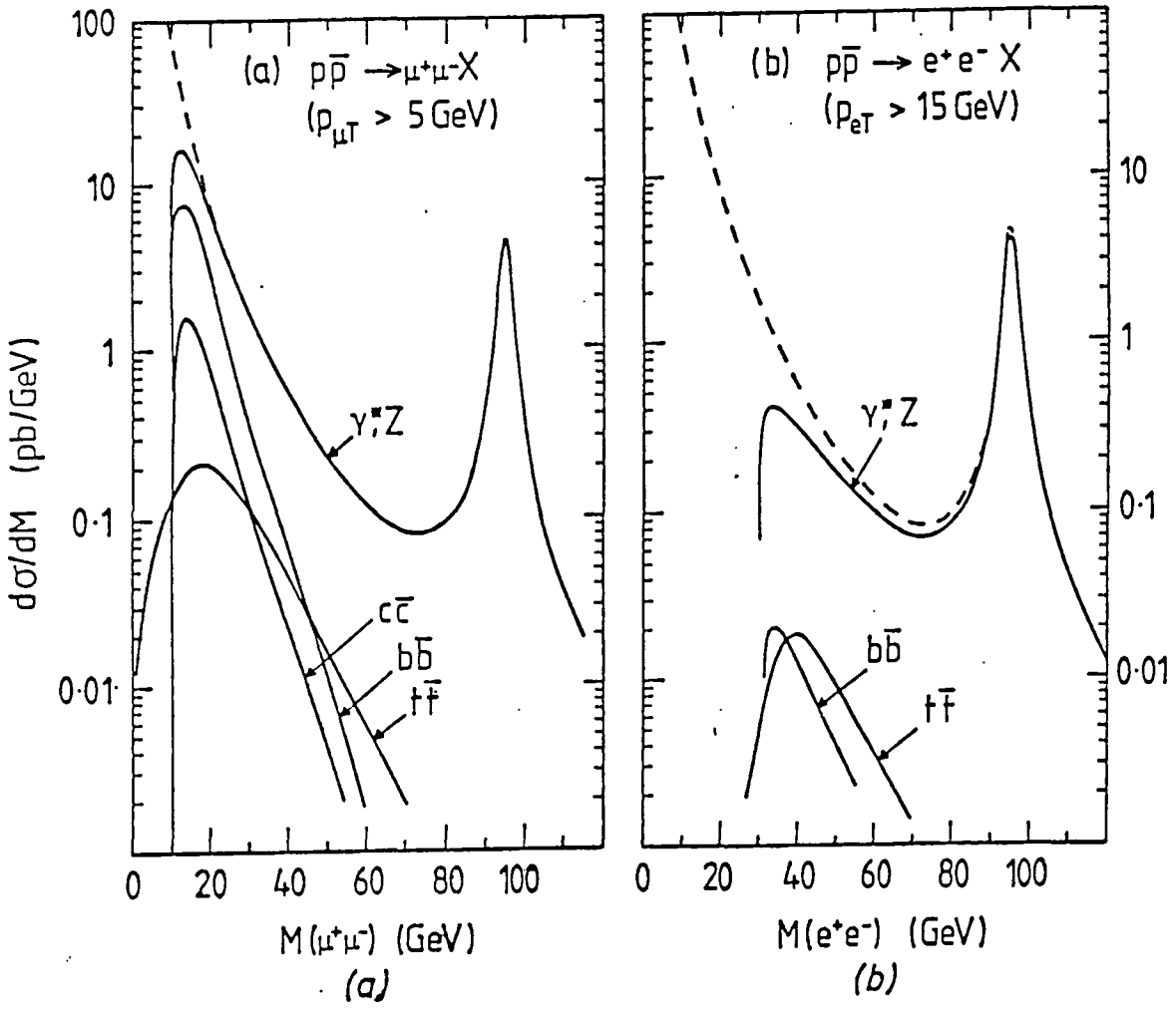

Figure 11

As Fig. 10 but with lepton p_T cuts imposed: (a) $p_{\mu T}$ > 5GeV, (b) p_{eT} > 15GeV. The dashed line shows the Drell-Yan curve of Fig. 10 for comparison.

plane) and so the leptons will be accompanied by the collimated hadronic decay products of the final state quark in the decay $Q \rightarrow q l \nu$. Typical isolation criteria [13] require an identified decay lepton to have summed hadronic p_T of less than 3GeV in a cone 30^o about the lepton direction. Such cuts are effective in suppressing $b\bar{b}$ and $c\bar{c}$ events whilst leaving the $t\bar{t}$ signal relatively unaffected. However, even if the probability, P, for one c(b) quark semileptonic decay to survive the isolation cut were sizeable, the probability that both the c and $\bar{c}$(b and $\bar{b}$) decays do so is P^2. Isolation cuts should therefore be very effective in rejecting $c\bar{c}(b\bar{b})$ initiated dilepton events while having small effect on Drell-Yan or $t\bar{t}$ events.

These cuts leave a data sample containing Drell-Yan events with a small $t\bar{t}$ background. The Drell-Yan events, unlike typical $t\bar{t}$ decays, should give decay leptons that are back-to-back in the transverse plane and which have little or no accompanying jet activity. Hence the seemingly large background shown in Figure 10 can easily eliminated to leave a clean Drell-Yan data sample. The isolation cut on the leptons should not affect the signal, although the minimum momentum cut does (see Figure 11) and should be taken into account when confronting theory with experiment.

Finally consider the $t\bar{t}$ initiated lepton pair events. Because of the large mass and relatively low p_T of the t quark these events will largely survive the lepton isolation cuts, which should eliminate lepton pairs of $c\bar{c}$ and $b\bar{b}$ origin. The b quark jet in the $t \rightarrow b\bar{l}\nu$ decay will accidentally overlap the lepton in comparatively few events, and the chance for this to occur simultaneously for the $\bar{t} \rightarrow \bar{b}$ $l\bar{\nu}$ decay will be even smaller, and so at least one decay lepton will

usually appear 'isolated'. Lepton pair events with $M(l^+l^-) \sim 20$GeV is therefore an ideal place to search for, or eventually confirm, the t quark. The Drell-Yan contribution may be removed by rejecting events in which the decay leptons are approximately back-to-back in the transverse plane, and which do not have considerable jet activity.

The Drell-Yan contamination of the $t\bar{t}$ events is, of course, totally absent from $e^+\mu^-$ and $e^-\mu^+$ events. In Figure 12 the expected $e\mu$ invariant mass distribution (with minimum p_T cuts imposed) is shown for various values of the top quark mass. Assuming a semi-leptonic branching ratio of 10% for each channel, the cross sections of lepton pairs from $t\bar{t}$ production calculated from $q\bar{q}$ and gg fusion at $\sqrt{s}$ = 540GeV are,

m_t(GeV)	$\sigma(t\bar{t})$	$\sigma(t\bar{t} \rightarrow \mu\bar{\mu})$	$\sigma(t\bar{t} \rightarrow \mu\bar{e})$
25	5.0 nb	200 pb	30 pb
35	0.8 nb	50 pb	20 pb
45	0.3 nb	20 pb	10 pb.

The lepton p_T cuts, $p_{\mu T} > 5$GeV and $p_{eT} > 15$GeV have been imposed. These numbers represent upper limits for the signal since a fraction of the $t\bar{t}$ events will be removed by particular isolation cuts [13] employed to eliminate $c\bar{c}$ and $b\bar{b}$ events. However, the dilution of the signal will be much less severe than in Ref. 13 since here isolation criteria can be imposed on two decay leptons.

To summarise, although the $t\bar{t}$ event rate is somewhat less than that of the $W \rightarrow t\bar{b}$ event rate [13], the $e\mu$ signal has however the

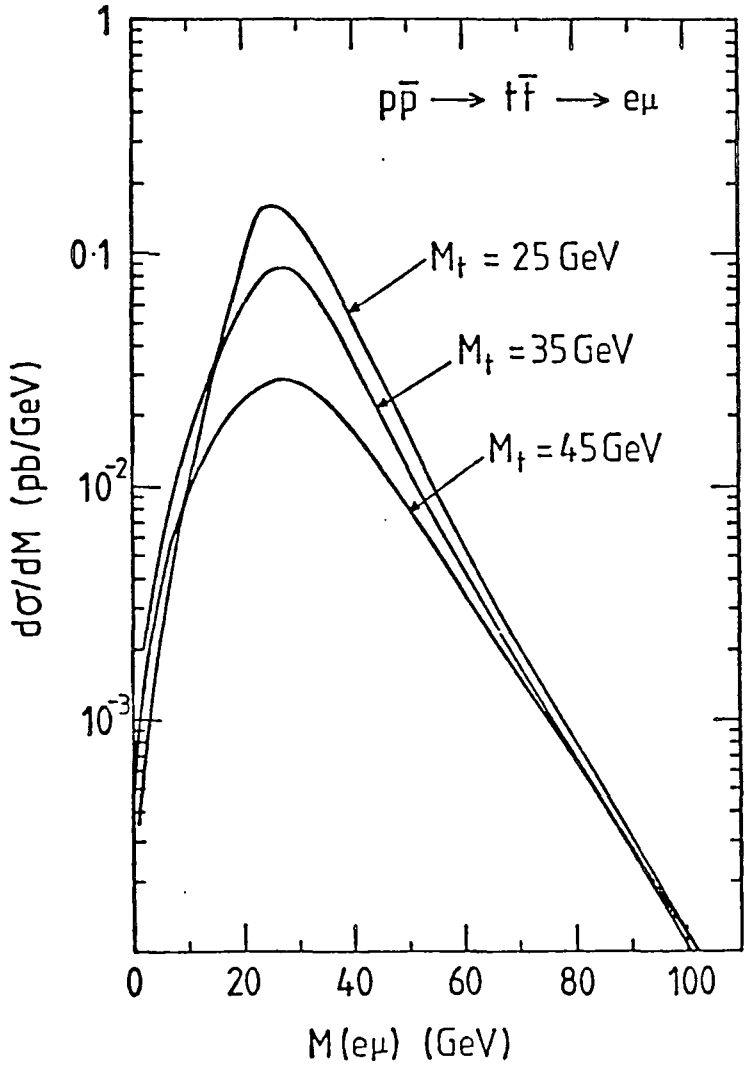

Figure 12

The eμ invariant mass distribution originating from $t\bar{t}$ production and decay for m_t = 25, 35 and 45GeV. The transverse momentum cuts p_{eT} > 15GeV and $p_{\mu T}$ > 5GeV are imposed.

advantage of being particularly clean and distinctive. The experimental measurement involves only charged letons and there are no competing backgrounds. Thus very few eμ events are required to establish a signal. Secondly, although the Drell-Yan process appears swamped by leptons from heavy quark decays, (see Fig. 10), the heavy quark background can be simply eliminated by cuts on the lepton p_T and the Drell-Yan process examined.

3.5 J/ψ as a trigger in $p\bar{p}$ collisions.

Since the top quark is expected to have a large mass, the charged leptons from its semileptonic decays are likely to have a large p_T and are likely to be isolated. This fact has resulted in many proposals for top quark signatures involving charged leptons [16-21]. The situation for the b and c quarks is somewhat different. Although the predicted $c\bar{c}$ and $b\bar{b}$ event rates in $p\bar{p}$ collisions are large, the decay leptons occur dominantly at relatively low transverse momenta and within jets where lepton identification problems are severe. The main difficulty is that one of the copiously produced hadrons is misidentified as a decay lepton or that the muon from $\pi \rightarrow \mu\nu$ decay, for example, is mistaken with that from a heavy quark decay $Q \rightarrow q\mu\nu$. Furthermore, it is very difficult to distinguish between the c and b parentage of a decay lepton.

In contrast, "hidden" flavour J/ψ or Υ production, with subsequent decay,

$$J/\psi \text{ or } \Upsilon \rightarrow \mu^+\mu^- \qquad (3.23)$$

has an extremely distinctive signature. In particular ψ production at

high p_T ($p_{\psi T} \geq$ 5GeV) is important because,

(a) the experimental signature should be especially free of background, and

(b) in this region the estimates of the ψ yield based on QCD perturbation theory should be reliable.

There are two questions to be answered. First, is the inclusive ψ yield large enough to provide a practical event rate? Second, what type of physics can be explored via the observation of ψ's? As shown in Fig. 13, there are two possible mechanisms for ψ production at large p_T. The ψ can be produced (A) via $c\bar{c}$ bound state production, such as,

$$gg \rightarrow \psi g, \tag{3.24}$$

$$q\bar{q},\ gg \rightarrow \chi_J g \text{ with } \chi_J \rightarrow \psi\gamma, \tag{3.25}$$

or (B) via $b\bar{b}$ production, $b \rightarrow B$ fragmentation, followed by $B \rightarrow \psi X$ decay [34]. A measurement from CLEO [4] of the branching ratio for $B \rightarrow \psi X$ gives $(1.0 \pm 0.5)\%$, in reasonable agreement with theoretical predictions based on the process circled in Fig. 13 with gluon corrections [35-37].

Consider first ψ production from mechanism (A). Baier and Ruckl [38,39] have studied in detail the production of charmonium states ($\psi, \chi_J, \ldots$) directly from the light quark and gluon constituents of the colliding hadrons. ψ production at large p_T is now thought to be well understood, and is calculated from the dominant $O(\alpha_s^3)$ QCD diagrams shown in Fig. 13. The differential cross sections for these processes are given in Ref. 37 and are rather complicated. The combination of the charmed quarks into the charmonium state is represented by a non-perturbative wavefunction which forces the quarks into the correct

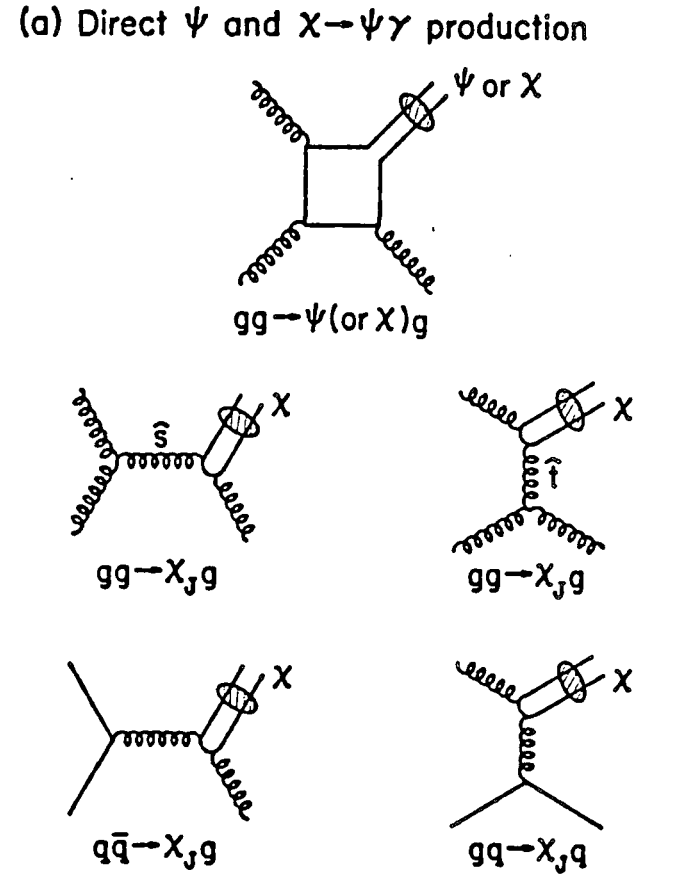

Figure 13

ψ production (A) via ($c\bar{c}$) bound-state production and $\chi \to \psi\gamma$, and (B) via $b\bar{b}$ production and $B \to \psi X$. χ_J denotes the ^3P_J (with J = 0, 1, 2) charmonium states. Diagrams with permutations of the gluon lines are implied. The $O(\alpha_s^2)$ subproceses $gg \to \chi_{0,2} \to \psi\gamma$ only produce ψ's of low transverse momentum and are omitted. For mechanism (B) only one of the possible $q\bar{q}$, $gg \to b\bar{b}$ QCD subprocesses is shown.

spin configuration for that particular state. The radial wavefunction at the origin (and it's derivatives) are typically calculated using non-relativistic potential models. In this calculation the radial wave functions are taken to be [39].

$$R_s^2 = 0.49 \qquad R_p'^2/m_\chi^2 = 0.009.$$

The $\chi \to \psi\gamma$ branching ratios are taken to be,

$$Br(\chi_0 \to \psi\gamma) = 0.027$$

$$Br(\chi_1 \to \psi\gamma) = 0.315$$

$$Br(\chi_2 \to \psi\gamma) = 0.154.$$

The resulting $p_{\psi T}$ distributions are shown in Fig. 14 for $p\bar{p}$ collisions at $\sqrt{s}$ = 540GeV. Table 1 lists the total cross sections, integrated over the region $p_{\psi T} > 5$GeV, for a range of collider energies.

Table 1

Contributions to the J/ψ production cross section (in nb), integrated over the range $p_T > 5$GeV/c, from the mechanisms (A) and (B) of Fig. 13, for $p\bar{p}$ collisions at energy $\sqrt{s}$.

		via $\chi_J \to \psi\gamma$			via $b\bar{b}$	total σ(nb)
$\sqrt{s}$(GeV)	$gg \to \psi g$	χ_0	χ_1	χ_2	$B \to \psi X$	$p_T > 5$GeV/c
540	0.31	0.13	3.9	1.1	11.2	16.6
620	0.42	0.15	4.9	1.4	17.3	24.2
2000	1.1	0.3	13.2	3.0	164.0	181.6

For these processes (at these energies and this p_T range) the dominant contribution comes from the subprocess,

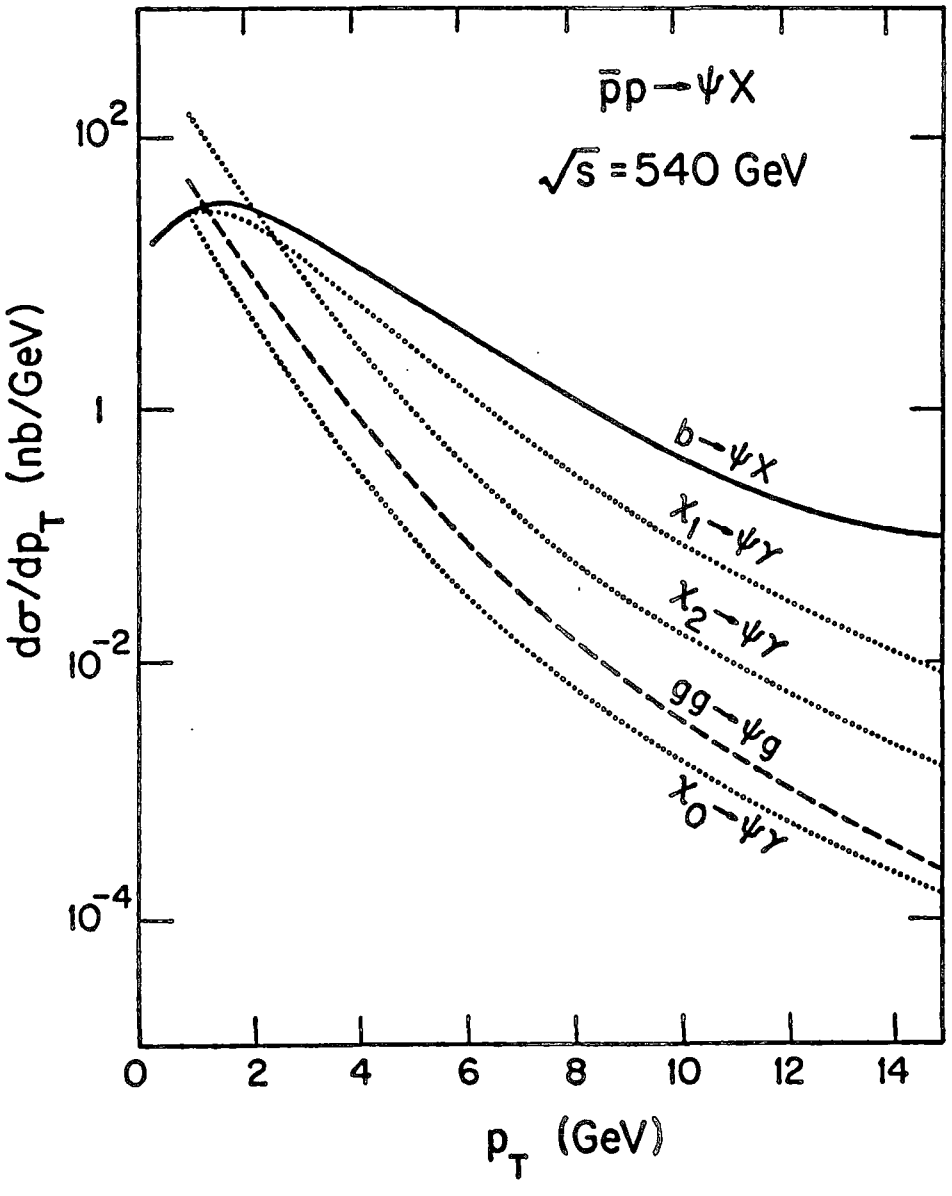

Figure 14

The ψ transverse momentum distributions arising from mechanisms (A) and (B) in $p\bar{p}$ collisions at $\sqrt{s}$ = 540GeV.

$$gg \rightarrow \chi_1 g \text{ with } \chi_1 \rightarrow \psi\gamma. \qquad (3.26)$$

The relative contribution to χ production from the subprocess $q\bar{q} \rightarrow \chi g$ is negligible while that of the subprocess $qg \rightarrow \chi q$ and $\bar{q}g \rightarrow \chi\bar{q}$ is small. This implies an approximate equality for the χ production rate at $\bar{p}p$ and pp colliders. At small s/M_χ^2 the contribution from the direct channel $gg \rightarrow \psi g$ is also comparably small. The main uncertainties in the prediction of the ψ yield are therefore related to the choice of structure function and to the value of α_s. The quoted yield correspond to using the non-scaling parton densities of Gluck et al. [25] and α_s given by (3.13) with $N_F = 4$, $\Lambda = 0.3$ GeV and $Q^2 = M_\chi^2$ or M_ψ^2. At $\sqrt{s} = 540$GeV, the uncertainty introduced by the gluon distribution is O(10) for the ψ yield from the subprocess $gg \rightarrow (\psi,\chi)g$. The highest rate can be achieved by taking scaling glue,

$$xg(x) = 3(1-x)^5; \qquad (3.27)$$

the non-scaling distribution used [25] predicts a rate approximately ten times smaller than that from scaling glue.

To calculate the ψ yield from mechanism (B) a QCD fusion calculation based on $q\bar{q}$, $gg \rightarrow b\bar{b}$ with $b \rightarrow B$ fragmentation folded in as in section 3.2. For the $B \rightarrow \psi X$ decay, a wide range of two- and three-body (isotropic) decays are considered with $X = K$, K^*, $K\pi$, $K^*\pi$,... taking $K^*(890)$ and $K^*(1430)$. The uncertainties are found to be well encompassed by the allowed range $(1.0 \pm 0.5)\%$ of the $B \rightarrow \psi X$ branching ratio [4]. The $b\bar{b}$ production cross section at $\sqrt{s} = 540$GeV is taken to be $6.6\mu b$ and the branching ratio for $B \rightarrow \psi X$ to be 1%. The resulting $p_{\psi T}$ is compared with that for the "direct" and χ-initiated production mechanisms in Fig. 14 and in Table 1.

Even though $\sigma(c\bar{c}) >> \sigma(b\bar{b})$ (see section 3.2) mechanism (B) gives the larger yield, particularly at larger $p_{\psi T}$ values. This is well illustrated by Figure 15 which shows the number of $\psi \rightarrow \mu^+\mu^-$ events expected for an integrated $\bar{p}p$ collider luminosity of $100nb^{-1}$ at $\sqrt{s}$ = 540GeV. The event rate is such that the proposed $\psi \rightarrow \mu\mu$ signal should be clearly visible in the $\bar{p}p$ collider data. It should thus allow a clean measurement of $b\bar{b}$ production. Besides their flatter $p_{\psi T}$ dependence, the $b\bar{b}$ initiated events may also be distinguished by the fact that the ψ will be accompanied by a strange particle and recoils against a b jet. On the other hand, in the χ-initiated events (mechanism (A)) the ψ should be predominantly accompanied by a relatively slow photon and recoil against a gluon jet.

It might be thought that the corresponding $\Upsilon \rightarrow \mu\mu$ signal could be exploited to measure $t\bar{t}$ production. Unfortunately, the expected $T \rightarrow \Upsilon X$ branching ratio is much too small. Interestingly, at $\sqrt{s}$ = 540GeV, the dominant QCD subprocess turns out to be the "direct" reaction $gg \rightarrow \Upsilon g$.

In summary, the value of measuring ψ production at the $p\bar{p}$ collider should be stressed. In understanding heavy flavour production in high energy $p\bar{p}$ collisions it is important to find a way to unravel b quark production from the much larger c quark background. It may then be possible to identify hadrons containing b quarks e.g., B, Λ_b. The $\psi \rightarrow \mu^+\mu^-$ signal (together with a strange particle) offers a unique "clean" trigger for b quark events. Hence it may provide a quantitative test of the QCD fusion mechanism for $b\bar{b}$ production (and perhaps may reveal whether or not there is a large diffractive $b\bar{b}$ component). The second major mechanism for producing ψ's, which has a

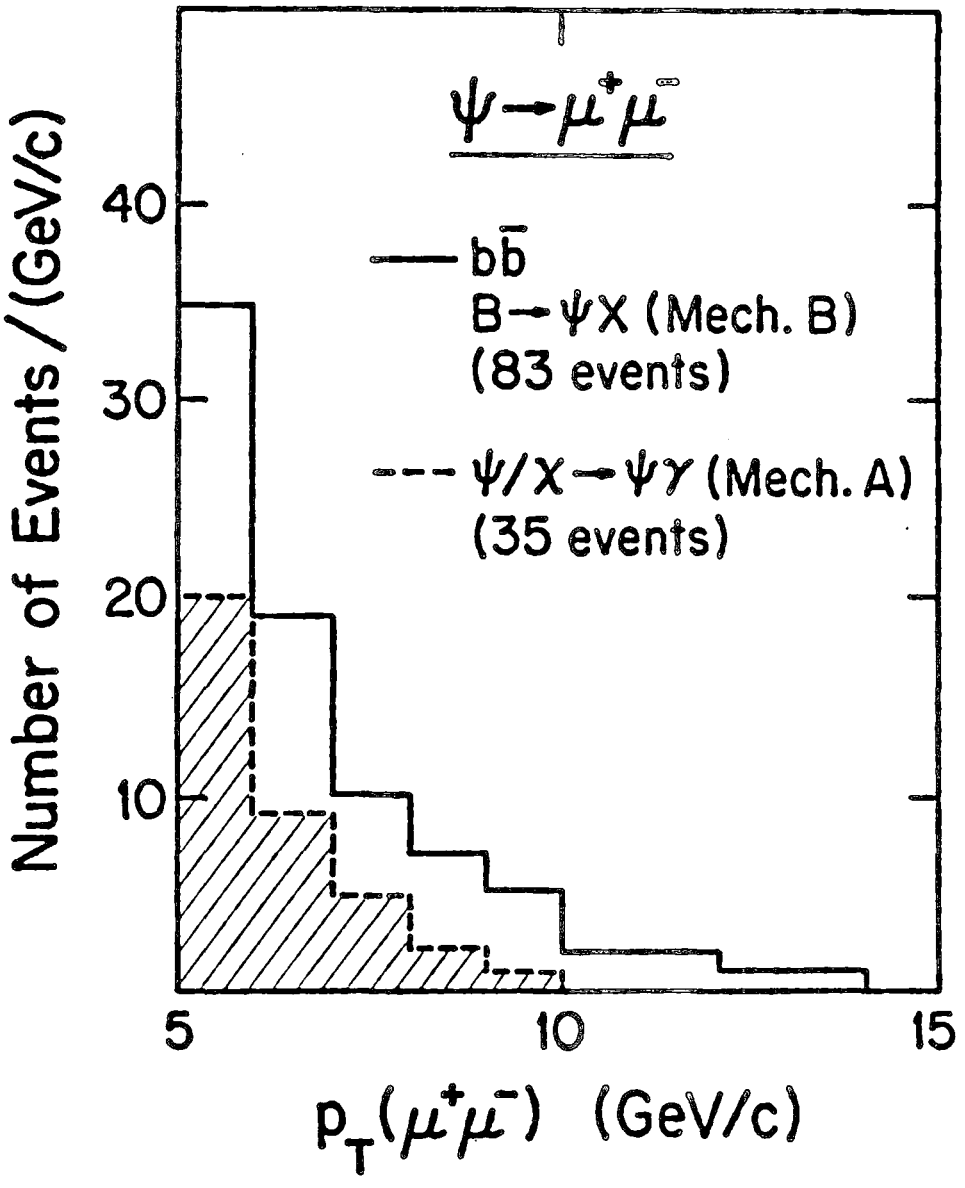

Figure 15

The number of events per (GeV/c) interval of $p_{\psi T} = P_T(\mu^+\mu^-)$ expected in $p\bar{p}$ collisions at $\sqrt{s}$ = 540GeV for an integrated luminosity of $100nb^{-1}$ arising from the mechanisms (A) and (B) of Fig. 14. The $\psi \rightarrow \mu^+\mu^-$ branching ratio is taken to be 7.4%.

steeper $p_{\psi T}$ dependence, is $gg \rightarrow \chi g$ with $\chi \rightarrow \psi\gamma$. Isolation of such events may give a valuable direct measurement of the gluon distribution of the proton at collider energies.

3.6 Summary

To avoid the difficulties of recognising a jet or missing p_T vector in heavy flavour semileptonic decays, a dilepton trigger is proposed. This has the experimental advantage that the possibility of misidentifying both leptons is small. Only unlike sign dileptons have been examined (like sign leptons from $W \rightarrow t\bar{b} \rightarrow l^+l^+X$ [16], B^0-$\bar{B}^0$ mixing [22] or even supersymmetric channels [40] have been discussed elsewhere) for $M(l^+l^-) < M_Z$. By making various cuts on the lepton transverse momentum or dilepton transverse momentum, the following processes may be isolated and examined,

(a) Drell-Yan lepton pair production,

(b) $t\bar{t}$ production,

(c) $b\bar{b}$ production,

(d) $gg \rightarrow \chi g$.

These four processes may yield a wealth of information about the details of heavy flavour production in high energy proton-antiproton collisions.

References

(1) G.Arnison et al., UA1 collab., Phys. Lett. 122B, 103, (1983)

M.Banner et al., UA2 collab., Phys. Lett. 122B, 476, (1983)

(2) G.Arnison et al., UA1 collab., Phys. Lett. 126B, 398, (1983)
P.Bagnaia et al., UA2 collab., Phys. Lett. 129B, 130, (1983)

(3) H.Schneider, Proc. Int. Europhysics Conference on High Energy Physics, Brighton, (1983)

(4) CLEO collab., presented by S.Stone, Proc. 1983 Int. Symp. on Lepton and Photon Interactions at High Energies, Cornell, (1983)

(5) G.Hanson, B.Gittelman and K.Berkelman, Proc. XXth International Conf., Madison, (1981)

(6) D.M.Scott, Proc. Conf. on Antiproton-proton Collider Physics, Madison, (1981)

(7) V.Barger, A.D.Martin and R.J.N.Phillips, Phys. Lett. 125B, 339, (1983); ibid 125B, 343, (1983); Phys. Rev. D28, 145, (1983)

(8) R.M.Godbole, S.Pakvasa and D.P.Roy, Phys. Rev. Lett. 50, 1539, (1983)

(9) G.Ballochi and R.Odorico, Phys. Lett. 136B, 126, (1984)

(10) F.Halzen and D.M.Scott, Phys. Lett. 129B, 341, (1983)

(11) L.Seghal and P.M.Zerwas, Nucl. Phys. B234, 61, (1984)

(12) K.Hagiwara and W.F.Long, Phys. Lett. 132B, 202, (1983)

(13) V.Barger, H.Baer, A.D.Martin and R.J.N.Phillips, Phys. Rev. D29, 887, (1984)

(14) R.Odorico, Nucl. Phys. B242, 297, (1984)

(15) G.Arnison et al., UA1 collab., Phys. Lett. 147B, 493, (1984)

(16) M.Abud, R.Gatto and C.A.Savoy, Phys. Lett. 79B, 435, (1978)

(17) S.Pakvasa, M.Dechantsreiter, F.Halzen and D.M.Scott, Phys. Rev. D20, 2862, (1978)

(18) L.L.Chau, W-Y.Keung and S.C.C.Ting, Phys. Rev. D24, 2862, (1981)

(19) F.E.Paige, Proc. Conf. on Antiproton-proton Collider Physics,

Madison, (1981)

(20) R.Kinnunen, CERN report EP/84-19 (1984)

(21) V.Barger and R.J.N.Phillips, Phys. Rev. D30, 1890, (1984)

(22) V.Barger and R.J.N.Phillips, Phys. Lett. 143B, 259, (1984)

(23) S.D.Drell and T.M.Yan, Ann. Phys. N.Y. 66, 578, (1971)

(24) B.L.Combridge, Nucl. Phys. B151, 429, (1979)

(25) M.Gluck, E.Hoffmann and E.Reya, Z.Phys. 13C, 119, (1982)

(26) J.F.Owens and E.Reya, Phys. Rev. D17, 3003, (1978)

(27) G.Altarelli, R.K.Ellis, M.Greco and G.Martinelli, Nucl. Phys. B246, 12, (1984)

(28) C.Peterson, D.Schlatter, I.Schmitt and P.M.Zerwas, Phys. Rev. D27, 105, (1983)

(29) P.Aurenche, R.Kinnunen and K.Mursula, Annecy report LAPP-TH-106 (1984)

(30) F.Halzen, A.D.Martin and D.M.Scott, Phys. Lett. 112B, 160, (1982)

(31) I.Schmitt, L.M.Seghal,H.Tholl and P.M.Zerwas, Phys. Lett. 139B, 99, (1984)

(32) S.Aronson, F.E.Paige and S.Protopopescu, reported Gordon Conference (1983), unpublished

(33) V.Barger, H.Baer, K.Hagiwara, A.D.Martin and R.J.N.Phillips, Phys. Rev. D29, 1923, (1984)

(34) H.Fritzsch, Phys. Lett. 86B, 164, (1979); ibid 86B, 343, (1979)

(35) M.B.Wise, Phys. Lett. 89B, 229, (1980)

(36) T.A.DeGrand and D.Toussaint, Phys. Lett. 89B, 256, (1980)

(37) J.H.Kuhn and R.Ruckl, Phys. Lett. 135B, 477, (1984)

(38) R.Baier and R.Ruckl, Phys. Lett. 102B, 364, (1981); Nucl. Phys. B208, 381, (1982)

(39) R.Baier and R.Ruckl, Z.Phys. C19, 251, (1983)

(40) V.Barger, W-Y.Keung and R.J.N.Phillips, Wisconsin report MAD/PH/219 (1984)

Chapter Four

Heavy lepton signatures from W decay

4.1 Introduction

One of the crucial questions in particle physics is whether or not there are more than three generations of quarks and leptons. In particular, does the sequence (e, ν_e), (μ, ν_μ), (τ, ν_τ) continue to a fourth weak isospin doublet (L, ν_L)? Similarly is there a fourth generation of quarks (a,v)? The new energy range opened up by the CERN $p\bar{p}$ collider offers the exciting possibility of searching for the fourth generation.

Experiments at e^+e^- colliders offer the possibility of finding new particles via the electromagnetic pair production process,

$$e^+e^- \rightarrow \gamma^* \rightarrow f\bar{f}, \qquad (4.1)$$

where f represents the new fermion of charge Q. Current mass bounds on new leptons and quarks are [1],

Q	m(GeV)
1	>20.6
2/3	>20.7
1/3	>19.8

Neglecting threshold effects, the mass of the fermion produced by this mechanism is upper-bounded by half the centre of mass energy. The LEP experiment will offer the possibility of pair producing particles with mass roughly less than half the Z mass towards the end of the decade.

The discovery of the W bosons [2,3] at the CERN $p\bar{p}$ collider opens up the possibility of searching for new charged heavy leptons [4-6] with mass less than the W mass if the partner neutrino, ν_L, is light. The non-diagonal nature of the W current means that a higher limit (than that likely to be found in e^+e^- experiments in the near future) on the heavy lepton mass may be found. Suppose that such a new sequential heavy lepton L exists, then it will be produced via the decay,

$$W \rightarrow L\bar{\nu}_L, \tag{4.2}$$

with the subsequent leptonic or hadronic decay of the L,

$$L \rightarrow e\bar{\nu}_e\nu_L,\ \mu\bar{\nu}_\mu\nu_L, \tag{4.3}$$

$$L \rightarrow d\bar{u}\nu_L,\ s\bar{c}\nu_L. \tag{4.4}$$

These two decay modes will be studied in turn.

First note that the leptonic decay chain,

$$W \rightarrow L\bar{\nu} \rightarrow e\bar{\nu}_e\nu_L\bar{\nu}_L, \tag{4.5}$$

has the same signature as the direct and initiated decay modes of the W,

$$W \rightarrow e\bar{\nu}_e, \tag{4.6}$$

$$W \rightarrow \tau\bar{\nu}_\tau \rightarrow e\bar{\nu}_e\nu_\tau\bar{\nu}_\tau, \tag{4.7}$$

namely an isolated energetic electron accompanied by missing transverse momentum. Section 4.2 contains a quantitative study of the properties of the electron spectrum from the leptonic decays of the W

bosons, including careful considerations of the background.

Section 4.3 considers ways of optimising the L leptonic decay signal with respect to the background. There is an additional background contribution from heavy quark production in which one of the quarks decays semileptonically and the hadronic debris from the quark decays is not seen. For example,

$$p\bar{p} \rightarrow b\bar{b}X \text{ with } b \rightarrow ce\bar{\nu}_e. \qquad (4.8)$$

The contribution from such heavy quark background processes can be suppressed by requiring that the lepton is not accompanied by hadrons. That is an isolation cut of the type mentioned in Chapter 3 may be imposed.

The hadronic decay signature of the L is,

$$W \rightarrow L\bar{\nu}_L \rightarrow q'\bar{q}\nu_L\bar{\nu}_L. \qquad (4.9)$$

Since there is an energetic primary neutrino ($\bar{\nu}_L$) and only one secondary neutrino (ν_L), these events are characterised by high missing transverse momentum balanced by two hadronic jets. Assuming that mass effects of the final state particles are negligible, the total hadronic decay rate should be six times that of a leptonic decay rate due to colour. In section 4.4 the heavy lepton hadronic decay signature is described and the background contributions from heavy quark production with subsequent semileptonic decays in which the charged leptons are not identified, eliminated. Background contributions also arise from τ-initiated events,

$$W \rightarrow \tau\bar{\nu}_\tau \rightarrow q'\bar{q}\nu_\tau\bar{\nu}_\tau. \qquad (4.10)$$

In section 4.5 this background contribution is investigated and a method of optimising the L hadronic decay signal is proposed. Section 4.6 contains a description of the hadronic decay signal after the UA1

jet algorithm has been applied. The results of these studies are summarised in section 4.7.

Before proceeding a note of caution is in order, in many supersymmetric theories the gauge fermions are lighter than the gauge bosons - this allows the decay chains,

$$W \rightarrow \tilde{W}\tilde{\gamma} \rightarrow e\bar{\nu}_e\tilde{\gamma}\tilde{\gamma}, \qquad (4.11)$$

$$W \rightarrow \tilde{W}\tilde{\gamma} \rightarrow q'\bar{q}\tilde{\gamma}\tilde{\gamma}. \qquad (4.12)$$

The photino ($\tilde{\gamma}$) and the wino ($\tilde{W}$) are the spin-1/2 partners of the γ and W respectively. The photino is usually considered to be extremely feebly interacting thus escaping the detector and giving rise to missing transverse momentum. Dicus et al. [7] have pointed out that for a wino mass of less than 50GeV it may not be possible to distinguish between a wino and a heavy lepton on the basis of the electron spectra.

4.2 Leptonic decays of W bosons

The matrix element for the leptonic decay of the W (see Fig. 1) is,

$$-iM = \epsilon_\mu(W)\bar{u}(L^-)(-i(g/\sqrt{2})\gamma^\mu((1 - \gamma_5)/2))v(\bar{\nu}_L). \qquad (4.13)$$

Squaring the amplitude and performing the spin summation yields,

$$\Sigma|M|^2 = g^2\ (L.\bar{\nu}_L + 2(L.W\ W.\bar{\nu}_L)/M_W^2), \qquad (4.14)$$

where, as usual, particle labels represent their four-momenta. The averaging over the initial spin of the W gives an additional factor of 1/3. Taking the neutrino mass to be negligible and performing the

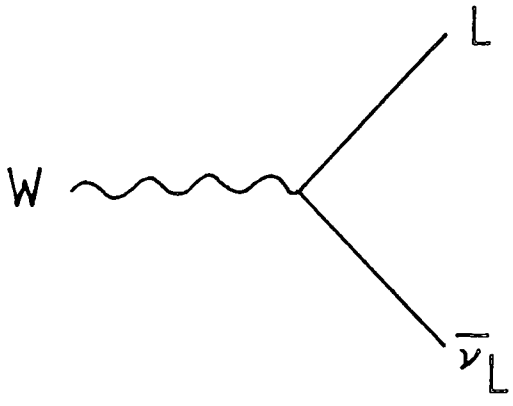

Figure 1

The vertex for W decay to $L\nu_L$.

phase space integration gives the W leptonic partial width to be,

$$\Gamma(W^- \rightarrow L^-\bar{\nu}_L) = G_F M_W^3/(6\sqrt{2})\ (1 - x)^2(1 + x/2) \qquad (4.15)$$

where $x = m_L^2/M_W^2$ [4]. Figure 2 shows the $W \rightarrow L\nu$ branching ratio as a function of x.

The leptonic branching ratio for the L is 1/9 which takes account of the $d\bar{u}\nu_L$, $s\bar{c}\nu_L$ and three primary leptonic decay channels. The W partial widths for the leptonic decay modes are in the ratio,

$$(W \rightarrow e):(W \rightarrow \tau \rightarrow e):(W \rightarrow L \rightarrow e) = 1 : 0.17 : 1/9(1 - x)^2(1 + x/2) \qquad (4.16)$$

where the observed $\tau \rightarrow e\nu\nu$ branching ratio of 17% has been used. For example, for a heavy lepton of mass 40GeV,

$$(W \rightarrow e) : (W \rightarrow L \rightarrow e) = 1 : 0.07.$$

Decay chains such as $W \rightarrow L \rightarrow \tau \rightarrow e$ and $W \rightarrow L \rightarrow c \rightarrow e$ which are smaller contributions and which give very soft electrons are ignored. Although the discussion is framed in terms of electrons, the results apply equally well to muons. Indeed, since transverse momenta of around 10GeV/c are emphasised, the observation of muons may be favoured from an experimental viewpoint.

The e^+ spectrum for $p\bar{p} \rightarrow W^+X \rightarrow e^+X$ resulting from the three decay modes of the W is calculated using the quark structure functions of Owens and Reya [8] evolved in Q^2 up to $Q^2 = \hat{s}$, where $\sqrt{\hat{s}}$ is the centre of mass energy of the annihilating u and $\bar{d}$ quarks. The structure functions of Gluck, Hoffmann and Reya [9] lead to essentially identical results. An SU(4)-symmetric sea is assumed, ie. u,d,s and c sea-quark contributions are included. This gives the largest estimate for the $W \rightarrow e$ background. In fact there is little difference in the predictions of an SU(2)-symmetric u,d sea and the

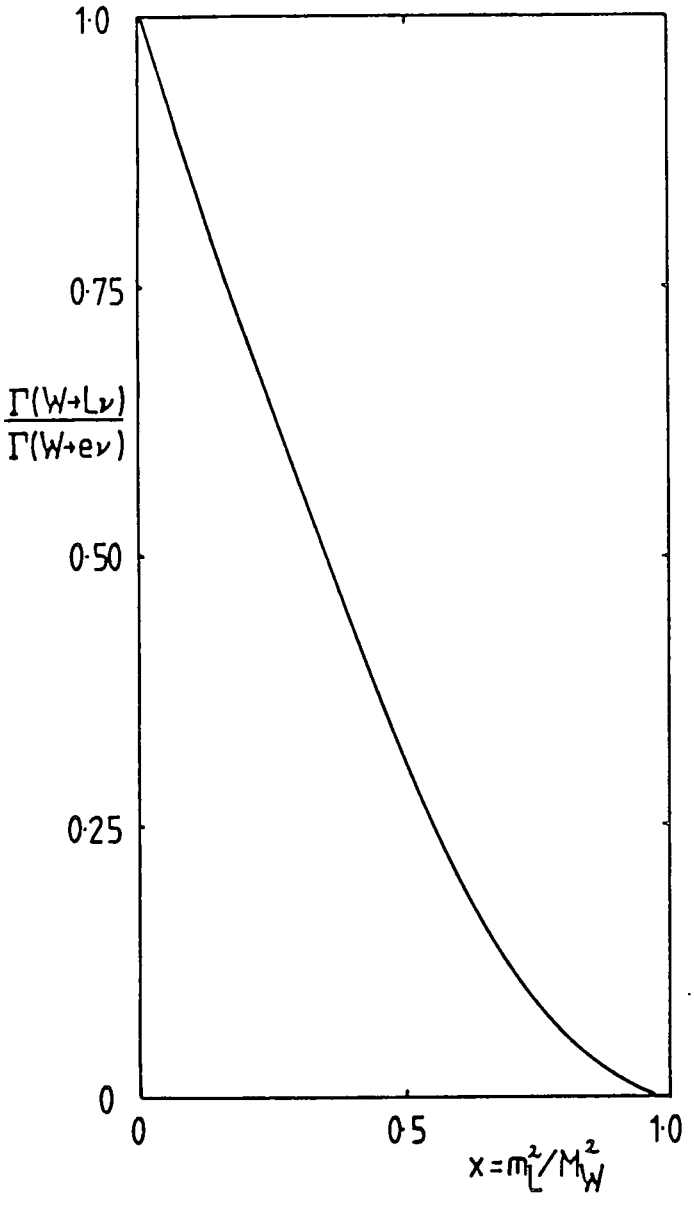

Figure 2

The width for the decay $W \rightarrow Lv_L$ as a function of x (= m_L^2/M_W^2) as given by 4.15, where $G_F M_W^3/(6\sqrt{2})$ has been replaced by $\Gamma(W \rightarrow ev)$.

SU(4) case, except for the height of the sharp peak at backward angles (i.e., with the e^+ antiparallel to the $\bar{p}$ direction) due to sea-sea interactions.

The amplitude for the sequential decay process of Fig. 3,

$$u\bar{d} \rightarrow W \rightarrow L^+\nu_L \rightarrow e^+\nu_e\bar{\nu}_L\nu_L, \tag{4.17}$$

is of the form,

$$\begin{aligned} -iM = {} & \bar{v}(d)(-i(g/\sqrt{2})\gamma_\mu((1-\gamma_5)/2)u(u)(-i(g^{\mu\nu} - W^\mu W^\nu/M_W^2))\bar{u}(\nu_L) \\ & x\ (-i(g/\sqrt{2})\gamma_\nu((1-\gamma_5)/2)(i(\not{p}_L + m_L)(-i(g/\sqrt{2})\gamma_\alpha((1-\gamma_5/2)v(\bar{\nu}_L)) \\ & x\ (-i(g^{\alpha\beta} - W_2^\alpha W_2^\beta/M_W^2))(\bar{u})(\nu_e)(-i(g/\sqrt{2})\gamma_\beta((1-\gamma_5)/2)v(e)) \\ & /\ ((\hat{s} - M_W^2) + i\Gamma_W M_W)(p_L^2 - m_L^2 + im_L\Gamma_L)(s_{ev} - M_W^2) \end{aligned} \tag{4.18}$$

where $\hat{s}$ and s_{ev} are shown in Fig. 3. Squaring and summing over the spin states reduces this to,

$$\begin{aligned} \Sigma|M|^2 = {} & 16g^4\ (\nu_L.d\ L.u\ L.\nu_e\ \bar{\nu}_L.e - m_L^2/2\ \nu_L.d\ \nu_e.u\ \bar{\nu}_L.e) \\ & x\ (\pi/m_L\Gamma_L)\delta(p_L^2 - m_L^2) \\ & /\ ((\hat{s} - M_W^2)^2 + \Gamma_W^2 M_W^2)(s_{ev} - M_W^2)^2) \end{aligned} \tag{4.19}$$

where the particle labels are used to denote their four-momenta and where the narrow width approximation is used for the L lepton, that is, it is assumed on-mass-shell. The initial spin and colour averages give an additional factor of 1/4x1/3. Quark and electron masses are neglected.

Rather surprisingly, the on-mass-shell approximation $\hat{s} = M_W^2$

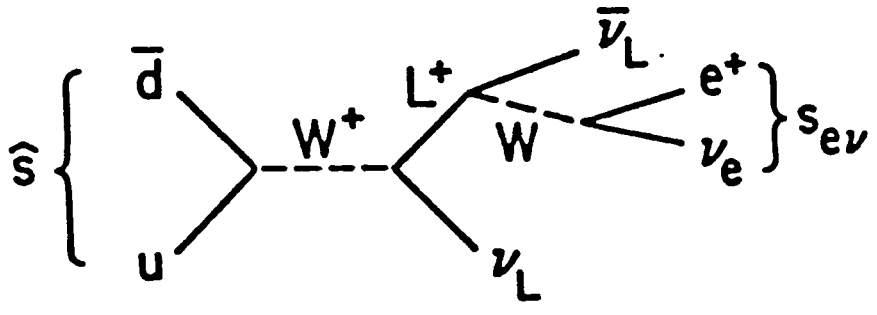

Figure 3

The production and leptonic decay of an L^+ heavy lepton.

cannot be made in calculating the $W \to e\nu$ background. It will be seen that off-mass-shell effects of the W are important in kinematic regions where the cross section is small. The cross section is multiplied by a QCD motivated enhancement factor K = 2 in the fusion subprocess.

The resulting cross section for $W^{\pm}$ production with $e^{\pm}$ decay, summed over both charges, is,

$$\sigma(p\bar{p} \to W^{\pm} \to e^{\pm}\nu) = 0.56 \text{ nb}, \tag{4.20}$$

which is in accord with the observed cross section [10],

$$\sigma_{UA1}(p\bar{p} \to W^{\pm} \to e^{\pm}\nu) = 0.53 \pm 0.08 \pm 0.09 \text{ nb}. \tag{4.21}$$

Figure 4 shows the predicted electron distributions transverse to the beam direction for $p\bar{p}$ collisions at $\sqrt{s}$ = 540GeV, with relative normalisations given by (4.16). Smearing due to the transverse motion of the produced W is included according to the approximate formula,

$$\frac{d\sigma}{dp_T^2} \propto \exp(-25p_T/\sqrt{\hat{s}}) \tag{4.22}$$

which reproduces calculations [11] of the W transverse momentum distribution arising from multiple gluon emission from the incident partons. The electron p_T distributions arising from heavy lepton decay are shown for various values of the lepton mass m_L. The curve for the direct $W \to e\nu$ decay continues to rise with increasing p_T to the Jacobian peak at $p_T \sim M_W/2$ which played a valuable role in the discovery of the W boson [2,3].

It can be seen from Fig. 4 that the L-initiated p_{eT} distribution is masked by the direct $W \to e$ and $W \to \tau \to e$ decays. However a study of the angular distributions of the emitted positrons allows these competing processes to be unravelled. The angular distributions

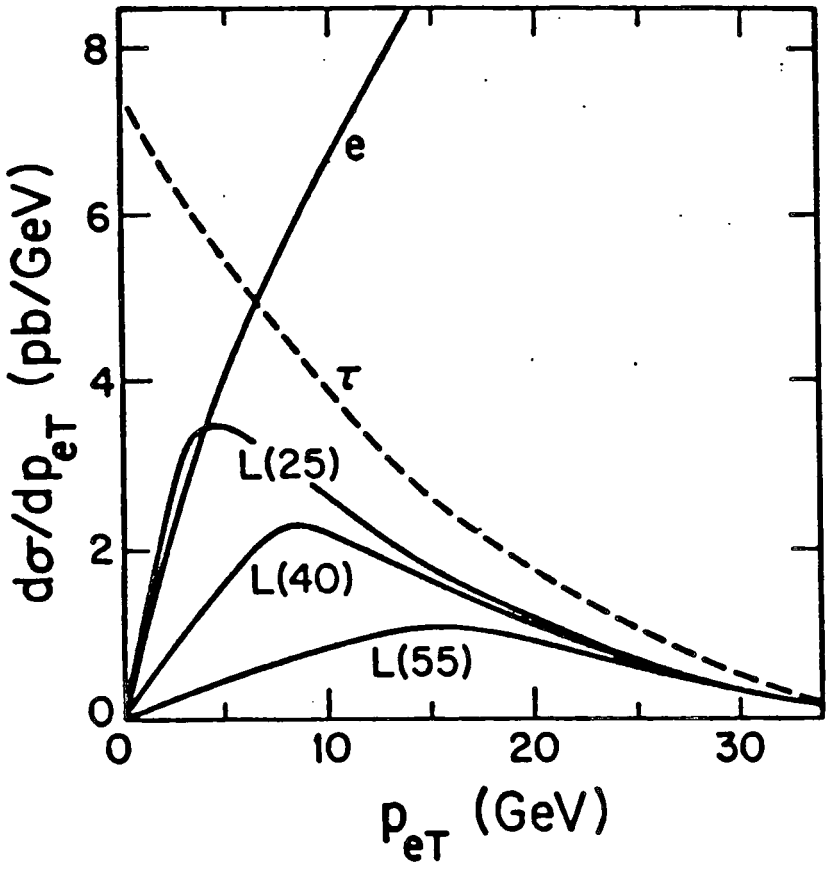

Figure 4

The momentum distribution of the electon transverse to the beam axis for $p\bar{p} \rightarrow W \rightarrow e\nu$ at $\sqrt{s}$ = 540GeV. The curves labelled e, τ and L correspond to the decay modes 4.6, 4.7 and 4.5 respectively. The distributions labelled $L(m_L)$ correspond to assuming three different values of the heavy lepton mass: m_L = 25, 40 and 55GeV. The e curve corresponding to the direct $W \rightarrow e\nu$ decay rises to a Jacobian peak at $p_{eT} \sim M_W/2$: M_W is taken to be 81GeV.

are shown in Fig. 5 for various intervals of p_{eT} , for each decay of the W boson. Inspection of the results shows that to optimise the L signal-to-background ratio the interval $8 < p_{eT} < 16GeV$ should be chosen. The comparison is made in Fig. 6. However, before embarking on a detailed discussion of the leptonic decay signature of the L and of other possible background contributions, it is useful to gain some physical insight into the distributions displayed in Fig. 5.

The angular distribution of an L^+ lepton, produced by the process $\bar{d}u \rightarrow L^+\nu_L$, has the characteristic asymmetrical form,

$$\bar{d}.\nu_L \; L^+.u \propto (1 + \cos\hat{\theta})(1 + v_L\cos\hat{\theta}), \qquad (4.23)$$

where v_L is the L^+ velocity in units of c and $\hat{\theta}$ is the angle between the L^+ and the incident $\bar{d}$ quark in the $\bar{d}u$ centre of mass frame. In the limit $m_L^2/M_W^2 \rightarrow 0$ (that is $v_L \rightarrow 1$) the L^+ lepton is produced in a state of positive helicity, whereas for a massive lepton both positive and negative helicity states are populated.

Fig. 5 shows that for the direct $W^+ \rightarrow e^+\nu$ decay the e^+ angular distribution is sharply peaked in the forward direction, relative to the $\bar{p}$ beam, for the relevant range 8 to 16GeV in p_{eT}, essentially arising from (4.23) boosted from the $\bar{d}u$ to the $\bar{p}p$ centre of mass frame. Only as p_{eT} approaches $M_W/2$ (i.e. $\theta \rightarrow \pi/2$) does the asymmetry disappear; in this case the e^+ angular distribution reflects the longitudinal momentum distribution of the W. On the other hand, for the τ^+ and the L^+, the sequential decays weaken the e^+ asymmetry, the more so the more massive the L^+.

An interesting feature of the angular distributions shown in Fig. 5(a) is that the off-mass-shell effects of the W must be included (ie. the full Breit-Wigner form must be taken for the propagator) to obtain

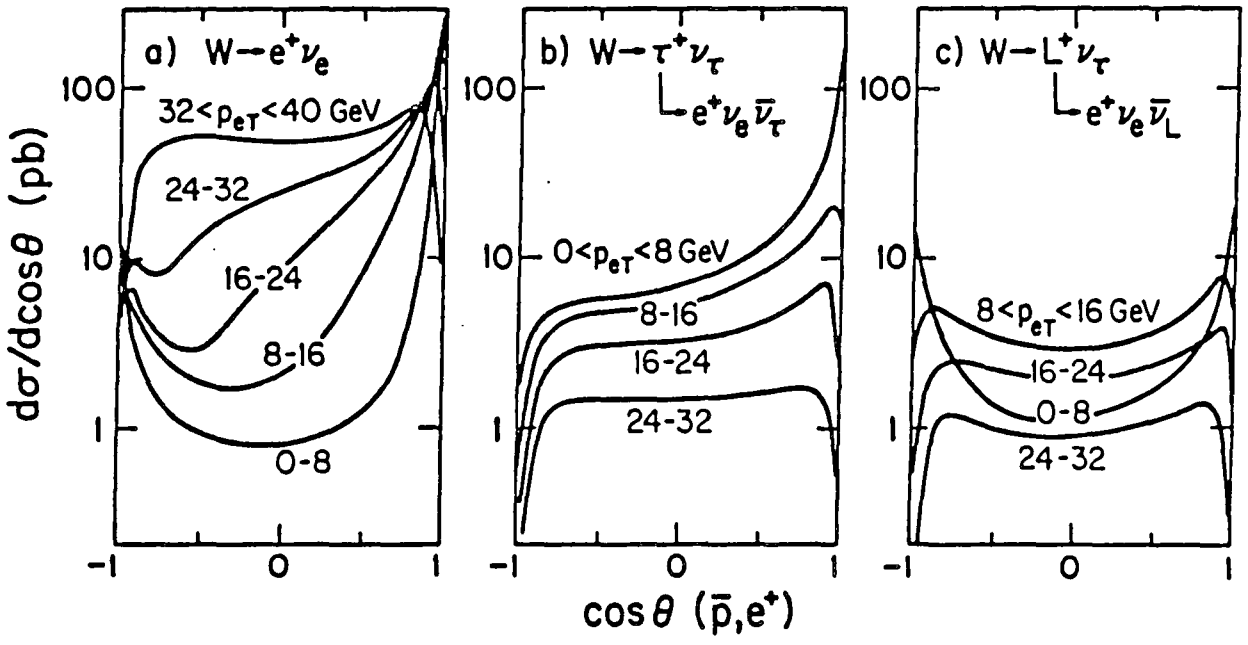

Figure 5

The angular distributions of the emitted e^+ for various intervals of p_{eT} for (a) $p\bar{p} \rightarrow W^+ \rightarrow e^+$, (b) $p\bar{p} \rightarrow W^+ \rightarrow \tau^+ \rightarrow e^+$, and (c) $p\bar{p} \rightarrow W^+ \rightarrow L^+ \rightarrow e^+$ with m_L = 40GeV. θ is the angle between the incident $\bar{p}$ and the outgoing e^+ in the $p\bar{p}$ centre-of-mass frame, $\sqrt{s}$ = 540GeV.

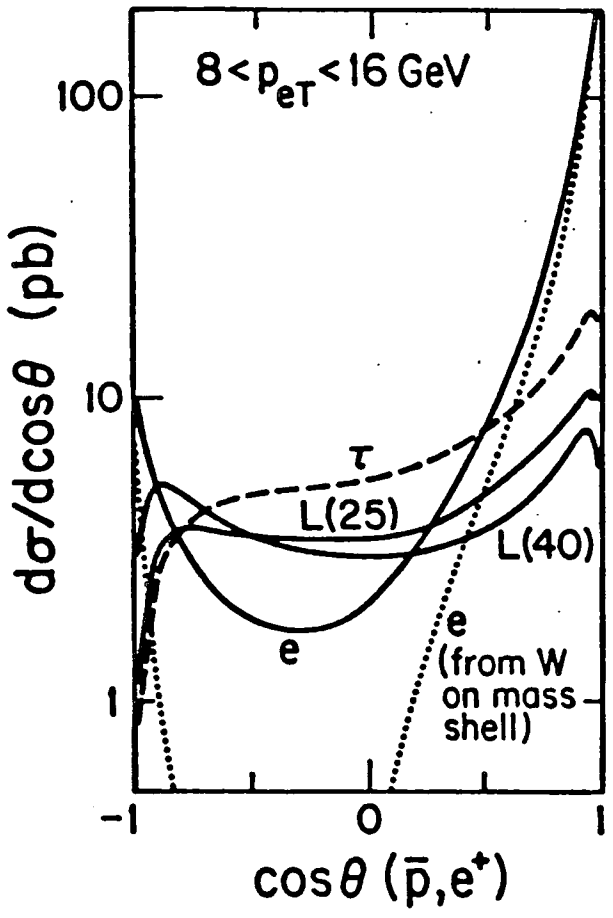

Figure 6

The e^+ angular distribution for the interval $8 < p_{eT} < 16$GeV, for m_L = 25 and 40GeV. The dotted curve represents the W-mass-shell approximation to the $W \rightarrow e\nu$ cross section.

the correct structure of the dips in the cross section which occur for $p_{eT} < 25GeV$. The contributions in the dip region arise from virtual W's at $\bar{d}u$ centre of mass energies $\sqrt{\hat{s}}$ far below M_W. Even though the far off-mass-shell amplitude is suppressed, there is a compensating feature in that the main contribution to the angular distribution occurs for $p_{eT} = \sqrt{\hat{s}}/2$ and has no dip. This is well illustrated in Fig. 6 by comparing the true distribution with the direct $W^+ \rightarrow e^+\nu$ distribution calculated assuming the W remains on shell, $\sqrt{\hat{s}} = M_W$ (the dashed curve).

Finally, note that the e^- angular distributions from W^- decay can be obtained from the $W^+ \rightarrow e^+$ angular distributions by the replacement $e^-(\theta) = e^+(\pi - \theta)$.

4.3 Leptonic-decay signature of the L

In Fig. 6 the p_{eT} interval of the emitted e^+ is selected to maximise the L signal relative to the backgrounds from W decay. This "window" in p_{eT} is the best that can be done; for larger values of p_{eT} the direct $W \rightarrow e\nu$ decay dominates, and for smaller p_{eT} there are many more τ-initiated events. The optimum interval corresponds to $-0.9 < \cos\theta < 0.2$ where is the angle between the emitted e^+ and the incident $\bar{p}$ beam. The cross sections for $W^+ \rightarrow e^+$, $W^+ \rightarrow \tau^+ \rightarrow e^+$ and $W^+ \rightarrow L^+ \rightarrow e^+$ for given (p_{eT}, $\cos\theta$) intervals of the outgoing e^+, and different mass values m_L (in GeV) of the heavy lepton are tabulated below for L production and decay in $p\bar{p}$ collisions at $\sqrt{s} = 540GeV$. The normalisation corresponds to $\sigma(\bar{p}p \rightarrow W^{\pm} \rightarrow e^{\pm}\nu) = 0.56$ nb.

Interval		Partial cross section σ(pb)					
							L
p_{eT}(GeV)	cosθ	e	τ	m_L(GeV)	= 25	40	55
(8,16)	(-0.9,0.2)	2.5	5.3		3.7	3.8	1.8
(10,15)	(-0.9,0.2)	1.5	3.3		2.2	2.3	1.2
(15,20)	(-0.8,-0.2)	1.0	1.4		0.9	0.9	0.8

For example, in the optimum p_{eT} and cosθ range and a heavy lepton mass m_L = 40GeV, the signal is,

$$\Delta\sigma(L) = 3.8 \text{ pb}, \tag{4.24}$$

whereas summing the contributions in this range from $W \rightarrow e$ and $W \rightarrow \tau$ gives,

$$\Delta\sigma(\text{background}) = 7.8 \text{ pb}. \tag{4.25}$$

If this were the whole story then it may be possible to identify such a signal from a heavy lepton, with mass up to about 50GeV, at the 3 standard deviation level, with the order of 1000 $W \rightarrow e$ events.

Unfortunately for the leptonic decay mode there is another background to consider. Namely, e^+'s emitted from the semi-leptonic decays of heavy quarks (c,b,t) which are pair produced in $\bar{p}p$ collisions; in particular consider,

$$p\bar{p} \rightarrow \bar{b}bX \text{ with } \bar{b} \rightarrow \bar{c}e^+\nu. \tag{4.26}$$

A QCD fusion calculation (as in Chapter 3) gives a contribution in the $8 < p_{eT} < 16$GeV interval some two orders of magnitude above the L signal. The calculation corresponds to a total $\bar{b}b$ production cross section of 6.6μb (taking m_b = 4.6GeV), assumes a semi-leptonic branching ratio of 10% and includes a b quark fragmentation function

(as described in Chapter 3). However, the $\bar{b}b$ background falls off rapidly with increasing p_{eT} as shown in Fig. 7.

In events of $\bar{b}b$ or $\bar{c}c$ origin the decay electron is accompanied by hadronic debris from the quark cascade decays (for example the $\bar{b}$ decay of (4.26)). Therefore, this background may be suppressed by imposing cuts on the accompanying hadronic p_T. For example, the heavy quark background can be essentially eliminated by rejecting events with hadronic $\Sigma|p_{Ti}| > 10GeV$, where the sum is over all hadrons, i, within a cone of 30^o of the electrom momentum. Note, of course, that there is a contribution to hadronic p_T within this cone from the proton/antiproton fragments. The minimum bias value for hadronic p_T must be subtracted from the event $\Sigma|p_{Ti}|$ in applying this cut.

To summarise, the detection of a heavy lepton L via the observation of its decay electron would require a $\bar{p}p$ collider experiment with an integrated luminosity in excess of $1000nb^{-1}$ for $\sqrt{s} = 540GeV$. If the mass is in the range $20 < m_L < 50GeV$, then in the optimum interval of p_{eT} and θ, the $W \rightarrow L \rightarrow e$ signal is at the 3-4pb level. Even then the background due to $W \rightarrow \tau \rightarrow e$ and $W \rightarrow e$ exceeds the signal. The advent of microvertex detectors in the CERN collider experiments may improve the situation by directly observing the production and decay vertices in τ-initiated and $\bar{b}b$ events, thus identifying background events.

4.4 Hadronic-decay signature of the L

A more promising signature for the L is via its hadronic decay modes. The relevant decay chains are,

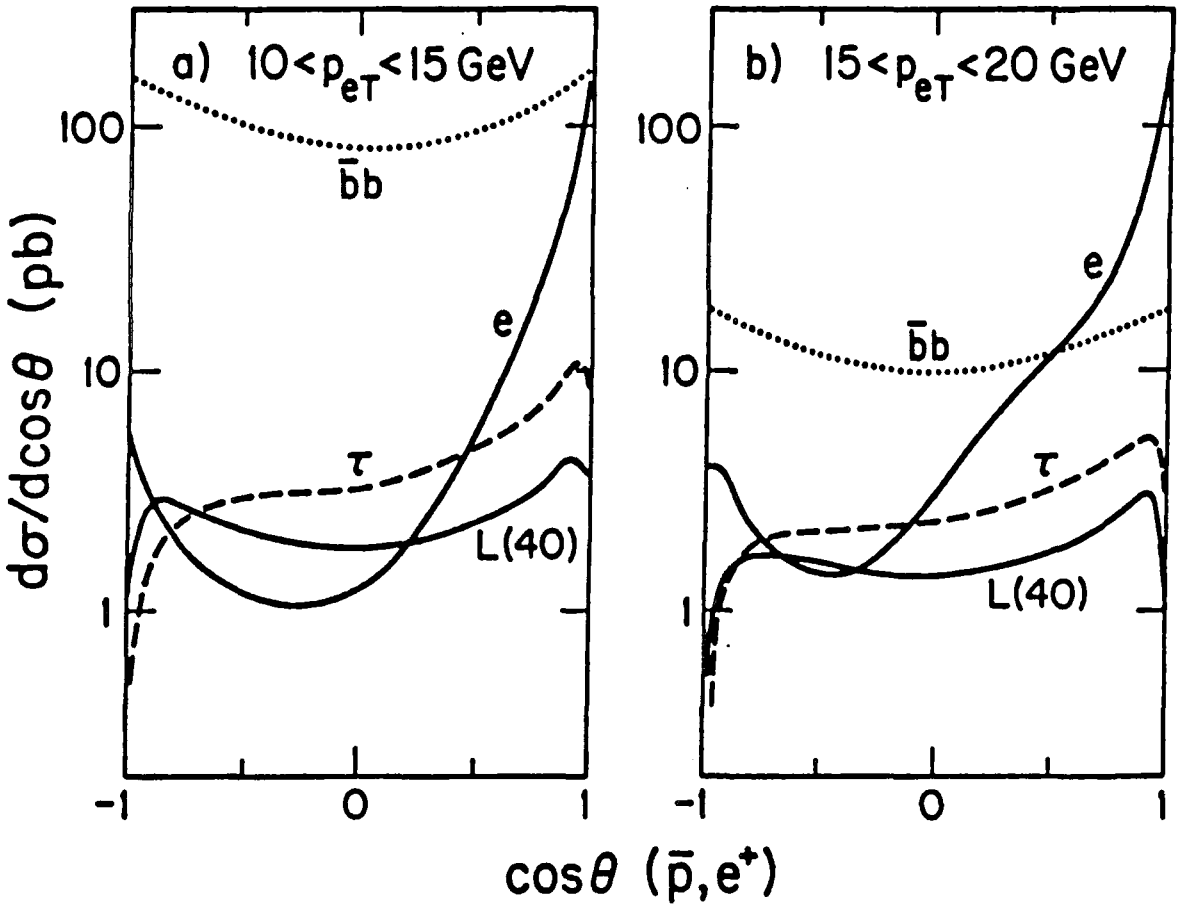

Figure 7

The e^+ angular distribution for the interval a heavy lepton of mass 40GeV, together with background contributions, for two intervals of p_{eT}. The effect of the $\Sigma p_T < 10$GeV cut on the debris reduces the $b\bar{b}$ and $c\bar{c}$ backgrounds to well below the signal.

$$W \rightarrow Lv_L \rightarrow u\bar{d}\bar{\nu}_L\nu_L \text{ or } c\bar{s}\bar{\nu}_L\nu_L. \qquad (4.27)$$

Colour enhances these decays relative to the leptonic decay modes so that the sum of the rates is ,

$$\Gamma(W \rightarrow Lv \rightarrow q'\bar{q}\bar{\nu}\nu) = 6/9\ (1 - x)^2(1 + x/2)\Gamma(W \rightarrow e\nu) \qquad (4.28)$$

where $x = m_L^2/M_W^2$ (cf. (4.15)). Since there is only one secondary decay neutrino to soften the energetic primary decay neutrino, these events have, on average, much larger missing transverse momentum than in the leptonic decays of the L. There is therefore a distinctive signature for the L of high missing transverse momentum (due to $\bar{\nu}_L\nu_L$) balanced by two (possibly overlapping) quark jets. The calculation of the rate proceeds in a similar way to that for the leptonic decay with the amplitude for

$$\bar{d}u \rightarrow W^+ \rightarrow L^+\nu_L \rightarrow (q'\bar{q}\bar{\nu}_L)\nu_L \qquad (4.29)$$

given by (4.18) with $e^+ \rightarrow \bar{q}$ and $\nu_L \rightarrow q'$. Folding in the structure functions gives the missing transverse momentum distribution for a lepton of mass m_L = 40GeV in $p\bar{p}$ collisions at $\sqrt{s}$ = 540GeV shown in Fig. 8.

Fig. 8 also shows possible background contributions from sequential decay,

$$W \rightarrow \tau\nu_\tau \rightarrow u\bar{d}\bar{\nu}_\tau\nu_\tau, \qquad (4.30)$$

and from heavy quark production with one or more subsequent semileptonic decays in which the charged leptons are not identified. Heavy quark production is estimated from the lowest order QCD processes $q\bar{q}$, $gg \rightarrow \bar{c}c$, $\bar{b}b$, $\bar{t}t$ and the hadronic W^+ decay modes $W^+ \rightarrow t\bar{b}$ with a top quark mass of 35GeV . As in Chapter 3, Owens-Reya scale violating structure functions are used, evolved in Q^2 up to $Q^2 = \hat{s}$.

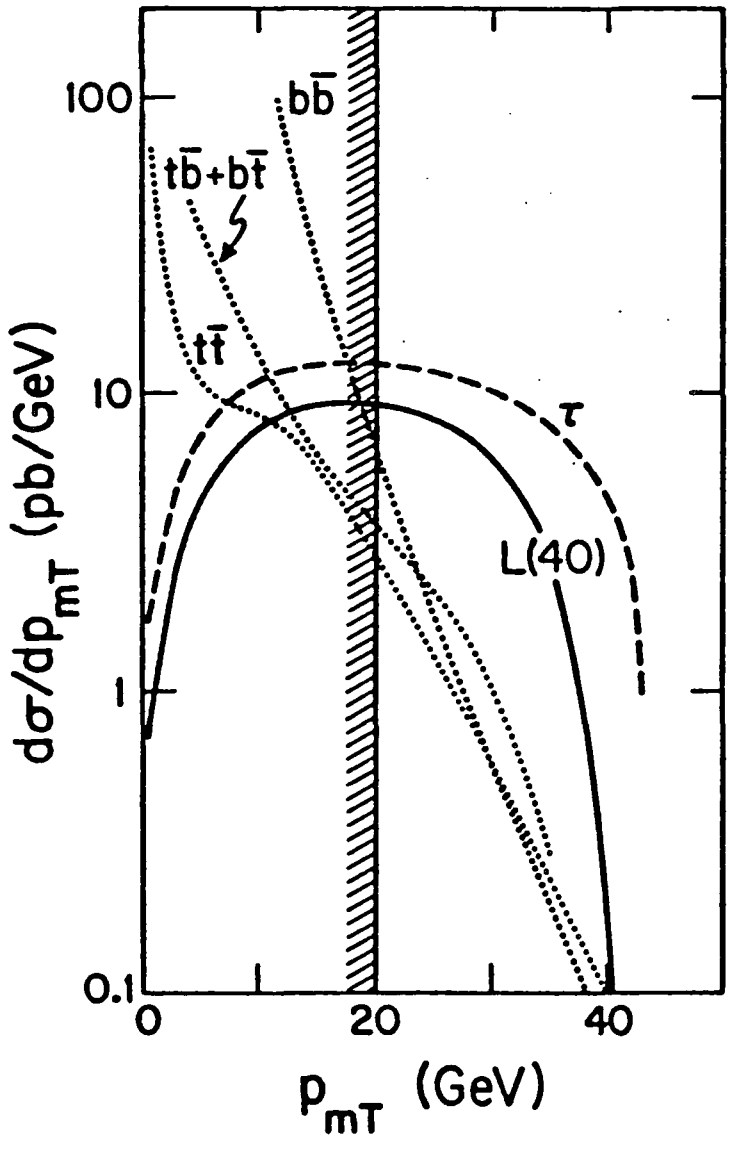

Figure 8

The missing transverse momentum (p_{mT}) distributions arising from $W \rightarrow L\nu_L \rightarrow q\bar{q}'\bar{\nu}_L\nu_L$ with m_L = 40GeV and L = τ, taking $\tau \rightarrow$ hadrons branching fraction of 65%. The normalisation is as Fig. 4 with $W^{\pm}$-initiated events summed over. The curves which decrease with increasing p_{mT} are background contributions coming from the production and subsequent decay of heavy quarks.

The semileptonic branching fractions are taken to be 10% for each mode, except for τ decay where the observed fraction of 17% is taken. The heavy quarks are assumed to fragment into heavy spinless or unpolarised hadrons of the same masses as the quarks. The fragmentation function used is that of Peterson et al. [12] with ε_c = 0.15 and $\varepsilon_b = \varepsilon_c(m_c^2/m_b^2)$ which is consistent with c and b production data. The heavy quarks are allowed to undergo a full cascade decay and the charged leptons from the semileptonic decays are assumed to be seen if, and only if, $p_{eT} > 10$GeV and $p_{\mu T} > 4$GeV.

Figure 8 shows that the missing p_T distribution (p_{mT}) arising from heavy-quark production falls off rapidly with increasing p_{mT} as expected, and that for $p_{mT} > 20$GeV/c the distribution comes mainly from L- and τ-initiated events. Fortunately experimental measurements of p_{mT} are most reliable for large p_{mT} which the L signal dominates.

For the heavy lepton L, the primary neutrino is unaccompanied by other decay debris, whereas for the heavy quark events the decay neutrino (or neutrinos) will be accompanied by decay debris. Consider the b quark semileptonic decay $b \rightarrow c e \nu$. Straightforward kinematics leads to the relation,

$$\sin^2(\theta_{T\nu i}/2) \leq (m_b^2 - m_c^2)/(4p_{\nu T}p_{iT}), \qquad (4.31)$$

where i = e or c and $\theta_{T\nu i}$ is the angle in the transverse plane between the "neutrino" and the decay fragment i. In the case $m_b = 4.6$GeV, m_c = 1.5GeV, $p_{\nu T} > 20$GeV, $p_{cT} > 8$GeV one has,

$$\theta_{T\nu c} < 20^{\circ}. \qquad (4.32)$$

This means that the heavy quark background can be suppressed by requiring that the missing transverse momentum vector is isolated. A

requirement that $\Sigma|p_{iT}| < 5GeV$, where the sum is over all the fragments, i, within 20^{o} of the missing p_T vector in the transverse plane, reduces the heavy quark background by over an order of magnitude.

The two quark jets (denoted JJ) emerging from the decay of the L are quite energetic and should be recognisable. For the results presented here both jets are required to have $p_T(jet) > 8GeV$ in addition to the $p_{mT} > 20GeV$ and the isolation cuts. Fig. 9 shows the prediction for the opening angle between the two jets (θ_{JJ}) for different masses of the parent lepton at $\sqrt{s} = 540GeV$. The invariant mass (M_{JJ}) distribution of the two jets is shown in Fig. 10, again for various lepton masses. This M_{JJ} distribution offers an excellent signature for $W \rightarrow L\nu_L$ events. The upper end-point of the distribution is a good indicator of the mass of the new lepton. Moreover, the total event rate is healthy. After imposing all the cuts the integrated heavy lepton signal relative to the total $W^{\pm} \rightarrow e^{\pm}\nu$ rate is

$$\frac{\sigma(W^{\pm} \rightarrow L\bar{\nu} \rightarrow JJ\nu\bar{\nu})}{\sigma(W^{\pm} \rightarrow e^{\pm}\nu)} = \begin{array}{l} 0.13 \text{ for } m_L = 25GeV \\ 0.11 \text{ for } m_L = 40GeV \\ 0.08 \text{ for } m_L = 50GeV \\ 0.05 \text{ for } m_L = 60GeV. \end{array} \qquad (4.33)$$

It can be seen that for a wide range of the lepton mass, the event rate is about 10% of the W signal.

4.5 The W -> tau background

It remains to eliminate the background from τ-initiated events,

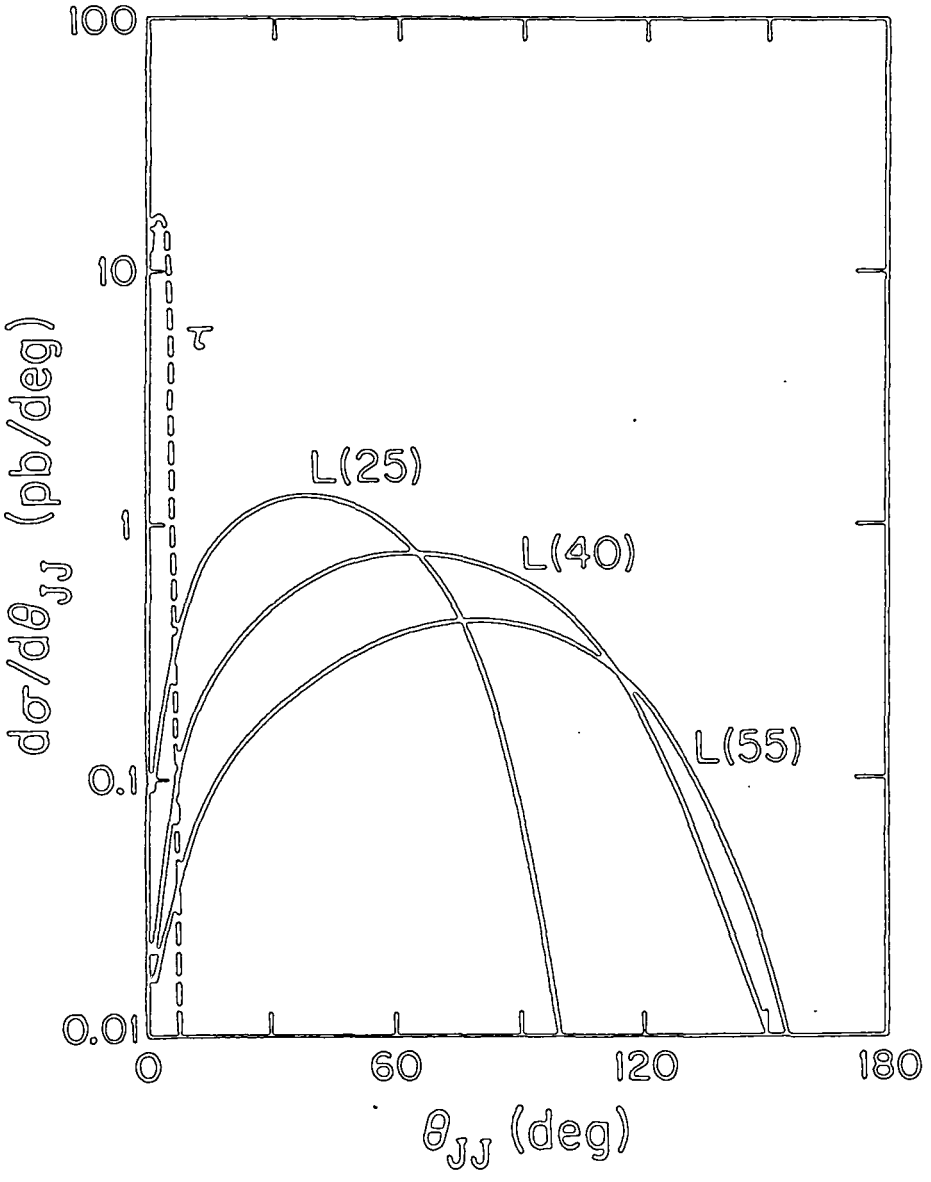

Figure 9

The distribution of the opening angle θ_{JJ}, as seen in the $p\bar{p}$ frame, between the two jets emerging from $p\bar{p} \rightarrow W \rightarrow Lv_L \rightarrow JJ\bar{v}_L v_L$, for different masses of the heavy lepton L. The cuts to remove the background events have been imposed.

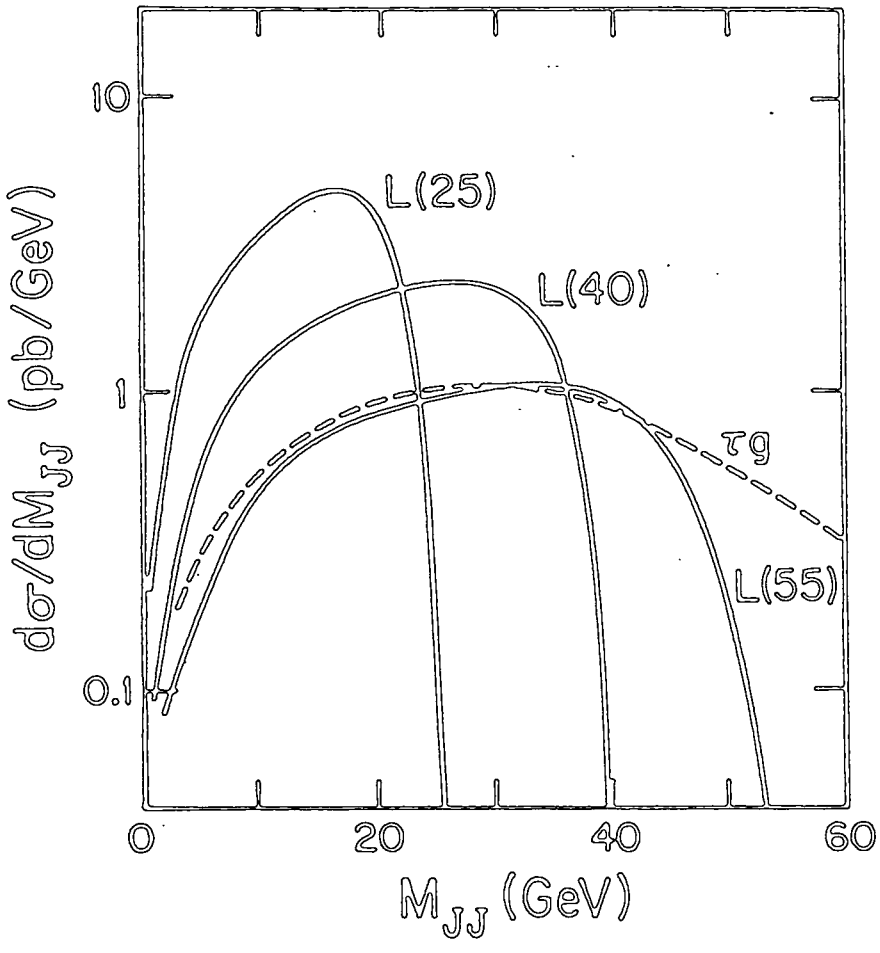

Figure 10

The invariant mass (M_{JJ}) distribution of the two jets arising from $W \rightarrow Lv_L \rightarrow JJ\bar{v}_L v_L$ for different masses of the heavy lepton L. The cuts to remove the background have been imposed. The dashed curve is the possible remaining background contribution from $p\bar{p} \rightarrow Wg \rightarrow \tau v_\tau g \rightarrow (u\bar{d})\bar{v}_\tau v_\tau g$ with $p_{gT} > 8$GeV and K = 2. The normalisation is as Fig. 4 and $W^\pm$-initiated events are summed over.

$$W \rightarrow \tau\nu_\tau \rightarrow u\bar{d}\bar{\nu}_\tau\nu_\tau. \qquad (4.34)$$

Figure 8 shows that the τ signal is comparable with the L signal. However, there is not the same difficulty in distinguishing between L and τ hadronic decay modes as there was in separating their leptonic decays. The $u\bar{d}$ system emerging from τ decay will be observed as a single narrow, energetic jet (with typically $20 < p_T(\text{jet}) < 40\text{GeV}$ using the above missing p_T cut) of low multiplicity, and should be readily recognisable. Moreover, the τ-initiated events will populate the $M_{JJ} < m_\tau$ region of the M_{JJ} plot and so, in principle, should give no background to the L distributions.

However, there is one contribution to the missing p_T + 2 jets signal that may cause confusion. In a fraction of events the W will be produced at large p_T (say, $p_{WT} > 8\text{GeV}$) recoiling against a visible parton jet, namely via,

$$\bar{q}q' \rightarrow W^+g \rightarrow \tau^+\nu_\tau g, \qquad (4.35)$$

or any of the crossed QCD processes. Thus it may be possible to construct M_{JJ} from the $(u\bar{d})$ jet from the τ decay together with the gluon jet. For these events the τ signal will be smeared over a wide range of M_{JJ}. Using lowest order QCD, the amplitude for the process of Fig. 11 is given by,

$$\begin{aligned} -iM = {} & \bar{v}(\bar{d})(-i(g/\sqrt{2})\gamma_\mu((1-\gamma_5)/2))(i/(\not{u}-\not{q})(-ig_s T_{ij}^a\gamma_\alpha)u(u) \\ & + \bar{v}(\bar{d})(-ig_s T_{ij}^a\gamma_\alpha)(i/(\not{u}-\not{W})(-i(g/\sqrt{2})\gamma_\mu((1-\gamma_5)/2))u(u) \qquad (4.36) \\ & \times (-i(g^{\mu\nu}-W^\mu W^\nu/M_W^2))\bar{u}(\nu)(-i(g/\sqrt{2})\gamma_\nu((1-\gamma_5)/2))v(\tau)\varepsilon^{\alpha *}(g) \\ & / ((\hat{s} - M_W^2) + i\Gamma_W M_W). \end{aligned}$$

The spin- and colour- averaged matrix element squared is then given

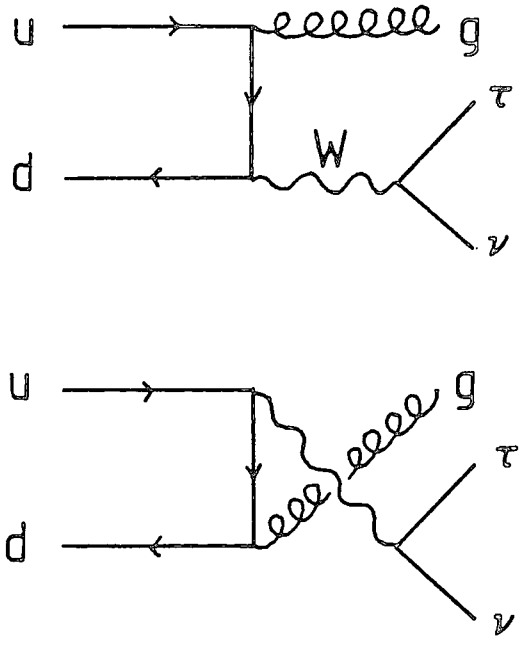

Figure 11

The $O(\alpha^2\alpha_s)$ Feynman graphs for the subprocess $u\bar{d} \rightarrow Wg \rightarrow \tau\nu g$.

by,

$$\Sigma|M|^2 = \frac{8g^4 g_s{}^2 M_W{}^2}{9((\hat{s}-M_W{}^2)^2 + \Gamma_W{}^2 M_W{}^2)} \left[- \bar{d}.v\ \bar{d}.\tau - \tau.u\ v.u \right.$$

$$\left. + \frac{(\hat{s} + \hat{u})\bar{d}.v}{2} + \frac{(\hat{s} + \hat{t})\tau.v}{2} \right] \frac{1}{\hat{u}\hat{t}} \qquad (4.37)$$

where, as usual, the particle names are used to denote their four momenta and the variables $\hat{s}$, $\hat{t}$, $\hat{u}$ refer to the subprocess $\bar{d}u \rightarrow W^+g$. The fermions are taken to be massless. This matrix element squared is multiplied by the τ-decay factor,

$$B_\tau d\Gamma_\tau/\Gamma_\tau, \qquad (4.38)$$

where B_τ is the $\tau \rightarrow \bar{\nu}_\tau q'\bar{q}$ branching ratio and,

$$d\Gamma_\tau = \Sigma|M(\tau \rightarrow q'\bar{q}\nu_\tau)|^2\ dLips(\tau \rightarrow q'\bar{q}\nu_\tau)/(2m_\tau) \qquad (4.39)$$

and,

$$\Sigma|M(\tau \rightarrow q'\bar{q}\nu_\tau)|^2 = 2g^4(\tau.q'\nu_\tau.q)/(W.W - M_W{}^2), \qquad (4.40)$$

with the particle names representing the particle momenta as shown in Figure 12. With the cut $p_{WT} > 8GeV$ (so that the gluon is recognised as a jet)and a K factor of 2, the cross section for this process is,

$$\sigma(p\bar{p} \rightarrow W^\pm g \rightarrow \tau\nu_\tau g) = 0.068nb. \qquad (4.41)$$

The contributions from the crossed subprocesses $qg \rightarrow W^\pm q$ and $\bar{q}g \rightarrow W^\pm\bar{q}$ are much smaller. Constructing M_{JJ} from the $(q'\bar{q})$ and g jets gives the τ background curve shown in Fig. 10. This is an upper estimate of this background since the τ may often be distinguished as a single particle jet.

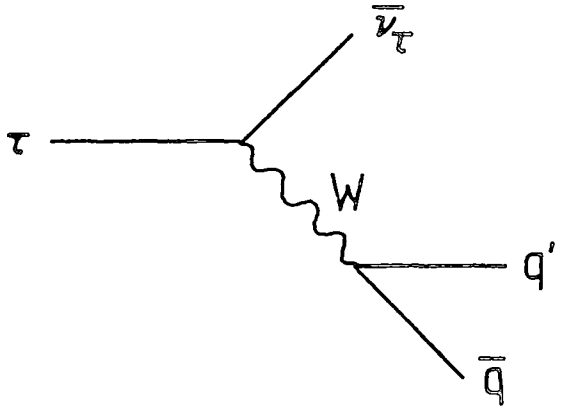

Figure 12

The semi-hadronic decay of the τ lepton.

4.6 The hadronic L signal and the UA1 jet algorithm

The above discussion of the hadronic decay signature of the heavy lepton assumes that the two jets from the heavy lepton would always be separable. In practise the UA1 jet algorithm [2] cannot resolve parton jets if,

$$((\Delta\varphi)^2 + (\Delta y)^2)^{1/2} < 1, \qquad (4.42)$$

where $\Delta\varphi$ is the difference in azimuth and Δy the difference in rapidity of the two parton jets. Hence some of these two parton events will appear as one "fat" jet and will be thrown away. Fig. 13 shows the opening angle in the $\bar{p}p$ centre of mass frame between the two jets after the UA1 jet algorithm has been applied. Events where the two partons are not well separated are discarded i.e.,events with small θ_{JJ} do not pass the cut. The coalescing of parton jets is most marked when the heavy lepton has a relatively low mass, for example, 50% of the previously accepted events for m_L = 25GeV are seen as single jet events, but for m_L = 60GeV only 20% fall into this category. After imposing the jet coalescing criteria (in addition to the other cuts) the integrated heavy lepton signal relative to the total $W^{\pm} \rightarrow e^{\pm}\nu$ rate is,

$$\frac{\sigma(W^{\pm} \rightarrow L\nu \rightarrow JJ\bar{\nu}\nu)}{\sigma(W^{\pm} \rightarrow e^{\pm}\nu)} = \begin{array}{l} 0.065 \text{ for } m_L = 25\text{GeV} \\ 0.085 \text{ for } m_L = 40\text{GeV} \\ 0.070 \text{ for } m_L = 50\text{GeV} \\ 0.040 \text{ for } m_L = 60\text{GeV} \end{array} \qquad (4.43)$$

that is, for a wide range of heavy lepton mass the event rate is about 7% of the $W^{\pm} \rightarrow e^{\pm}\nu$ rate. The invariant mass distribution is shown in

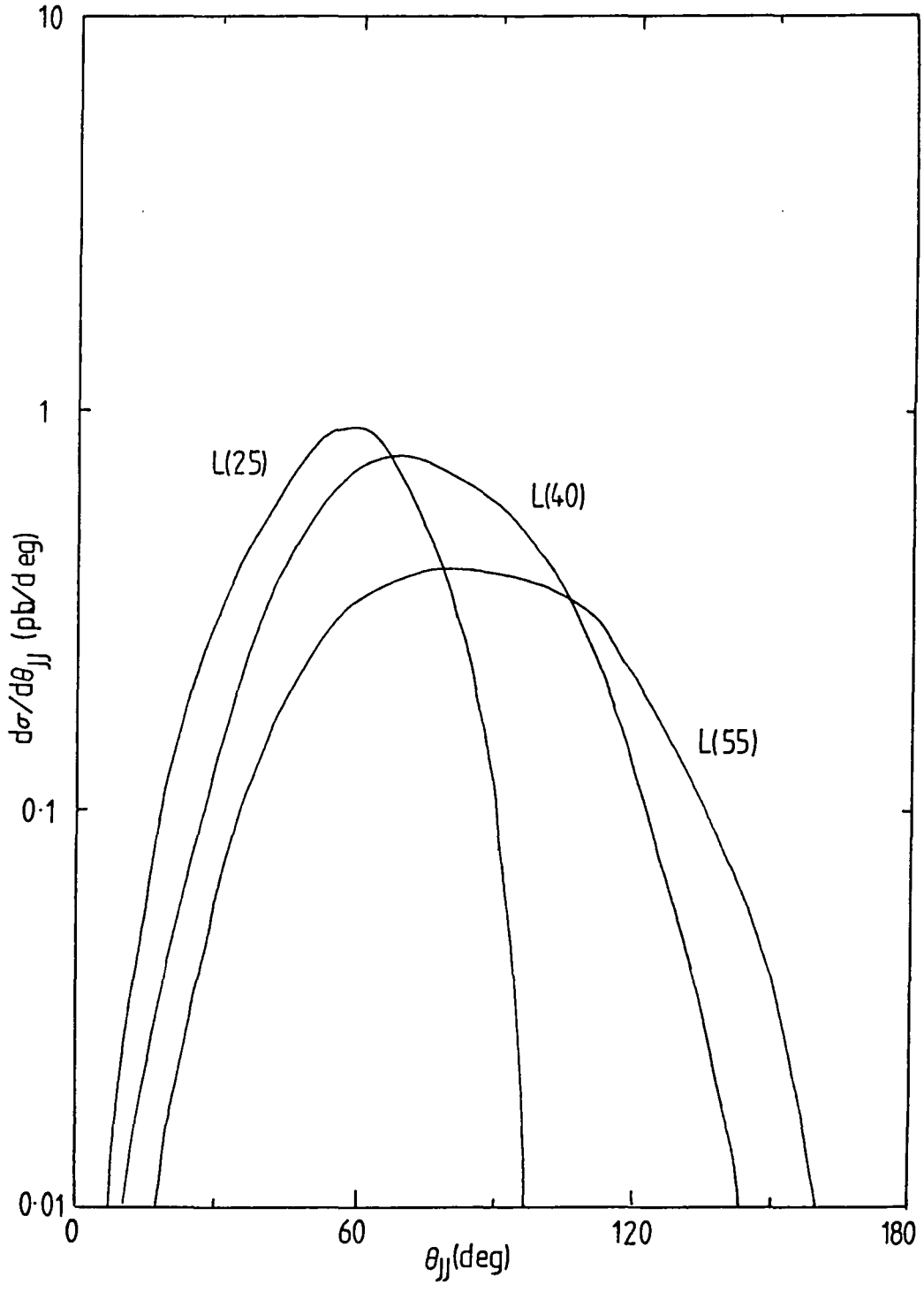

Figure 13

The distribution of the opening angle $\theta_{JJ'}$ as seen in the $p\bar{p}$ frame, between the two jets emerging from $p\bar{p} \rightarrow W \rightarrow Lv_L \rightarrow JJ\bar{v}_L v_L$, for different masses of the heavy lepton L. The cuts to remove the background events have been imposed. The UA1 jet algorithm has been applied.

Figure 14. Previously the low M_{JJ} events contained two nearly parallel partons - these events have now been eliminated resulting in a shift of the lower end point to higher M_{JJ} values. Clearly the M_{JJ} and θ_{JJ} distributions contain useful information on the mass of the heavy lepton.

4.7 Conclusion

The $W \rightarrow L\nu$ decay can be used to detect new sequential charged heavy leptons in $\bar{p}p$ collisions. Signatures from both the leptonic decay and hadronic decay of the L are possible, though in the former case there are serious backgrounds from $W \rightarrow e$ and $W \rightarrow \tau \rightarrow e$ decays. It should be emphasised, however, that these backgrounds are well known. This signal, which integrated over the optimum kinematic range of the emitted electron is about 4pb , is never above the background.

On the other hand, the hadronic decay signature of the L is much more promising. The events have the distinctive signal of large missing transverse momentum balanced by two energetic jets. After selective cuts to minimise the background the event rate is about 10% of the $W^{\pm} \rightarrow e^{\pm}\nu$ rate provided the mass of the new lepton is in the range 20 to 50 GeV.

In practise the UA1 experiment has studied missing transverse momentum by triggering on an energetic jet [13]. Several events with missing p_T > 40GeV (accompanied by an energetic jet) have been observed and do not appear consistent with either $W \rightarrow \tau$ or $W \rightarrow L$ origin (see Fig. 8). The events are more fully described in Chapter

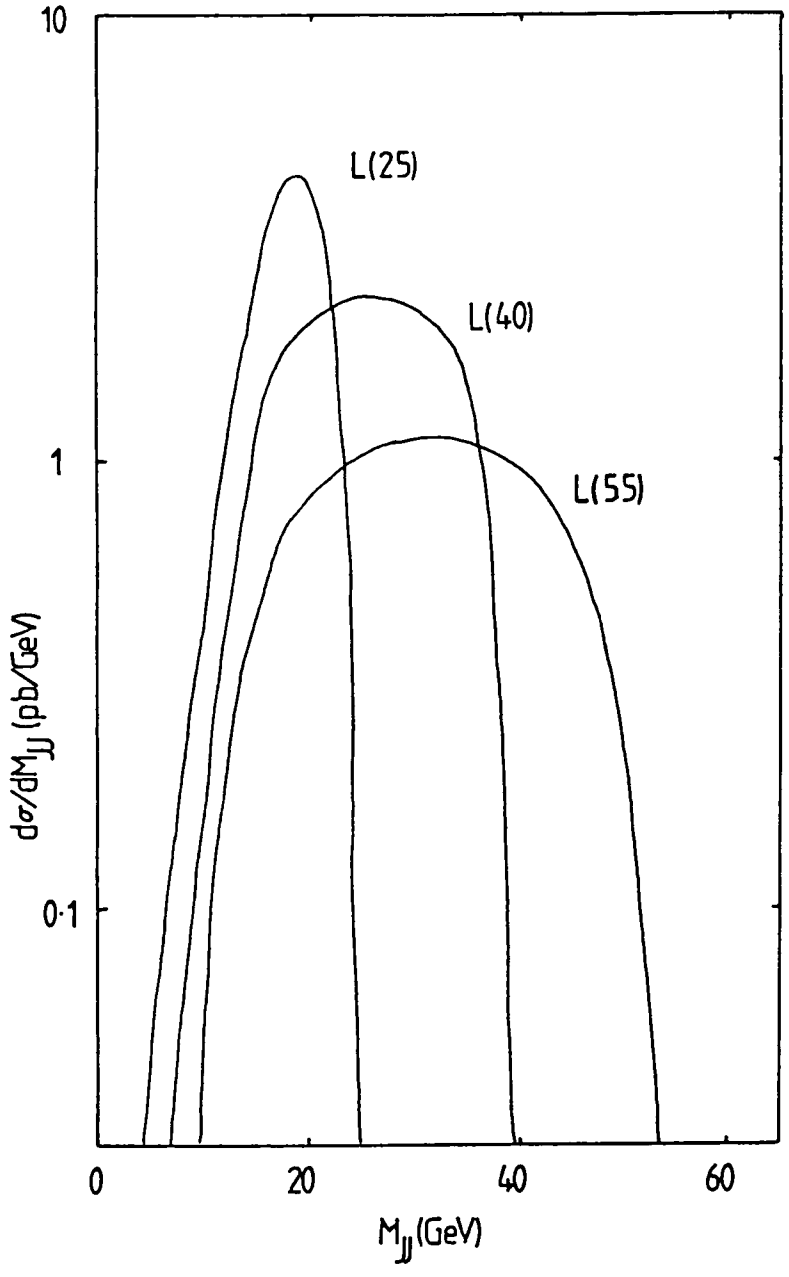

Figure 14

The invariant mass (M_{JJ}) distribution of the two jets arising from $W \rightarrow Lv_L \rightarrow JJ\bar{v}_L v_L$ for different masses of the heavy lepton L. The cuts to remove the background have been imposed. The dashed curve is the possible remaining background contribution from $p\bar{p} \rightarrow Wg \rightarrow \tau v_\tau g \rightarrow (u\bar{d})\bar{v}_\tau v_\tau g$ with $p_{gT} > 8$GeV and K = 2. The normalisation is as Fig. 4 and W^*-initiated events are summed over. The UA1 jet algorithm has been applied.

5. Because of the difficulty in removing the background from misidentified QCD jet pair production, events with lower missing p_T are not so well documented. For the 1984 run of the CERN $\bar{p}p$ collider, the UA1 experiment implemented a missing p_T trigger and so the region p_T(missing) < 40GeV may be examined more fully for heavy lepton events.

References

(1) JADE and TASSO collab., reported by S.Yamada, Proc. 1983 Int. Symp. on Lepton and Photon Interactions at High Energies, Cornell (1983)

(2) G.Arnison et al., UA1 collab., Phys. Lett. 122B, 103, (1983)

(3) M.Banner et al., UA2 collab., Phys. Lett. 122B, 476, (1983)

(4) D.B.Cline and C.Rubbia, Phys. Lett. 127B, 277, (1983)

(5) S.Gottlieb and T.Weiler, Phys. Rev. D29, 2005, (1984)

(6) P.Aurenche and R.Kinnunen, Annecy report, LAPP-TH-104, (1984)

(7) D.A.Dicus, S.Nandi, W.W.Repko and X.Tata, Phys. Rev. D29, 568, (1984)

(8) J.F.Owens and E.Reya, Phys. Rev. D17, 3003, (1978)

(9) M.Gluck, E.Hoffmann and E.Reya, Z.Phys. C13, 119, (1982)

(10) G.Arnison et al., UA1 collab., Phys. Lett. 129B, 273, (1983)

(11) F.Halzen, A.D.Martin and D.M.Scott, Phys. Lett. 122B, 160, (1982)

(12) C.Peterson, D.Sclatter, I.Schmitt and P.M.Zerwas, Phys. Rev. D27, 105, (1983)

(13) G.Arnison et al., UA1 collab., Phys. Lett. 139B, 115, (1984)

Chapter Five

Collider Monojets

5.1 Introduction

The UA1 detector has 4π calorimetry and detectors covering all but a small region close to the beam pipe. Therefore, for events with no non-interacting particles, the energy balance should be determined by overall calorimeter resolutions. Because energetic particles can escape down the beam pipe the longitudinal energy balance can not be measured. The transverse components are fairly well measured. When a non-interacting particle, for example the neutrino, is produced the momentum it carries is not deposited in the calorimeter and a transverse energy imbalance (missing p_T) is created. Events in which an energetic electron is accompanied by large missing p_T have been identified as the decay $W \rightarrow ev$ [1].

Several events [2] have been found in which an energetic hadronic jet is accompanied by large missing momentum (p_T(missing) $>$ 35GeV). These events have caused great surprise since the missing p_T's are very large and apparently defy explanation within the Standard Model. Section 5.2 describes these events in more detail, while section 5.3 discusses some of the theoretical ideas proposed to account for these strange events.

5.2 Events with large missing transverse energy and hadronic jets

During the 1983 $p\bar{p}$ collider run, the UA1 collaboration collected $113nb^{-1}$ of data which was aimed at the observation of W and Z particles [2]. There was no direct trigger for missing transverse energy and hence a subsidiary trigger was required, for example, a jet of $E_T > 25GeV$. The reduced sample was then scanned for events with missing energy using the selection cuts,

(a) p_T(missing) does not point to within $\pm 20^o$ of the vertical due to reduced efficiency in that region.

(b) p_T(missing) $> 4\sigma$ with $\sigma = 0.7\sqrt{E_T}$, where E_T is the total scalar transverse energy in the event.

The 4π calorimetry of the UA1 detector enables missing energy to be measured in all events. For "standard" events the missing transverse momentum x and y components are centred about zero with an approxomately gaussian shape and standard deviation σ. Imposing (b) therefore requires a four standard deviation effect for ordinary events to pass the cut. The remaining events (the $W \rightarrow e\nu$ events have been removed) are shown in Fig. 1. The events with jets separate into the following topologies,

(i) 17 events with single jets,

(ii) 5 events with two jets,

(iii) 3 events with more than two jets.

The six single jet events (A-F) with the highest p_T(missing) have been fully analysed. All (approximately) pass the cut,

$$p_T(\text{missing}) > 35GeV. \qquad (5.1)$$

In this region approximately one event from $W \rightarrow \tau\nu$ followed by the

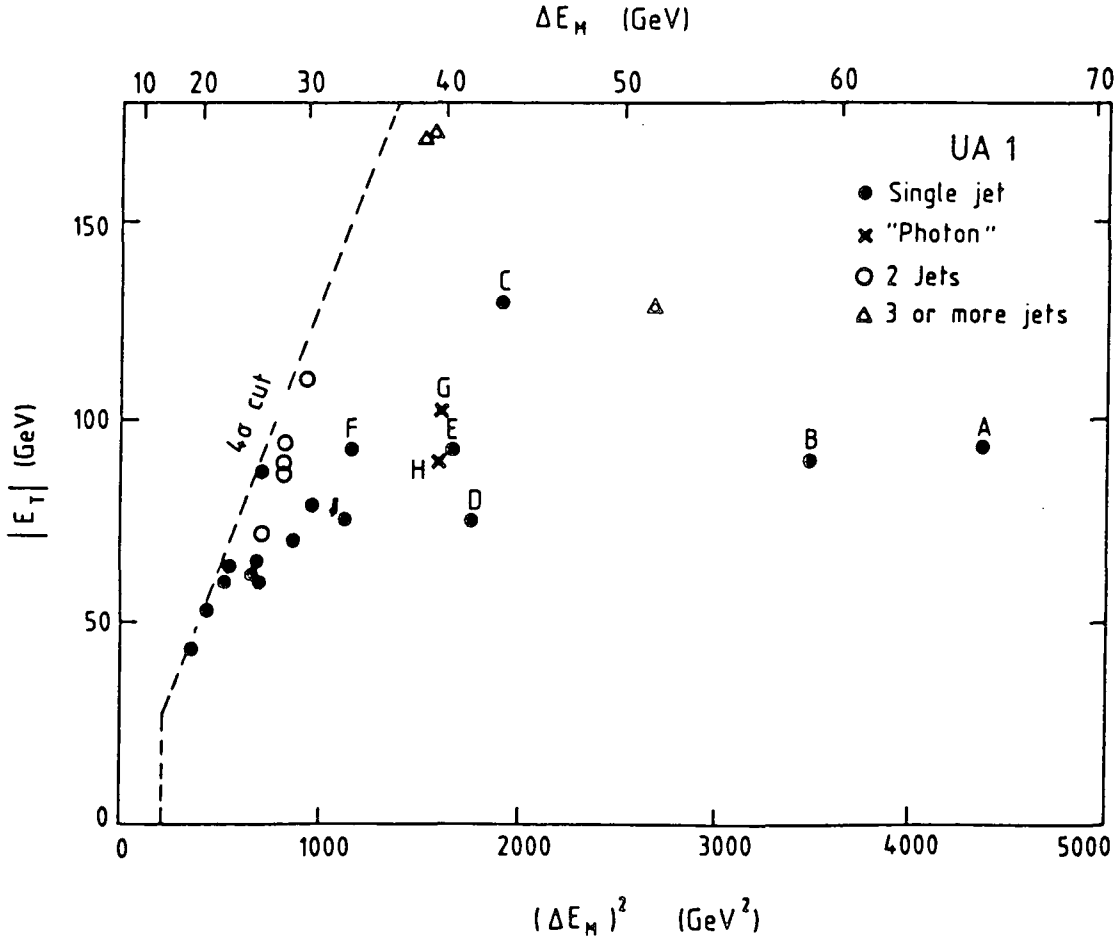

Figure 1

Scatter plot of the missing transverse energy squared versus total scalar transverse energy for the events observed by the UA1 collab. during 1983 which have missing E_T more than four standard deviations from zero. The events are labelled according to their topology.

hadronic decay of the τ is expected [2] and event F fits this category reasonably well. Event A is extremely strange since the jet contains a muon with very large p_T. The jets are generally of low multiplicity and have relatively small invariant masses. Figure 2 shows the transverse energy flow (plotted against azimuth φ and pseudorapidity η) seen in the detector for event B. The absence of deposited energy opposite the hadronic jet is clearly shown.

In order to assess the background to the single jet events with the largest missing p_T, the acceptance cut is relaxed to,

$$p_T(\text{missing}) > \max(2\sigma, 15\text{GeV}) \qquad (5.2)$$

and an isolation cut of $\cos\varphi < -0.8$ is made where φ is the azimuthal angle between the jet and the residual visible p_T. Such events which are approximately back-to-back in the transverse plane are candidates for a background contribution from QCD jet events in which all but one jet is missed. About half of the increased sample have $\cos\varphi < -0.8$, although none of the events A-F are in this region.

Since jet recognition plays an important role in these unusual events it is worth mentioning the UA1 jet algorithm [3]. In this algorithm, hadrons are considered to have come from the same parent parton if,

$$((\Delta\varphi)^2 + (\Delta y)^2)^{1/2} < 1 \qquad (5.3)$$

where $\Delta\varphi$ and Δy are the difference in azimuth and rapidity of the final state hadrons. For a set of hadrons to be recognised as a jet, the constituent hadrons must form a transverse momentum such that,

$$p_T(\text{jet}) > 12\text{GeV}. \qquad (5.4)$$

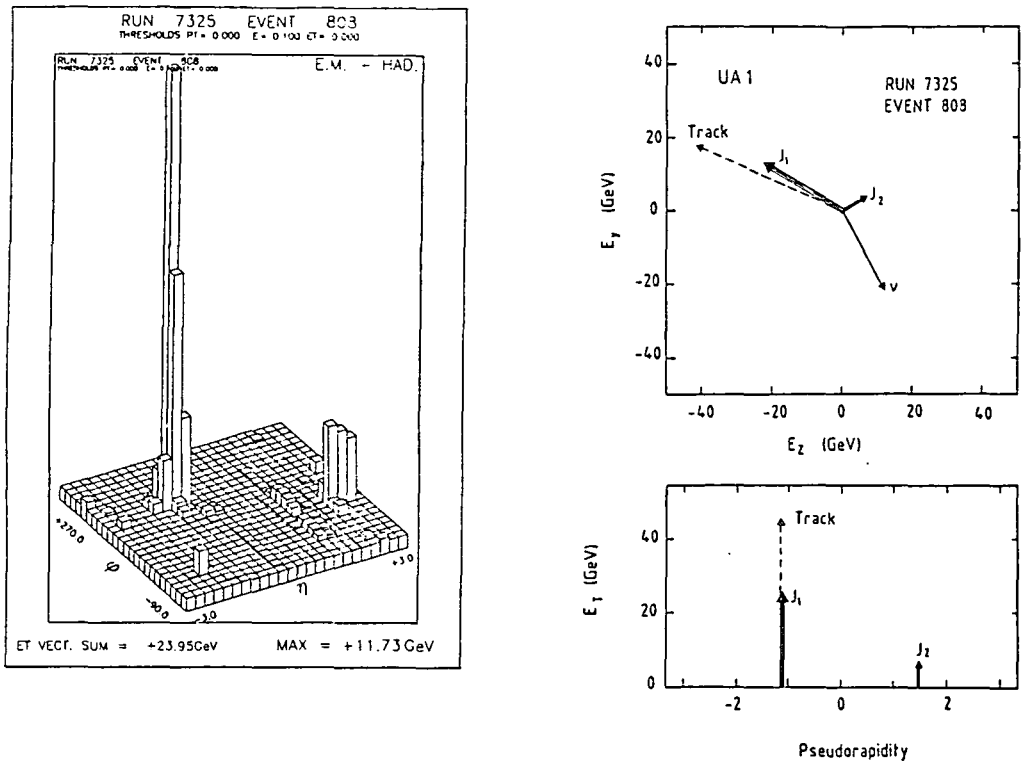

Figure 2

Transverse energy flow (φ versus η) seen in the calorimeters for monojet event B. Also shown are the transverse view and pseudorapidity distribution of the jets.

5.3 Monojets and new physics

The extremely large missing p_T's and the energetic nature of the jets, which apparently defy conventional explanation, has provoked much activity amongst phenomenologists. Many of the models suggested to explain these events separate into two categories which have differing mechanisms for producing missing p_T;

(a) supersymmetric models in which the photino ($\tilde{\gamma}$) is weakly interacting and leads to a missing transverse momentum, and,

(b) models in which the decay $Z \rightarrow \nu\bar{\nu}$ provides the missing p_T. The transverse momentum of the Z is equal to the observed missing p_T.

In Chapter 6 supersymmetric sources of missing p_T are examined and a scenario to account for the strange events is proposed. The pair production of scalar quarks ($\tilde{q}$) via QCD fusion,

$$q\bar{q},\ gg \rightarrow \tilde{q}\bar{\tilde{q}}, \tag{5.5}$$

and the subsequent decay,

$$\tilde{q} \rightarrow q\tilde{\gamma}, \tag{5.6}$$

can generate events of this type.

The models of category (b) split into two subclasses. Firstly, those in which a large mass intermediate state, X, is produced which then decays into a Z accompanied by a jet,

$$X \rightarrow Z + \text{jet}. \tag{5.7}$$

The transverse momentum of the Z forms a Jacobian peak at around 40GeV if the object X has mass O(150GeV). The second subclass, which is examined in Chapter 7, interprets the monojet events as being due to a new four point effective interaction. These interactions, for example,

$$q\bar{q} \rightarrow Zg, \qquad (5.8)$$

are assumed to originate from a theory unbroken at some scale Λ much larger than the weak scale. The transverse momentum of the Z produced in effective interactions does not form a Jacobian peak. As an example of the production of an intermediate state X, the production of excited quarks (up and down quarks with mass O(150GeV)) is examined.

References

(1) G.Arnison et al., UA1 collab., Phys. Lett. 122B, 103, (1983)

(2) G.Arnison et al., UA1 collab., Phys. Lett. 139B, 115, (1984)

(3) G.Arnison et al., UA1 collab., Phys. Lett. 136B, 294, (1984)

Chapter Six

Scalar quark interpretations of "monojets"

6.1 Introduction

One of the problems associated with the Standard Model is the so-called "naturalness" or "fine-tuning" problem [1,2]. This problem arises when the radiative corrections to the Higgs boson are calculated, see Fig. 1. This diagram diverges quadratically and thus gives a correction $O(\Lambda^2)$ where Λ is the scale at which the Standard Model is no longer a good approximation. (Because the Standard Model is not asymptotically free, i.e. its interactions become strong at high mass scales, it suggests that the Standard Model is only the low energy effective theory of a more complete theory.) Therefore the Higgs acquires a mass $O(\Lambda)$, leading to a large Higgs self-coupling and a breakdown of the low energy perturbation theory that seems successful. To prevent this large correction, there must exist a large degree of "fine tuning" which is "unnatural" and aesthetically unpleasing.

Supersymmetry [3-7] offers one way round this by proposing a set of partners to the ordinary particles with spin differing by 1/2, but all other quantum numbers the same. In an unbroken supersymmetry theory the masses of the standard particles and the new "sparticles" are identical, and, since the fermion and boson loops give

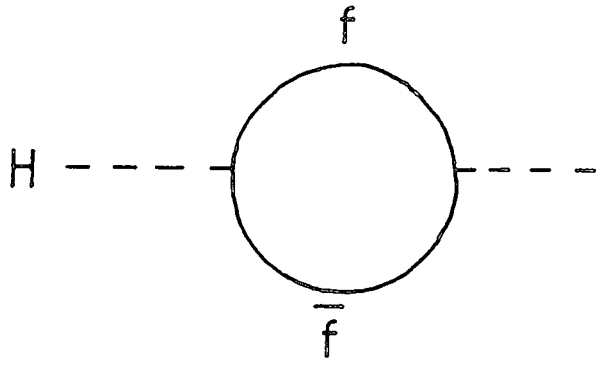

Figure 1

The contribution to the Higgs self-energy from fermion loops to lowest order.

contributions of opposite sign, the correction to the Higgs mass disappears. In the real world particles and sparticles do not exist with the same mass and so supersymmetry, if it exists, must be broken. However, if there is a large breaking, i.e. the mass difference between the particles and sparticles is large, the fine tuning problem returns. Therefore, one expects that if supersymmetry is a solution to the naturalness problem, new particles with mass $\lesssim$ O(1TeV) should exist.

Although supersymmetry is broken, a discrete symmetry (almost) always remains, and a multiplicatively conserved quantum number, R-parity [8-10], is generated. All the ordinary particles have R = +1, whereas the spartners have R = -1. This leads to the following restrictions,

1) supersymmetric particles are always produced in pairs,

2) the lightest supersymmetric particle must be stable.

In locally supersymmetric theories the photino $\tilde{\gamma}$ (the partner of the photon) is likely to be the lightest and so will occur in the final state of all supersymmetric particle decays. The photino interacts with ordinary matter via scalar fermions, e.g. Fig. 2, and the strength of the interaction decreases as the scalar fermion mass rises. This means that the photino is weakly interacting and hence likely to escape the detector and give rise to missing energy.

In supersymmetric theories there is a gluino ($\tilde{g}$) for every gluon and a scalar and pseudoscalar quark ($\tilde{q}$) (or squark) for every quark. Since these particles are coloured there is the possibility that they may be produced in hadron-hadron collisions, and then be detected via their decays to ordinary coloured particles accompanied by photinos

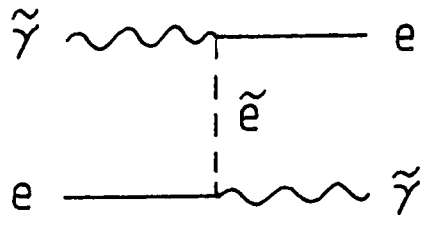

Figure 2

The lowest order diagram for photino ($\tilde{\gamma}$) interactions with electrons via a scalar electron $\tilde{e}$.

(missing energy). The interactions with quarks and gluons are fixed by gauge invariance so that only the masses are unknown.

The UA1 and UA2 collaborations have reported [11,12] a number of exotic events consisting of a large missing p_T accompanied by one or more hadronic jets, or a lepton with jet(s). Although the statistics are poor, these events do not appear to be consistent with the Standard Model. In this Chapter the interpretation of these events as being of supersymmetric origin is examined. A brief of summary squark and gluino production in proton-antiproton collisions is given in section 6.2, while the different scenarios leading to missing p_T with jet(s) are explained in section 6.3.

One particular scenario, that of scalar quark pair production with $\tilde{q} \rightarrow q\tilde{\gamma}$, is proposed as a possible explanation of the strange events in section 6.4. A consequence of the freedom in choosing the supersymmetric particle masses is that many different models also appear to explain the data. These are briefly summarised in section 6.5. Additional subprocesses are examined, within the scalar quark scenario of section 6.4, (section 6.6) leading to a bound on the gluino mass (section 6.7). The results of these calculations are summarised in section 6.8.

6.2 Squark and gluino production

Since the photino is taken to be the lightest supersymmetric particle and it is assumed to be feebly interacting, the monojet events [11] (see Chapter 5) have caused great excitement amongst theorists who favour supersymmetry. One of the features of

supersymmetric phenomenology is that the masses are essentially unknown [13]. The mass bounds that exist usually rely on assumptions about other sparticle masses. What this means in practical terms is that almost any combination of masses is allowed.

Gluinos may be pair produced from gg or $q\bar{q}$ fusion, as shown in Fig. 3,

$$gg \rightarrow \tilde{g}\tilde{g}, \quad q\bar{q} \rightarrow \tilde{g}\tilde{g}. \tag{6.1}$$

The differential cross sections for these processes are [13,14],

$$\frac{d\hat{\sigma}(gg \rightarrow \tilde{g}\tilde{g})}{d\hat{t}} = \frac{9\pi\alpha_s^2}{4\hat{s}^2}\left[\frac{(M^2-\hat{t})(M^2-\hat{u})}{\hat{s}^2} + \frac{(M^2-\hat{t})(M^2-\hat{u}) - 2M^2(M^2+\hat{t})}{(M^2-\hat{t})^2}\right.$$

$$\left. + \frac{M^2(\hat{s}-4M^2)}{2(M^2-\hat{t})(M^2-\hat{u})} - \frac{(M^2-\hat{t})(M^2-\hat{u}) + M^2(\hat{u}-\hat{t})}{\hat{s}(M^2-\hat{t})} + (\hat{u} \leftrightarrow \hat{t})\right] \tag{6.2}$$

$$\frac{d\hat{\sigma}(q\bar{q} \rightarrow \tilde{g}\tilde{g})}{d\hat{t}} = \frac{8\pi\alpha_s^2}{9\hat{s}^2}\left[\frac{3((M^2-\hat{t})^2 + M^2\hat{s})}{\hat{s}^2} + \frac{4(M^2-\hat{t})^2}{3(m^2-\hat{t})^2}\right.$$

$$\left. + \frac{M^2\hat{s}}{6(m^2-\hat{t})(m^2-\hat{u})} - \frac{3((M^2-\hat{t}))^2 + M^2\hat{s})}{\hat{s}(m^2-\hat{t})} + (\hat{u} \leftrightarrow \hat{t})\right] \tag{6.3}$$

where M is the gluino mass and m the squark mass. Since the squark acts as a mediating particle in some of the diagrams its mass enters the final cross section.

Similarly scalar quarks can be pair produced from $q\bar{q}$ or gg fusion (shown in Fig. 4),

$$gg \rightarrow \tilde{q}\tilde{q}, \quad q\bar{q} \rightarrow \tilde{q}\tilde{\bar{q}}. \tag{6.4}$$

The differential cross sections are [13,14],

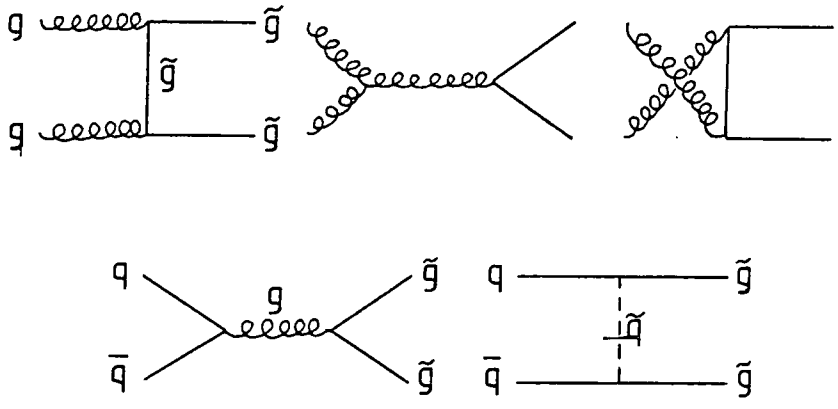

Figure 3

The $O(\alpha_s^2)$ Feynman graphs for (a) $gg \to \tilde{g}\tilde{g}$ and (b) $q\bar{q} \to \tilde{g}\tilde{g}$.

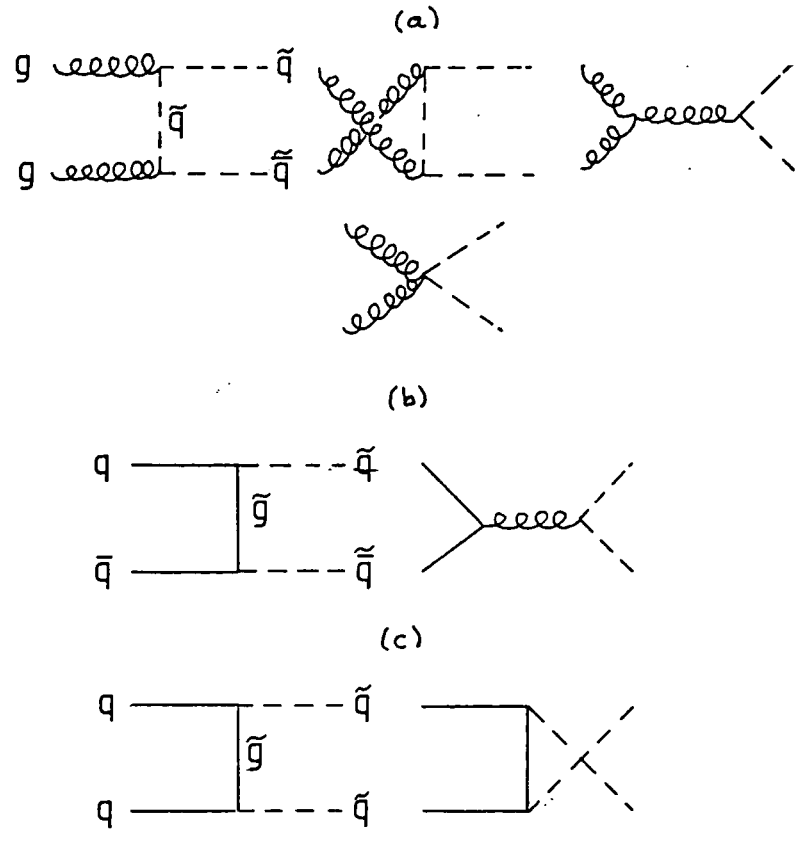

Figure 4

The $O(\alpha_s^2)$ Feynman graphs for (a) $gg \to \tilde{q}\tilde{\bar{q}}$, (b) $q\bar{q} \to \tilde{q}\tilde{\bar{q}}$ and (c) $qq \to \tilde{q}\tilde{q}$.

$$\frac{d\hat{\sigma}(gg \to \tilde{q}\bar{\tilde{q}})}{d\hat{t}} = \frac{F\pi\alpha_s^2}{4\hat{s}^2}\left[\frac{3(4\hat{s}(4m^2-\hat{s})+2(\hat{u}-\hat{t})^2)}{32\hat{s}^2}+\frac{(m^2+\hat{t})^2}{3(m^2-\hat{t})^2}+\frac{7}{24}\right.$$

$$+\frac{3((\hat{t}-\hat{u})(4m^2+4\hat{t}-\hat{s})-2(m^2-\hat{u})(6m^2+2\hat{t}-\hat{s}))}{32\hat{s}(m^2-\hat{t})}$$

$$\left.-\frac{(4m^2-\hat{s})^2}{96(m^2-\hat{t})(m^2-\hat{u})}+\frac{7(4m^2+4\hat{t}-\hat{s})}{96(m^2-\hat{t})}+(\hat{u}\longleftrightarrow\hat{t})\right] \quad (6.5)$$

where F is the number of squark flavours,and,

$$\frac{d\hat{\sigma}(q\bar{q} \to \tilde{q}\bar{\tilde{q}})}{d\hat{t}} = \frac{2\pi\alpha_s^2}{9\hat{s}^2}\left[\frac{\hat{s}(M^2-\hat{t})-(m^2-\hat{t})^2}{(M^2-\hat{t})^2}-\frac{2(m^2-\hat{t})(\hat{u}-\hat{t})+\hat{s}(m^2+\hat{t})}{3\hat{s}(M^2-\hat{t})}\right.$$

$$\left.+\frac{F(\hat{s}(\hat{s}-4m^2)-(\hat{u}-\hat{t})^2)}{\hat{s}^2}\right] \quad (6.6)$$

$$\frac{d\hat{\sigma}(qq \to \tilde{q}\tilde{q})}{d\hat{t}} = \frac{4\pi\alpha_s^2}{9\hat{s}^2}\left[\frac{(\hat{s}(M^2-\hat{t})-(m^2-\hat{t})^2}{(M^2-\hat{t})^2}+\frac{M^2\hat{s}}{3(M^2-\hat{t})(M^2-\hat{u})}\right.$$

$$\left.+(\hat{u}\longleftrightarrow\hat{t})\right]. \quad (6.7)$$

There is also the possibility of a quark and a gluon scattering to a gluino squark pair, shown in Fig. 5,

$$qg \to \tilde{q}\tilde{g}, \quad (6.8)$$

with differential cross section given by [14,15],

$$\frac{d\hat{\sigma}(qg \to \tilde{q}\tilde{g})}{d\hat{t}} = \frac{4\pi\alpha_s^2}{9\hat{s}^2}\left[\frac{(M^2-\hat{u})}{9\hat{s}}-\frac{(M^2-\hat{t})(m^2+\hat{t})}{9(m^2-\hat{t})^2}\right.$$

$$\left.+\frac{(M^2-\hat{u})(M^2-\hat{t})+3(M^2-\hat{u})(m^2-\hat{u})}{4(M^2-\hat{u})^2}\right.$$

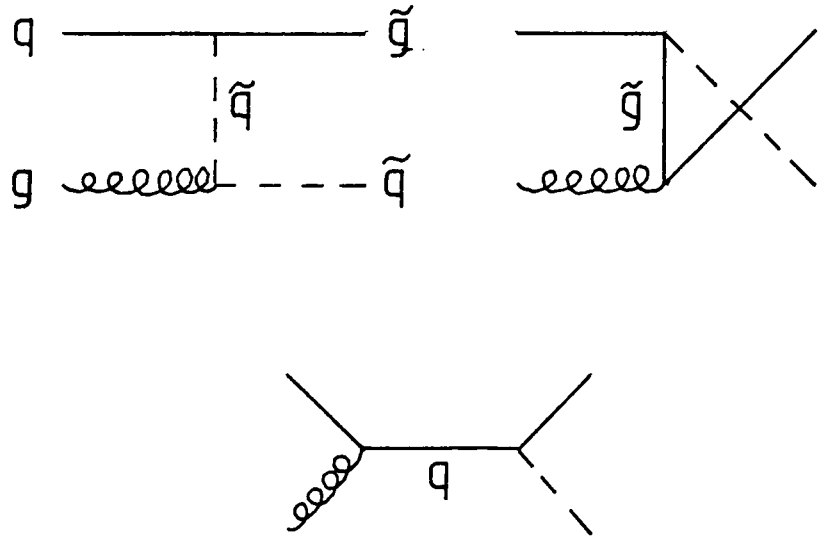

Figure 5

The $O(\alpha_s^2)$ diagrams for $qg \to \tilde{q}\tilde{q}\tilde{g}$.

$$- \frac{\hat{s}(m^2 + M^2 + 2\hat{t}) - (m^2 - M^2)(4M^2 - 4\hat{t} - \hat{s})}{144s(m^2 - \hat{t})}$$

$$+ \frac{(m^2 - \hat{u})(2\hat{t} + \hat{u} + M^2) - (M^2 - \hat{t})(2m^2 + M^2 + \hat{u}) + (M^2 - \hat{u})(2m^2 - 2\hat{u} - \hat{s})}{16(m^2 - \hat{t})(M^2 - \hat{u})}$$

$$+ \frac{(m^2 - \hat{u})(m^2 - M^2 - \hat{s}) - M^2\hat{s}}{4\hat{s}(M^2 - \hat{u})} \Bigg] . \qquad (6.9)$$

The interplay between the squark and gluino masses is clearly shown in these differential cross sections. The number of squark flavours also enters and plays an important role in determining the total cross sections. Although each quark must have a scalar (pseudoscalar) partner the masses of the partners need not be identical. The most important contributions then come from the squark of lowest mass.

The total cross sections for squark and gluino production at $\sqrt{s}$ = 540GeV are shown in Fig. 6 as functions of the squark and gluino masses. The parton densities of Ref. 15 have been folded in with the subprocess differential cross sections. Two degenerate flavours (u and d) of scalar and pseudoscalar quarks have been assumed. In Fig. 6(a) the gluino mass has been fixed at 100GeV, thus suppressing $\tilde{g}\tilde{g}$ and $\tilde{g}\tilde{q}$ production. If the gluino is heavy then squark-antisquark production gives the largest cross section. However, for very large squark mass ($> O(m_{\tilde{g}})$) then the Compton like process (6.8) dominates.

The total cross sections with fixed squark mass (= 100GeV) are shown as functions of the gluino mass in Fig. 6(b). The role is now reversed and $\tilde{g}\tilde{g}$ production dominates. Rather surprisingly, the $\tilde{q}\bar{\tilde{q}}$ cross section does not vary very much with the gluino mass. Finally,

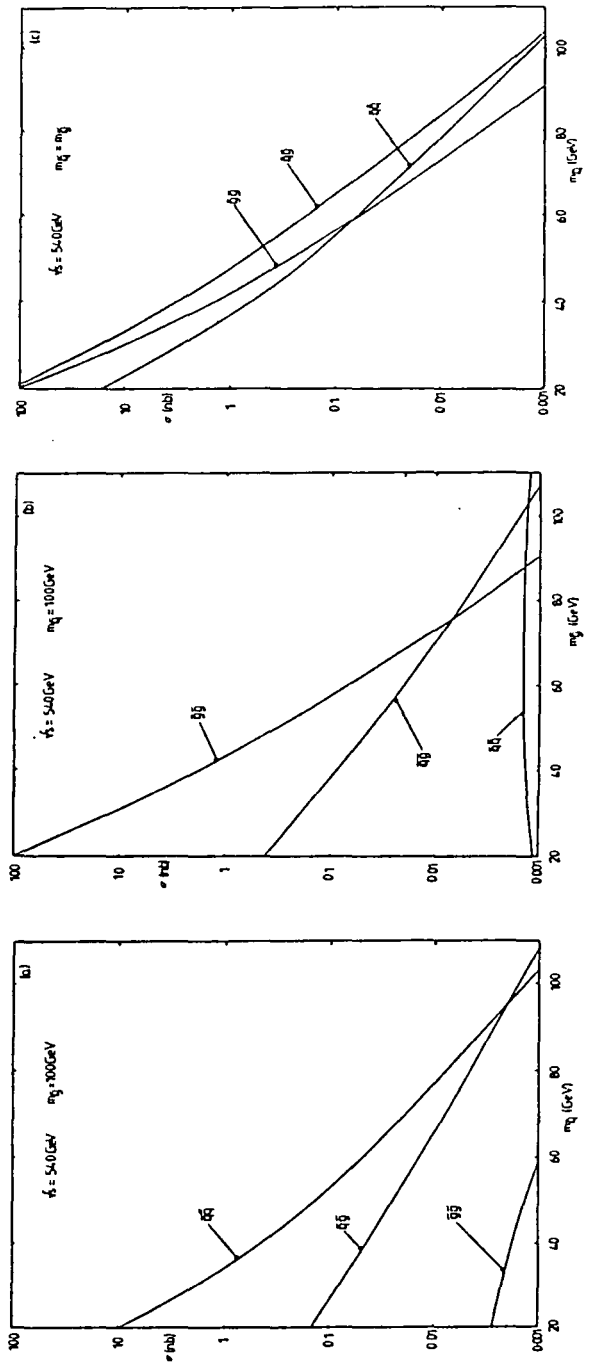

Figure 6

The cross sections for $\tilde{g}\tilde{g}$, $\tilde{q}\tilde{g}$ and $\tilde{q}\tilde{q}$ production in $p\bar{p}$ collisions at $\sqrt{s}$ = 540GeV based on QCD fusion. The three cases shown are (a) as a function of squark mass, $m_{\tilde{g}}$ = 100GeV, (b) as a function of gluino mass, $m_{\tilde{q}}$ = 100GeV, and (c) as a function of squark mass, $m_{\tilde{q}} = m_{\tilde{g}}$.

Fig. 6(c) shows the cross sections when the gluino and squarks have the same mass. The hardness of the quark structure functions ensures that $\tilde{q}\tilde{g}$ dominates $\tilde{g}\tilde{g}$ production for large values of the gluino mass, while for very large squark mass $\tilde{q}\bar{\tilde{q}}$ production dominates. These curves illustrate the fact that unless one of the masses (either squark or gluino) is much larger than the other, all processes should be considered simultaneously.

In performing these calculations, the QCD coupling constant is taken to be,

$$\alpha_s = \frac{12\pi}{b\ln(Q^2/\Lambda^2)} \qquad (6.10)$$

with Λ = 0.4GeV and b = 23 (corresponding to 5 active quark flavours). Allowing for one loop contributions from active supersymmetric particles [16-18] would give a smaller b and a larger α_s. On the other hand, choosing a smaller value of Λ would give a smaller α_s. These uncertainties, together with those of the structure functions [15], mean that there is an uncertainty of O(2) in the cross section predictions.

6.3 Missing energy from supersymmetric sources

As discussed earlier, broken supersymmetric theories with light feebly interacting photinos naturally give rise to missing transverse momentum. The supersymmetric mass spectrum determines the dominant decay modes of the squarks and gluinos. Two distinct classes exist, one where the squark is heavier than the gluino and the other where the squark is lighter than the gluino. The decays are different for

these two classes and lead to different numbers of final state partons.

Consider the case $m_{\tilde{q}} < m_{\tilde{g}}$. The gluino and squark decays are predominantly,

$$\tilde{q} \rightarrow q\tilde{\gamma} \text{ and } \tilde{g} \rightarrow \bar{q}\tilde{q} \rightarrow q\bar{q}\tilde{\gamma}. \tag{6.11}$$

For the three processes of interest (6.1,6.4,6.8), the preferred final states are,

$$q\bar{q} \text{ or } gg \rightarrow \tilde{g}\tilde{g} \rightarrow q\bar{q}q\bar{q}\tilde{\gamma}\tilde{\gamma}, \tag{6.12}$$

$$(q \text{ or } \bar{q})g \rightarrow (\tilde{q} \text{ or } \bar{\tilde{q}})\tilde{g} \rightarrow (q \text{ or } \bar{q})q\bar{q}\tilde{\gamma}\tilde{\gamma}, \tag{6.13}$$

$$q\bar{q} \text{ or } gg \rightarrow \tilde{q}\bar{\tilde{q}} \rightarrow q\bar{q}\tilde{\gamma}\tilde{\gamma}. \tag{6.14}$$

That is, the number of partons in the final state varies between 2 and 4. The missing p_T vector is the vector sum of the two photinos transverse momentum.

If, on the other hand, the gluino is lighter than the squark, the expected decays are,

$$\tilde{q} \rightarrow \tilde{g}q, \tag{6.15}$$

and,

$$\tilde{g} \rightarrow q\bar{q}\tilde{\gamma}. \tag{6.16}$$

The decay $\tilde{q} \rightarrow q\tilde{\gamma}$ will be suppressed relative to (6.15) by $O(\alpha/\alpha_s)$. This suppression will be modified by phase space factors since the gluino mass may be appreciable. The supersymmetric particle production mechanisms lead to the following final states,

$$q\bar{q} \text{ or } gg \rightarrow \tilde{q}\bar{\tilde{q}} \rightarrow q\bar{q}q\bar{q}q\bar{q}\tilde{\gamma}\tilde{\gamma}, \tag{6.17}$$

$$(q \text{ or } \bar{q})g \rightarrow (\tilde{q} \text{ or } \bar{\tilde{q}})\tilde{g} \rightarrow (q \text{ or } \bar{q})q\bar{q}q\bar{q}\tilde{\gamma}\tilde{\gamma}, \tag{6.18}$$

$$q\bar{q} \text{ or } gg \rightarrow \tilde{g}\tilde{g} \rightarrow q\bar{q}q\bar{q}\tilde{\gamma}\tilde{\gamma}. \tag{6.19}$$

There are many more partons in the final state for this scenario. Furthermore, the photinos are produced in three body decays and will

individually have a rather softer p_T spectrum than in the previous case.

Since the experimental information from the 1983 run indicates mainly one or two jet events, it would suggest that processes with small numbers of partons in the final state are most likely to fit the data. The process (6.14) with $m_{\tilde{q}} < m_{\tilde{g}}$ has least partons in the final state and so is a good candidate for a supersymmetric explanation of the "monojet" data. By taking into account the UA1 acceptance cuts [11], it will be shown that this process does yield large missing p_T events at about the observed rate, and that they are dominantly accompanied by a single jet, provided that $m_{\tilde{q}}$ is about 30GeV.

6.4 Scalar quarks and monojets

Assuming that $m_{\tilde{g}} > m_{\tilde{q}}$ and that $m_{\tilde{g}}$ is sufficiently large (> 100GeV) for gluino pair production (6.12) and the Compton like process (6.13) to be neglected, a phenomenological analysis is possible. The calculation proceeds as in section 6.2 with (i) the $q\bar{q}$ and gg fusion mechanisms (6.4), (ii) two degenerate squarks ($\tilde{u}$, $\tilde{d}$) of mass $m_{\tilde{q}}$, (iii) the structure functions of Gluck et al. [15] and (iv) α_s given by (6.10) Again there is an uncertainty of O(2) in the cross section predictions. The squarks are allowed to undergo two body decay to a massless quark and a massless photino.

To simulate the UA1 acceptance cuts [11] the following requirements are made on Monte Carlo simulated events for,

$$p\bar{p} \rightarrow \tilde{q}\bar{\tilde{q}} \rightarrow q\bar{q}(\tilde{\gamma}\tilde{\gamma}) \qquad (6.20)$$

(1) One parton jet (either q or $\bar{q}$) with

$$p_T(\text{jet}) > 25\text{GeV}, \qquad (6.21)$$

(2) The missing p_T is calculated by adding vectorially the p_T of the two photinos,

(3) $$p_T(\text{missing}) > 4\sigma \qquad (6.22)$$

with $\sigma = 0.7\sqrt{E_T}$, where E_T is the total scalar transverse energy of the event = $E_T(q) + E_T(\bar{q}) + 20\text{GeV}$. $E_T(q, \bar{q})$ are the E_T values of the outgoing partons and the addition of 20GeV represents the minimum bias value for the proton-antiproton debris at $\sqrt{s}$ = 540GeV.

(4) The outgoing q and $\bar{q}$ are combined to form a single large p_T hadronic jet if $((\Delta\varphi)^2 + (\Delta y)^2)^{1/2} < 1$, where $\Delta\varphi$ is the azimuth difference and Δy the rapidity difference of the two jets in accordance with the UA1 jet finding algorithm [17].

(5) A jet is recognised if $p_T(\text{jet}) > 12\text{GeV}$.

The missing p_T spectrum arising from $\tilde{q}\tilde{q}$ production and decay at $\sqrt{s}$ = 540GeV is shown in Fig. 7 for a range of squark mass. The event rate is greatly suppressed by imposing cuts (1) and (2) as shown in Fig. 7(b). For the smaller $m_{\tilde{q}}$ values the jet trigger (6.21) requires the parent scalar quark to have large p_T, for instance, for $m_{\tilde{q}}$ = 25GeV the average squark p_T is around 30GeV for events that pass the jet trigger. As the squark mass increases the parent p_T becomes less important and a greater proportion of events pass the trigger requirement.

The total $\tilde{q}\bar{\tilde{q}}$ cross section at $\sqrt{s}$ = 540GeV is shown in Fig. 8 as a function of $m_{\tilde{q}}$. The effect of imposing the UA1 acceptance cuts (1) and (3) is also shown. Here the difference between the total and 1-

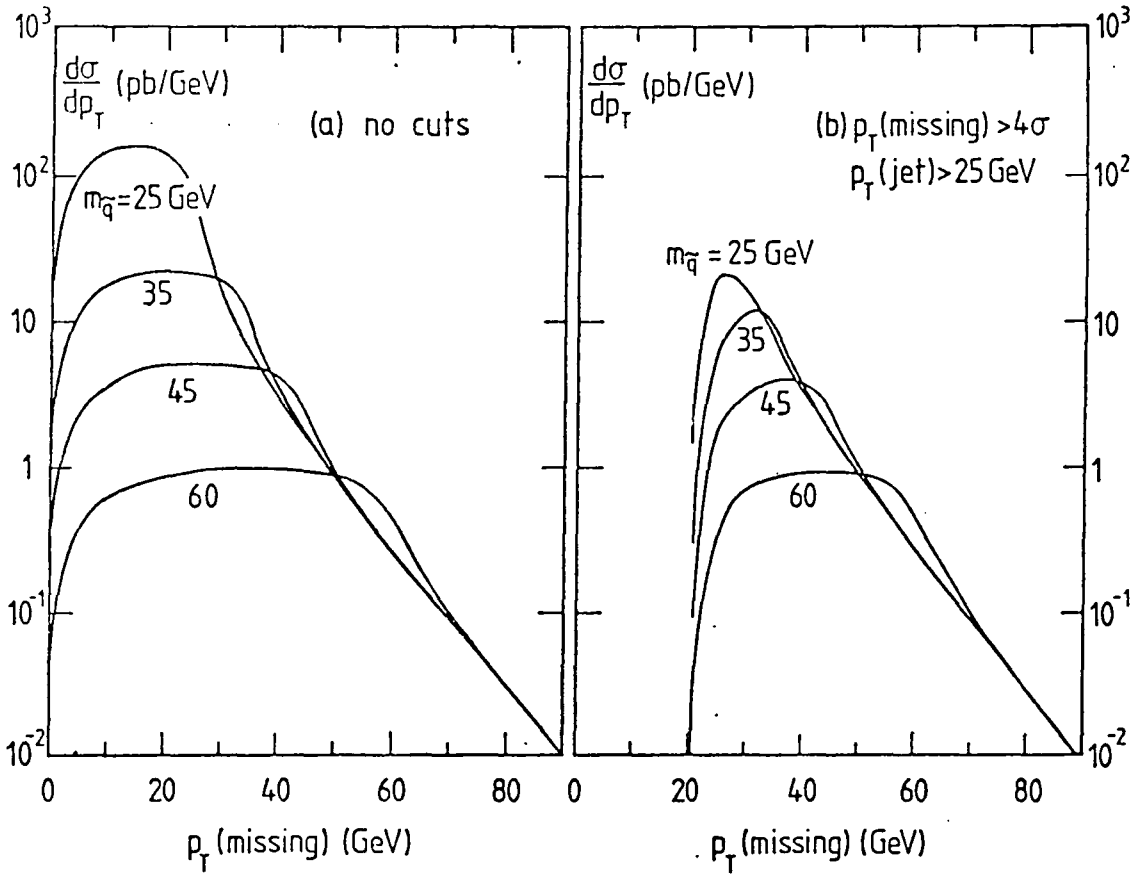

Figure 7

The missing p_T distribution arising from $\tilde{q}\bar{\tilde{q}}$ production and decay in $p\bar{p}$ collisions at $\sqrt{s}$ = 540GeV for various choices of the squark mass. Diagram (b) shows the suppression which results from imposing the cuts of 6.21 and 6.22.

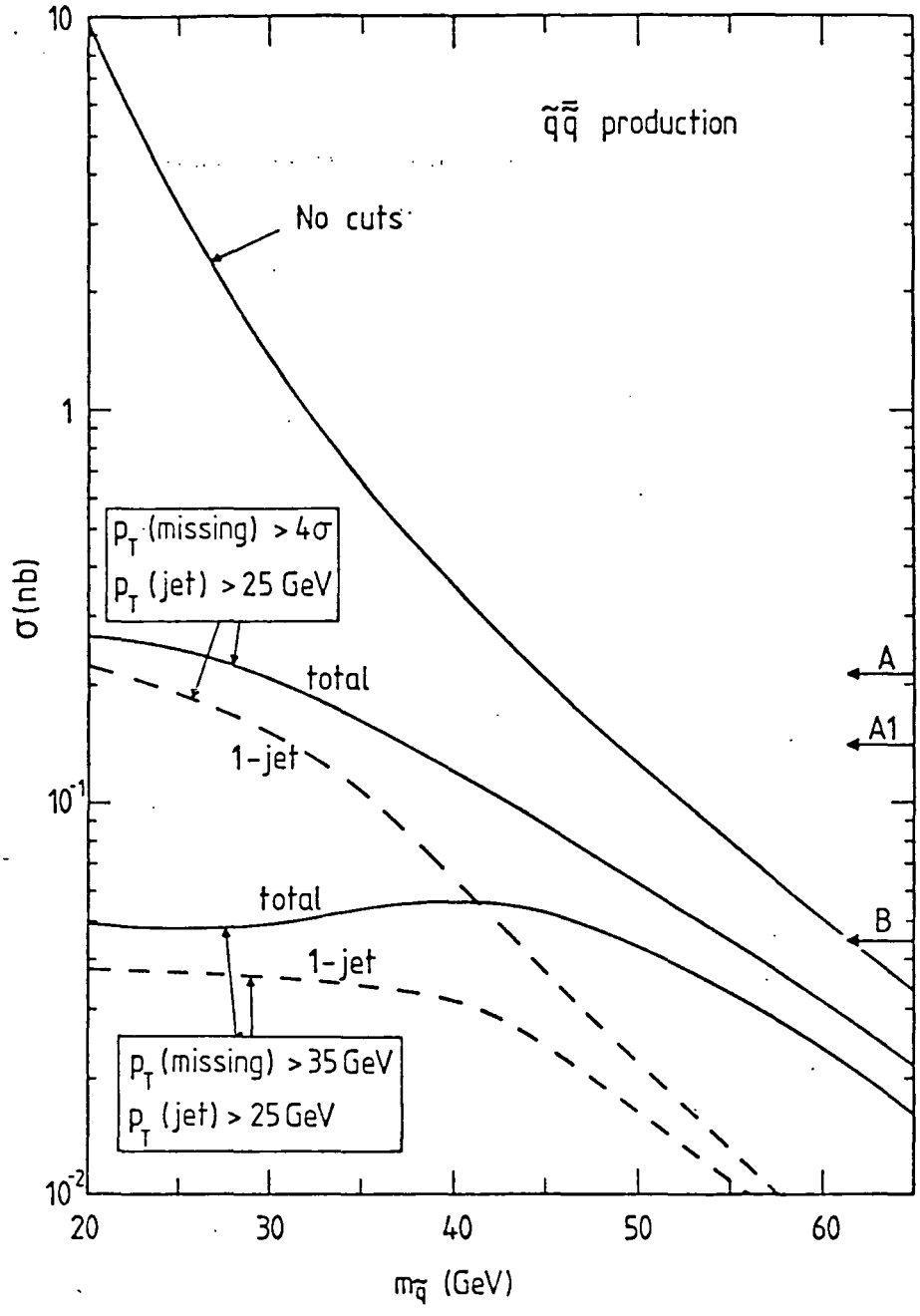

Figure 8

The $\tilde{q}\bar{\tilde{q}}$ production as a function of the squark mass. The effect of imposing the cuts of 6.21 and 6.22 is also shown, where the dashed curve represents the fraction of the total events with a single visible jet. The lower pair of curves correspond to the further requirement that the missing p_T is greater than 35GeV. The UA1 event rates [11] are shown to the right of the figure, for an integrated luminosity of $113nb^{-1}$: A) the 1- and 2-jet events with p_T(missing) > 4σ; A1) 1-jet events only; B) 1-jet events with p_T(missing) > 35GeV.

jet cross section is due to events with two visible jets. For low squark masses, the requirement that the photino-pair and one jet each have large p_T forces the second parton to be soft, resulting in the dominance of 1-jet events. On the other hand, for large squark masses two visible jets are expected. For squark masses up to about 40GeV, the predicted event rate is consistent with the 16 1-jet and 5 2-jet events reported by UA1, although there are uncertainties in the theoretical prediction of O(2).

To examine events with the largest missing p_T the missing p_T trigger is modified to,

(3′) $$p_T(\text{missing}) > 35\text{GeV}. \qquad (6.23)$$

The lowest set of curves on Fig. 8 shows the effect of this cut. 1-jet events dominate for squark mass in the range $20 < m_{\tilde{q}} < 35$GeV (the PETRA data [20] require the squark mass to be greater than 17.8GeV). Furthermore, for an integrated luminosity of 100nb^{-1} about 4 such "monojets" are expected.

To make a comparison with the experimental distributions, the squark mass is set to 25GeV. Fig. 9(a) compares the missing p_T of the 24 observed events that passed cut (3) with the model prediction. The experimental uncertainty on missing p_T is about ± 7GeV, a little over the bin width shown in the figure. The experimental jet p_T distribution is shown in Fig. 9(b) for the five events with $p_T(\text{missing}) > 35$GeV along with the predicted distribution. Considering the low statistics and the theoretical uncertainties, there is good overall agreement with the observed UA1 rate and p_T distributions.

UA1 [11] have also made an assessment of the background to their

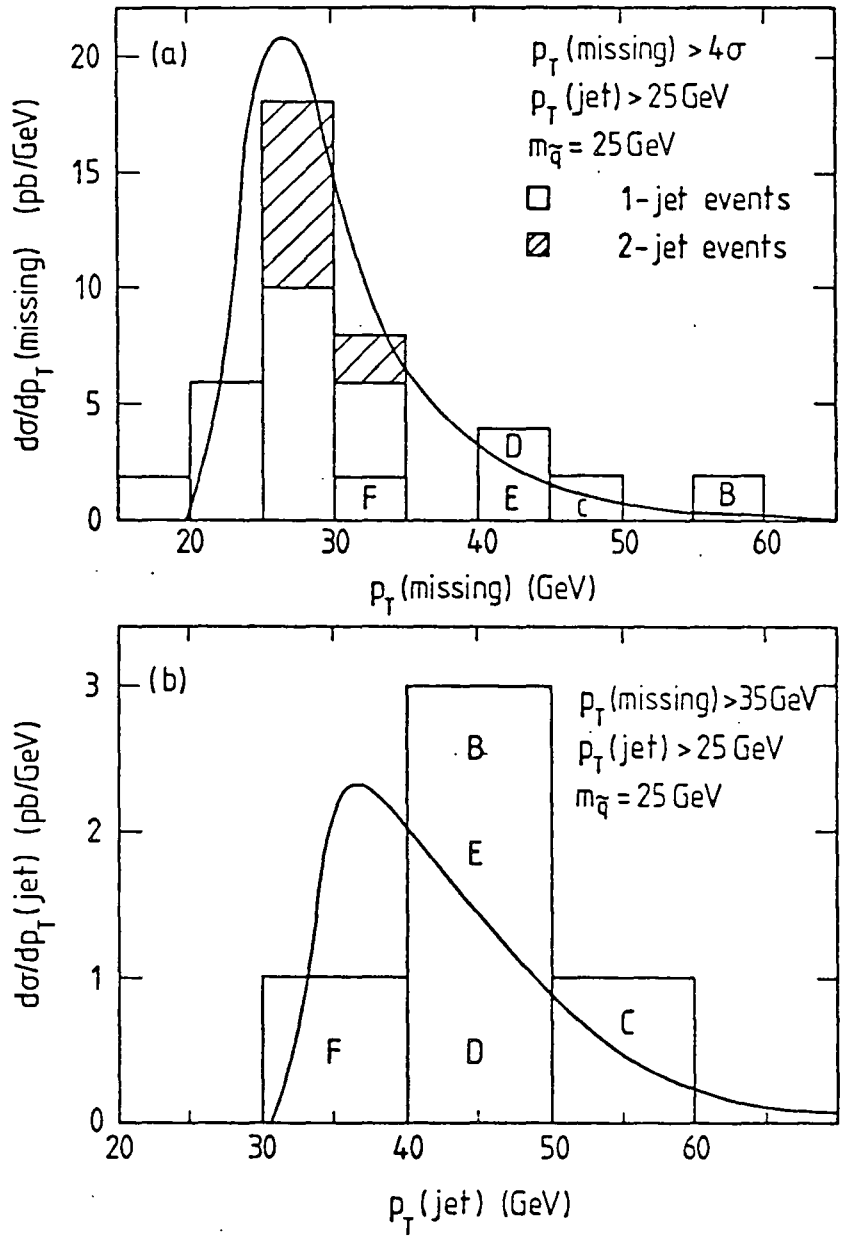

Figure 9

(a) The missing p_T distribution and (b) the jet p_T distribution (for 1-jet events with p_T(missing) > 35GeV) compared with the UA1 data [11] assuming no contamination from QCD jets. UA1 events B-F are those with the largest missing p_T; event A, which contains an energetic muon is omitted.

single jet events from misidentified QCD jets. The acceptance cuts are relaxed to p_T(missing) > max (2σ,15GeV) as described in chapter 5. An isolation cut of cosφ < -0.8 is made, where φ is the angle between the jet and the residual visible p_T (excluding the jet). For a squark mass of 25GeV, none of the predicted 1-jet events with p_T(missing) > 4σ (and p_T(jet) > 25GeV) are in the region cosφ < -0.8.

In summary, it has been shown that scalar quark production,

$$q\bar{q} \text{ or } gg \rightarrow \tilde{q}\bar{\tilde{q}} \rightarrow q\bar{q}(\tilde{\gamma}\tilde{\gamma})$$

can lead to events with a single visible jet and large missing p_T in accord with observations [11] if the squark mass is O(30GeV) and the gluino mass is O(100GeV). The dominant configuration is where the jet comes from one $\tilde{q} \rightarrow q\tilde{\gamma}$ decay and the missing p_T mainly from the other decay.

6.5 Alternative supersymmetric scenarios

Several supersymmetric scenarios have been proposed to account for the monojet data. All have a light photino (< 10GeV) that carries the missing transverse momentum. The three main supersymmetry scenarios can be categorised as follows,

(A) gluino pair production with $\tilde{g} \rightarrow q\bar{q}\tilde{\gamma}$; $m_{\tilde{q}} > m_{\tilde{g}} \sim 40$GeV.

Several authors [21-23] have supported the mechanism of (6.19). Monojets and dijets from this mechanism contain a significant contribution from the coalition of final state partons. Such jets would appear broader than seems to be the case [11].

(B) single heavy squark production with $\tilde{q} \to q\tilde{\gamma}$ and a light gluino; $m_{\tilde{q}} \sim 100GeV$, $m_{\tilde{g}} \sim 3\text{-}10GeV$.

The relevant subprocesses are [24-26],

$$qg \to \tilde{q}\tilde{q}g \to q\tilde{\gamma}\tilde{g} \tag{6.24}$$

and [27],

$$q\tilde{g} \to \tilde{q} \to q\tilde{\gamma}. \tag{6.25}$$

Because the gluino is so light it can be perturbatively generated as a component of the proton [25] and (6.25) is allowed. The squark is produced with little p_T and the subsequent two-body decay gives rise to a Jacobian peak in the missing p_T spectrum. The explanation due to Barger et al. [24] based on (6.24) relies on a long gluino lifetime in order to evade current experimental gluino mass bounds. This requires the $\tilde{g}$ and $\tilde{\gamma}$ to be approximately degenerate: they take $m_{\tilde{g}} = 0.9\ m_{\tilde{\gamma}}$ which seems rather contrived. The authors of Ref. 26 calculate the fragmentation of light gluinos and show that low mass gluinos are not ruled out experimentally. Supergravity mass relations suggest $m_{\tilde{g}} \sim 7m_{\tilde{\gamma}}$ so in their scenario the photino is expected to be extremely light $O(0.4\text{-}1.2GeV)$. This violates the cosmological bounds on the photino energy density. This need not be a serious problem since there is no compelling supergravity model at present and the mass relations may be sidestepped. Nevertheless models with low mass gluinos run the risk of gluino pair production being very large and giving a sizeable contribution to the standard QCD two-jet cross section.

(C) Squark pair production with $\tilde{q} \to q\tilde{\gamma}$ decay; $m_{\tilde{g}} > m_{\tilde{q}} \sim 25\text{-}40GeV$.

As in section 6.4, squark-antisquark production (6.14) is taken to explain [23,28] the UA1 missing p_T data. Barger et al. [28] assume

five squark flavours (and degenerate left- and right-handed components) and use the calculated 1- and 2-jet cross sections to put a lower bound of O(40GeV) on the squark mass by comparison with the data. Given the uncertainties in the actual recognition of jets in a detector, these bounds are at the best very approximate. A similar bound is obtained by Ellis and Kowalski [23] who also assume five flavours of degenerate squarks. Their analysis depends on an accurate subtraction by UA1 of the QCD background which fakes missing p_T events in the region $(p_T(\text{missing}))^2 < 1000\text{GeV}^2$. The use of an estimate of the large background at small values of p_T(missing) to rigorously exclude relatively low squark masses must necessarily involve large uncertainties.

To distinguish between the different models it is important to explore all the consequences of the chosen mass spectrum. For example, just as ordinary heavy quarks may be produced by both QCD fusion and from W decay, so may squarks be produced via the W boson,

$$q_L\bar{q}_L' \rightarrow W \rightarrow \tilde{q}_L\bar{\tilde{q}}_L' \rightarrow q_L\bar{q}_L'(\tilde{\gamma}\tilde{\gamma}), \qquad (6.26)$$

where $\tilde{q}_L$ represents the combination of scalar and pseudo scalar quarks that couples to the W.

A second subprocess that can give rise to appreciable cross sections for small squark masses (especially if the photino is very light) is [29],

$$(q \text{ or } \bar{q})g \rightarrow (\tilde{q} \text{ or } \bar{\tilde{q}})\tilde{\gamma} \rightarrow (q \text{ or } \bar{q})\tilde{\gamma}\tilde{\gamma}. \qquad (6.27)$$

This process only contributes to the single jet + missing p_T signal.

In the next section, the effect of these subprocesses on the range of possible squark masses is investigated.

6.6 Electroweak contributions to squark production

The matrix element for the process,

$$u\bar{d} \rightarrow W \rightarrow \tilde{q}_{iL}\bar{\tilde{q}}_{jL} \tag{6.28}$$

shown in Fig. 10 is,

$$-iM = -\frac{ig}{\sqrt{2}} U_{ud}\, \bar{d}\frac{\gamma_\nu(1-\gamma_5)}{2}u\, i\frac{(-g^{\mu\nu}+W^\mu W^\nu/M_W^2)}{(\hat{s}-M_W^2+i\Gamma_W M_W)}\frac{ig}{\sqrt{2}}(\tilde{q}_i - \bar{\tilde{q}}_j)_\mu U_{ij} \tag{6.29}$$

where particle labels represent their four momenta. U_{ij} is the supersymmetric equivalent of the Kobayashi-Maskawa mixing matrix. Absence of flavour changing neutral currents require that this is equal to the Standard Model K-M matrix [30]. Squaring the amplitude and performing all summations and averaging yields,

$$\Sigma|M|^2 = g^4|U_{ud}|^2|U_{ij}|^2(\hat{u}\hat{t} - m_i^2 m_j^2)/(4((\hat{s} - M_W^2)^2+\Gamma_W^2 M_W^2)). \tag{6.30}$$

The differential cross section is then,

$$\frac{d\hat{\sigma}}{d\hat{t}} = \frac{\pi\alpha^2|U_{ij}|^2|U_{ud}|^2}{4\hat{s}^2\sin^4\theta_W}\quad\frac{(\hat{u}\hat{t} - m_i^2 m_j^2)}{((\hat{s} - M_W^2)^2 + \Gamma_W^2 M_W^2)} \tag{6.31}$$

where m_i and m_j are the masses of the two squarks i and j. The electroweak parameters are taken to be $|U_{ij}|^2 = |U_{ud}|^2 = 1$, M_W = 81GeV, Γ_W = 3GeV, α = 1/137 and $\sin^2\theta_W$ = 0.25. The cross section is normalised to the experimentally observed value [31] $\sigma(W \rightarrow e\nu)$ = 0.53nb and note that the W branching ratio to squarks is,

$$Br(W \rightarrow \tilde{q}_i\bar{\tilde{q}}_j) = 3/2\,Br(W \rightarrow e\nu)(1+x_i^2+x_j^2-2x_i-2x_j-2x_ix_j)^{3/2} \tag{6.32}$$

where $x_{i,j} = m_{i,j}^2/M_W^2$. The factor 3 comes from colour and the 1/2 reflects the scalar nature of the squark.

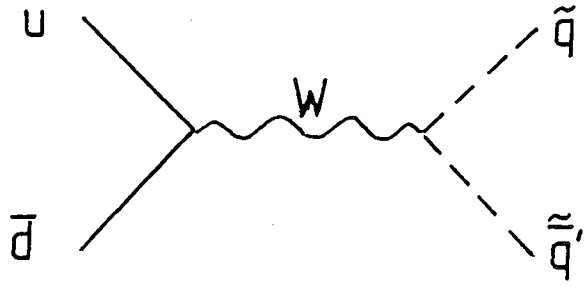

Figure 10

The lowest order contribution for the process $u\bar{d} \rightarrow W^{+} \rightarrow \tilde{q}\tilde{q}'$.

The differential cross section for the subprocess (see Fig. 11),

$$(q \text{ or } \bar{q})g \rightarrow (\tilde{q} \text{ or } \bar{\tilde{q}})\tilde{\gamma}, \tag{6.33}$$

is [13],

$$\frac{d\hat{\sigma}(qg \rightarrow \tilde{q}\tilde{\gamma})}{d\hat{t}} = \frac{\alpha_s \alpha e_q^2 \pi}{3\hat{s}^2}\left[-\frac{\hat{t}}{\hat{s}} + \frac{\hat{u}(\hat{u} + m^2)}{(\hat{u} - m^2)^2} - \frac{\hat{u}(\hat{s} - 2m^2)}{\hat{s}(\hat{u} - m^2)} \right] \tag{6.34}$$

where m is the squark mass and e_q the electric charge. $\hat{s}$,$\hat{t}$ and $\hat{u}$ are the Mandelstam variables.

The calculation proceeds as in section 6.4. The branching ratio for the squark decay,

$$\tilde{q} \rightarrow q\tilde{\gamma}, \tag{6.35}$$

is taken to be 100%. If the weak gauginos are lighter than the squark this branching ratio will be reduced. This gives an additional uncertainty in the cross section normalisation.

Fig. 12 shows the cross sections for the subprocesses (6.26) and (6.27) as functions of the squark mass at $\sqrt{s}$ = 540GeV. The effects of the experimental cuts are shown. The difference between the total and 1-jet cross section in Fig. 12(a) is due to events with two recognisable parton jets. Although the total event rates for the two subprocesses are comparable, many more W-initiated events survive the cuts due to the Jacobian peak in the squark transverse momentum. Fig. 13 shows the cross section for both these subprocesses and QCD fusion (6.14) as a function of the squark mass at $\sqrt{s}$ = 540GeV. The uncertainties inherent in the calculation are such that more restrictive bounds on the squark mass than those given in section 6.4 (20GeV $< m_{\tilde{q}} <$ 35GeV) are not justified.

All events from subprocesses (6.26) and (6.27) that pass the 4σ cut also survive the relaxed cuts of p_T(missing) $>$ max(2σ, 15GeV) and

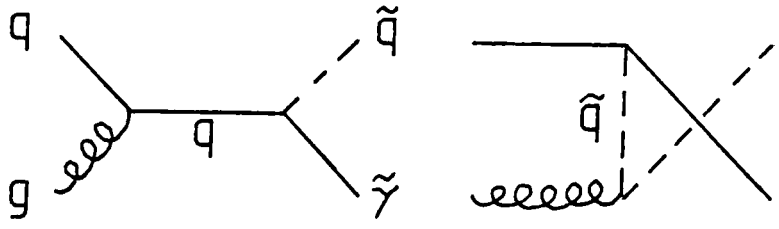

Figure 11

The $O(\alpha\alpha_s)$ diagrams for $qg \to \tilde{q}\tilde{\gamma}$.

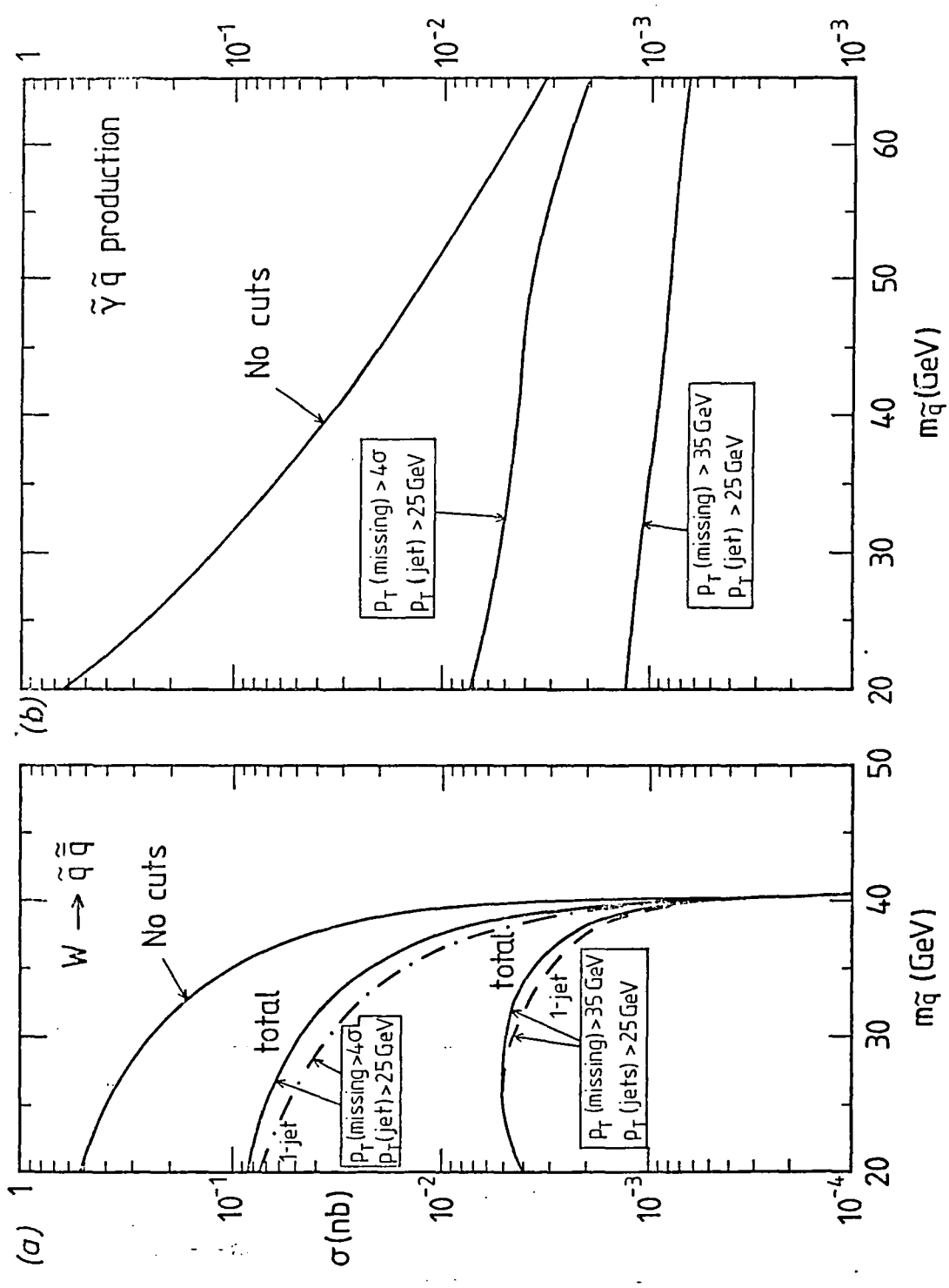

Figure 12

(a) The $W \rightarrow \tilde{q}_L^s \bar{\tilde{q}}_L^{s'}$ cross section as a function of the squark mass. The effect of imposing the missing momentum cuts is also shown. The dashed lines represent the 1-jet cross sections.

(b) The $\gamma \tilde{q}^s$ production cross section as a function of the squark mass. The effect of imposing the missing momentum cuts is shown.

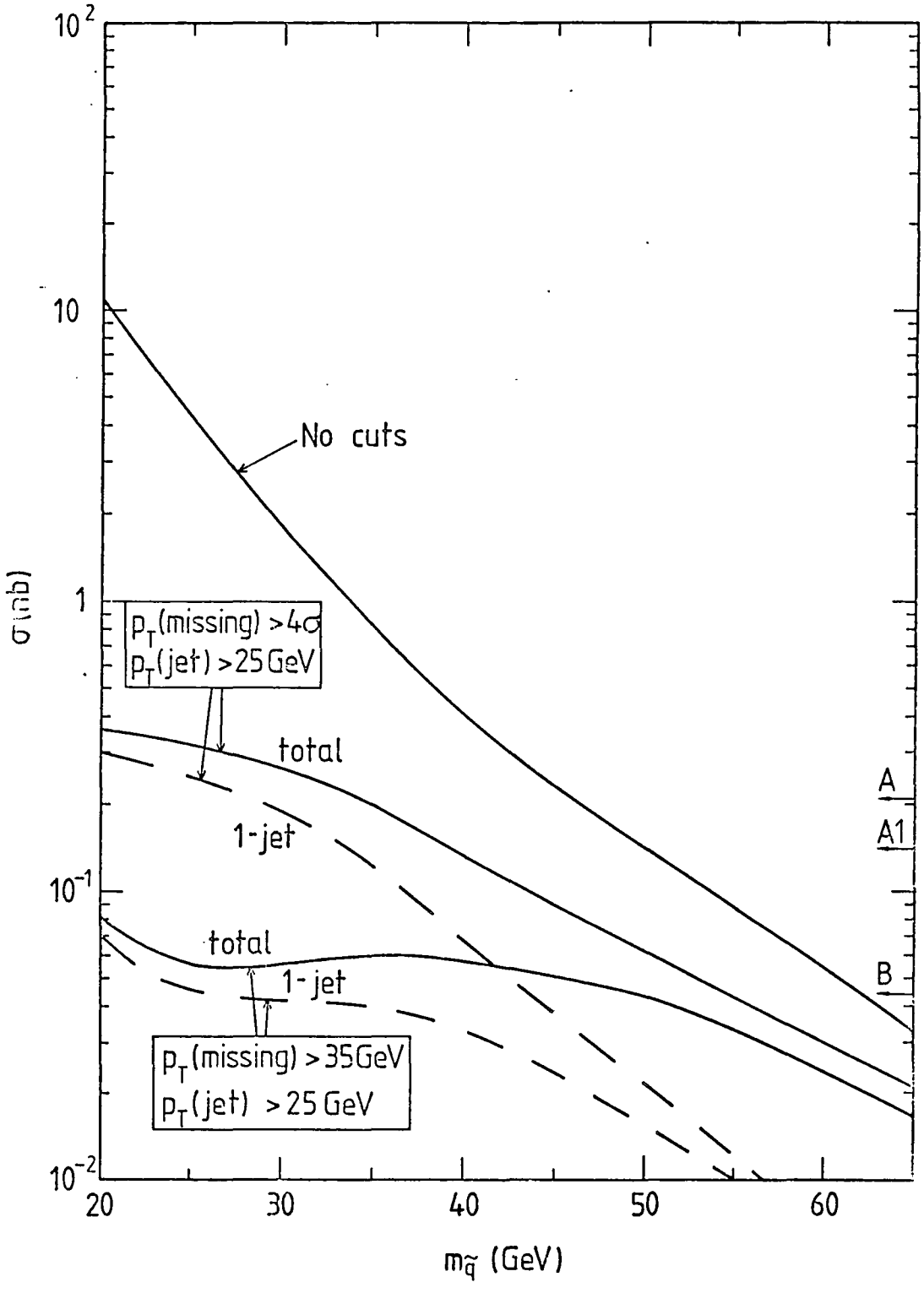

Figure 13

The combined cross section for processes 6.14, 6.26 and 6.27 as a function of the squark mass at $\sqrt{s}$ = 540GeV. The effect of imposing the missing momentum cuts is also shown, where the dashed curve represents the fraction of the total events with a single visible jet. The UA1 data [11] is shown as in Fig. 8.

$\cos\varphi < -0.8$ as described in chapter 5.

To further investigate the event topology, the jet recognition criterion is relaxed from $p_T(\text{jet}) > 12\text{GeV}$ to $p_T(\text{jet}) > 8\text{GeV}$. This may help to distinguish between subprocesses that predict differing numbers of partons in the final state. The relaxed jet criterion increases the number of events with two visible jets as shown in Table 1.

Table 1

Predictions for the number of 1-jet and 2-jet events for processes (6.14), (6.26) and (6.27) in an integrated luminosity $L = 0.113\text{pb}^{-1}$ at $\sqrt{s} = 540\text{GeV}$. The effect of varying the jet recognition criterion is shown for missing p_T cuts of 4σ (35GeV in brackets).

	$m_{\tilde{q}} = 25\text{GeV}$				$m_{\tilde{q}} = 35\text{GeV}$			
	$p_T(\text{jet}) > 12$		$p_T(\text{jet}) > 8$		$p_T(\text{jet}) > 12$		$p_T(\text{jet}) > 8$	
$N_{1\text{-jet}}$	27	(4.5)	20	(3.4)	14	(4.5)	10	(3.4)
$N_{2\text{-jet}}$	8	(1.1)	15	(2.2)	8	(2.3)	12	(3.4)

There are experimental difficulties in recognising jets with low transverse energy, indeed the actual calibration of jet momenta may be rather different for the theoretical parton jets and the experimental hadron jets. However, it may be possible to use such an analysis to distinguish between squark-antisquark production and gluino-gluino production.

6.7 Bounding the gluino mass

Since the data may be explained in terms of squark-antisquark production, it may be possible to place a bound on the gluino mass by forcing the contribution from the Compton-like subprocess (6.13) to be small. This mechanism can give rise to as many as three visible parton jets. Fig. 14 shows the cross section for this process at $\sqrt{s}$ = 540GeV as a function of the gluino mass before and after the missing momentum cuts with a squark mass of 25GeV. In this case the dashed curves represent the cross sections for events with either two or three visible jets. For a gluino mass of 60GeV or less, it can be seen that at least O(20) 2- or 3-jet events pass the 4σ cut in p_T(missing) (in addition to the O(7) 2-jet events fron squark-antisquark production). Even allowing for the generous uncertainties in the absolute normalisation of the calculation, this is excluded by the data. Thus there is a lower bound of O(60)GeV on the gluino mass. Although the curve shown is for a squark mass of 25GeV, varying the squark mass in the range 25 - 40GeV does not change this conclusion. Unfortunately the low statistics mean that the cleaner cut of p_T(missing) $>$ 35GeV does not give a more stringent bound. The experimental confirmation of 3-jet events with p_T(missing) $>$ 35GeV would be very informative. Note that a gluino mass of O(60GeV) means that $\tilde{g}\tilde{g}$ production contributes at most O(10) events before cuts and O(2) events after cuts.

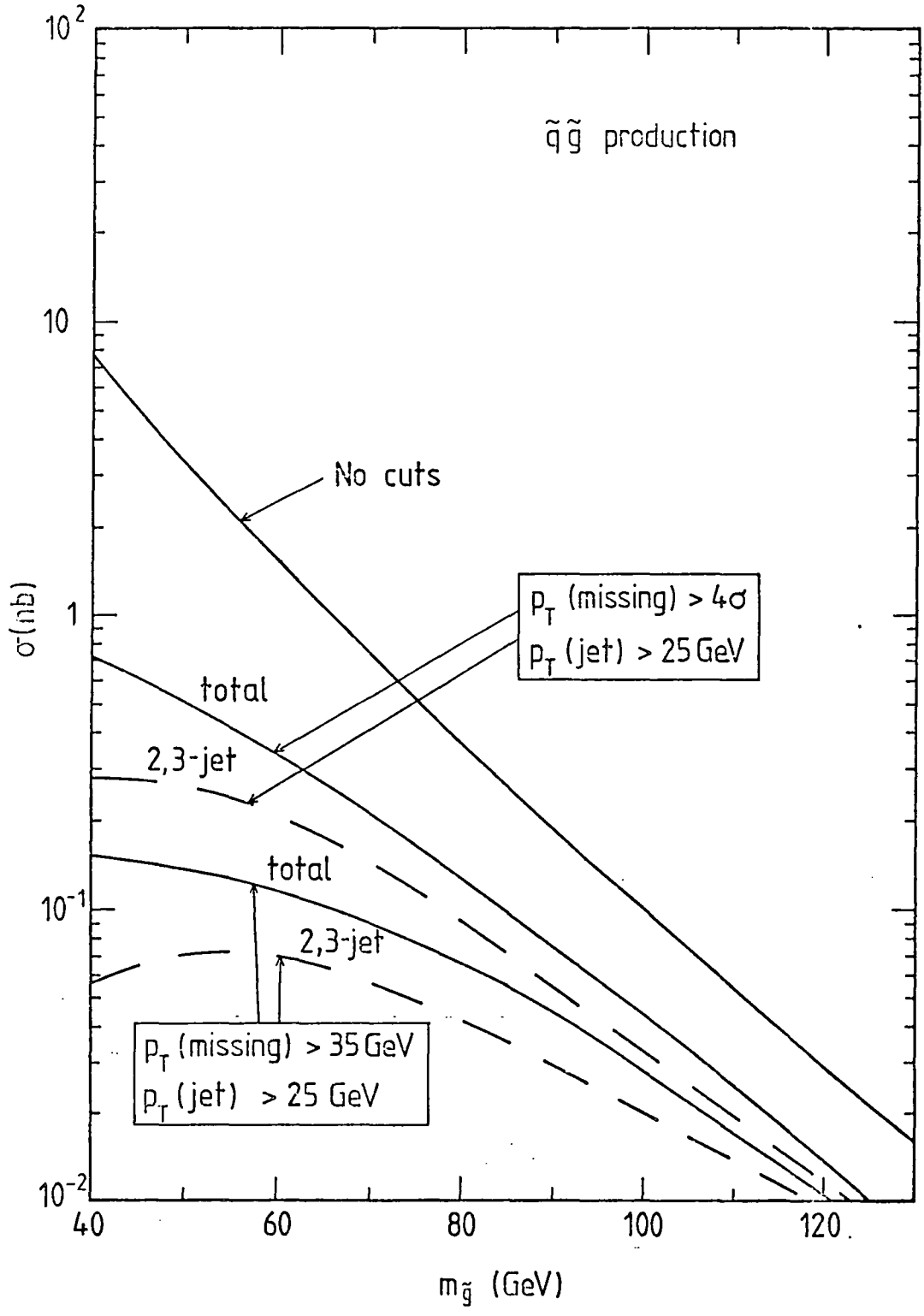

Figure 14

The $\tilde{q}\tilde{g}$ production cross section as a function of the gluino mass at $\sqrt{s}$ = 540GeV. The squark mass is taken to be 25GeV. The effect of imposing the missing p_T cuts is also shown, where the dashed curve represents the fraction of events with 2 or 3 visible jets.

6.8 Summary

In this chapter a supersymmetric scenario has been described which may account for the 1983 UA1 "monojet" events. The features of this scenario are,

(1) a light doublet of degenerate scalar and pseudoscalar quarks,

(2) a heavy gluino $m_{\tilde{g}} > m_{\tilde{q}}$,

(3) a light photino which is weakly interacting.

Contributions to events with large missing p_T accompanied by hadronic jets are dominantly from squark-antisquark production with subsequent decay to photinos,

$$q\bar{q} \text{ or } gg \rightarrow \tilde{q}\bar{\tilde{q}} \rightarrow q\bar{q}\tilde{\gamma}\tilde{\gamma}. \tag{6.36}$$

Additional processes,

$$u\bar{d} \rightarrow W \rightarrow \tilde{q}\bar{\tilde{q}}' \rightarrow q\bar{q}'\tilde{\gamma}\tilde{\gamma} \tag{6.37}$$

and,

$$qg \rightarrow \tilde{q}\tilde{\gamma} \rightarrow q\tilde{\gamma}\tilde{\gamma} \tag{6.38}$$

are also considered. By imposing the UA1 triggering requirements it is possible to generate mass bounds on the scalar quarks. Allowing for uncertainties of O(2) in the normalisation (from α_s, Λ and the structure functions) gives the bound,

$$25 < m_{\tilde{q}} < 40\text{GeV}. \tag{6.39}$$

In generating this bound the relative numbers of one and two jet events has been used to constrain the squark mass.

The gluino mass has been lower bounded by examining the process,

$$qg \rightarrow \tilde{q}\tilde{g} \rightarrow qq\bar{q}\tilde{\gamma}\tilde{\gamma} \tag{6.40}$$

which may have an appreciable rate if the gluino is not very heavy. Bearing in mind the rather large uncertainties the bound,

$$m_{\tilde{g}} > O(60GeV) \qquad (6.41)$$

is found.

If, on the other hand, the monojet events do not come from a supersymmetric source, then higher mass bounds may be found. In particular, in the scenario discussed here, requiring less than one event with p_T(missing) > 35GeV associated with a jet of p_T > 25GeV leads to the rather more restrictive bound of (see Fig. 13),

$$m_{\tilde{q}} > O(50GeV), \qquad (6.42)$$

given the uncertainties of O(2) in the cross section normalisation.

Note that in many supergravity models the soft supersymmetry breaking mass terms are universal at some large scale > 10^{16}GeV, The mass parameters can be calculated at scales $O(M_W)$ through the renormalisation group [32] and lead to relations of the form,

$$m_{\tilde{s}}^2 = m_o^2 + C_{\tilde{s}}\, m_{1/2}^2 \qquad (6.43)$$

for the scalar particle $\tilde{s}$ and,

$$m_{\tilde{f}} = C_{\tilde{f}}\, m_{1/2} \qquad (6.44)$$

for the spin-1/2 sparticle $\tilde{f}$. $C_{\tilde{s}}$ and $C_{\tilde{f}}$ are calculable coefficients [33] and m_o ($m_{1/2}$) the scalar (gaugino) mass at the supersymmetry breaking scale. There are only two free parameters and, using bounds on the right handed slepton mass (from e^+e^- experiments) and on the scalar quark mass, bounds on the other sparticle masses may be found. In particular, for light squarks of mass $m_{\tilde{q}} \sim$ 25GeV, the gluino is forced to have a mass $m_{\tilde{g}} \sim$ 16GeV which is at variance with the scenario described in this chapter. This not necessarily a problem since reliable renormalisation from 10^{16}GeV to 10^2GeV requires knowledge of all physics in those mass ranges.

References

(1) K.Wilson, Phys. Rev. D3, 1818, (1971)

(2) H.Georgi and A.Pais, Phys. Rev. D10, 539, (1974)

(3) Y.A.Gol'fand and E.P.Likhtman, Pis'ma Zh. Eksp. Teor. Fiz. 13, 323, (1971)

(4) D.Volkov and A.P.Akulov, Phys. Lett. 46B, 109, (1973)

(5) J.Wess and B.Zumino, Nucl. Phys. B70, 39, (1974); Phys. Lett. 49B, 52, (1974); Nucl. Phys. B78, 1, (1974)

(6) A.Salam and J.Strathdee, Nucl. Phys. B76, 477, (1974); ibid B80, 499, (1974)

(7) J.Wess and J.Bagger, Supersymmetry and Supergravity, Princeton University Press (1983)

(8) P.Fayet, Nucl. Phys. B90, 104, (1975)

(9) A.Salam and J.Strathdee, Nucl. Phys. B87, 85, (1975)

(10) P.Fayet and S.Ferrara, Phys. Rep. 32C, 249, (1977)

(11) G.Arnison et al., UA1 collab., Phys. Lett. 139B, 115, (1984)

(12) P.Bagnaia et al., UA2 collab., Phys. Lett. 139B, 105, (1984)

(13) S.Dawson, E.Eichten and C.Quigg, Phys. Rev. D31, 1581, (1985)

(14) P.R.Harrison and C.H.Llewellyn-Smith, Nucl. Phys. B213, 223, (1983); E:B223, 542, (1983)

(15) M.Gluck, E.Hoffmann and E.Reya, Z.Phys. C13, 119, (1982)

(16) S.Dimopoulos, S.Raby and F.A.Wilczek, Phys. Rev. D24, 1681, (1981)

(17) L.E.Ibanez and G.G.Ross, Phys. Lett. 105B, 439, (1982)

(18) M.B.Einhorn and D.R.T.Jones, Nucl. Phys. B196, 475, (1982)

(19) G.Arnison et al., UA1 collab., Phys. Lett. 122B, 103, (1983)

(20) JADE collab., reported by H.Takeda, 1983 EPS Int. Conf. on High Energy Physics, Brighton (1983)

(21) J.Ellis and H.Kowalski, Phys. Lett. 142B, 441, (1984)

(22) E.Reya and D.P.Roy, Phys. Rev. Lett. 53, 881, (1984)

(23) J.Ellis and H.Kowalski, Nucl. Phys. B246, 189, (1984); CERN report CERN-TH 4072/84, (1984)

(24) V.Barger, K.Hagiwara, W-Y.Keung and J.Woodside, Phys. Rev. Lett. 53, 641, (1984)

(25) R.M.Barnett, H.E.Haber and G.L.Kane, SLAC report SLAC-PUB-3551, (1985)

(26) A.De Rujula and R.Petronzio, CERN report CERN-TH 4070/84, (1984)

(27) M.J.Herrero, L.E.Ibanez, C.Lopez and F.J.Yndurain, Phys. Lett. 132B, 199, (1983); ibid 145B, 430, (1984)

(28) V.Barger, K.Hagiwara and W-Y.Keung, Phys. Lett. 145B, 147, (1984)

(29) H.E.Haber and G.L.Kane, Phys. Lett. 142B, 212, (1984)

(30) J.Ellis, CERN report TH-3802 (1984) and refs. therein.

(31) G.Arnison et al., UA1 collab., Phys. Lett. 129B, 273, (1983)

(32) K.Inoue, A.Kakuto, H.Komatsu and S.Takeshita, Prog. Theor. Phys. 68, 927, (1982); ibid 71, 453, (1984)

(33) C.Kounnas, A.B.Lahanas, D.V.Nanopoulos and M.Quiros, Phys. Lett. 132B, 135, (1983); Nucl. Phys. B236, 438, (1984)

Chapter Seven

Monojets and effective interactions

7.1 Introduction

The Appelquist-Carrazone decoupling theorem [1] states that low energy physics can be described without knowledge of high energy physics. In other words, the contribution of ultraviolet physics to an infrared world is small. This means that to understand the high energy regime either the small power suppressed effects that filter down to to the infrared world must be measured with high accuracy or a larger accelerator must be built to enable the observer to move towards the ultraviolet limit. One example of the former approach was the detection of the weak interaction many years before sufficient energy was obtained in hadron-hadron colliders to actually make the weak bosons.

Consider energies much beneath the weak interaction scale, where the gauge theory of $SU(3)_C \times U(1)_Q$ is a good approximation to the real world. At such energies there are certain phenomena that violate the conserved quantities of QCD and QED albeit at a low rate. For example,

a) decays of particles stable against strong and electromagnetic decay, e.g.,

$$n \rightarrow pe\nu \tag{7.1}$$

b) interactions of particles that are singlets under SU(3) x U(1), e.g.,

$$n\nu_\mu \rightarrow \mu^- X \tag{7.2}$$

c) parity violation.

Although these rates are small, because they are forbidden under QCD and QED they stand out. These interactions can be accounted for by adding four-fermion interactions to the Lagrangian, which for the process,

$$\bar{u}d \rightarrow e^-\nu, \tag{7.3}$$

shown in Fig. 1. gives the matrix element,

$$M = (4G_F/\sqrt{2})\ J_\mu^{had}\ J^{\mu+}_{lep}, \tag{7.4}$$

where,

$$\begin{aligned} J_\mu^{had} &= \bar{v}(u)\gamma_\mu((1-\gamma_5)/2)u(d), \\ J^{\mu+}_{lep} &= \bar{u}(e)\gamma^\mu((1-\gamma_5)/2)v(\nu). \end{aligned} \tag{7.5}$$

Because the fermion fields have dimension 3/2 and the Lagrangian has dimension 4, the Fermi coupling constant G_F must have dimension -2. Explicitly showing these dimensions yields,

$$G_F = \sqrt{2}g^2/8M_W^2 \tag{7.6}$$

where g is the dimensionless coupling constant of the full $SU(2)_L$ theory and M_W the mass of the mediating W boson.

Naively the cross sections from this type of interaction rises like $\hat{s}/M_W^4$ and would eventually violate unitarity (the theory is also unrenormalisable since G_F has negative dimension). However, as energy increases short distance effects become more important, the spin-1 W boson that connects the fermion currents is "seen", and the full $SU(3)_C$ x $SU(2)_L$ x $U(1)_Y$ gauge theory is required. The appropriate matrix element for (7.3) is then,

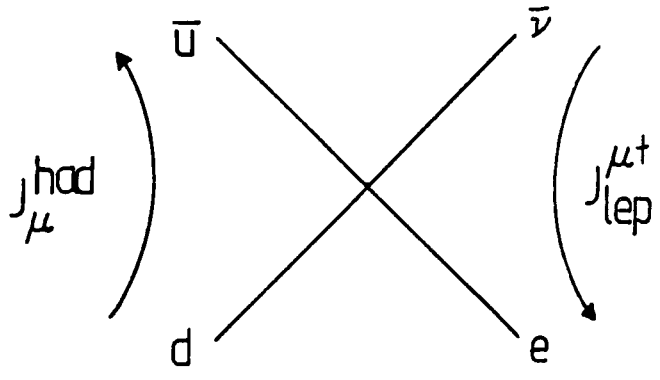

Figure 1

The Fermi four-point interaction for the process $\bar{u}d \rightarrow e^{-}\nu$.

$$M = (g^2/2)\ J_\mu^{had}\ ((-g^{\mu\nu} + W^\mu W^\nu/M_W^2)/(\hat{s}-M_W^2))J_\nu^{+lep}, \qquad (7.7)$$

where $\sqrt{\hat{s}}$ is the centre of mass energy and W_μ the four momentum of the W boson as shown in Fig. 2. Clearly in the limit $\hat{s} \ll M_W^2$, this reduces to (7.4).

It is possible that there are interactions beyond the Standard Model at scales Λ much larger than the weak scale. This gives rise to the obvious question, can such interactions be seen at the collider? Since there are few exact conservation laws remaining (colour, charge, baryon and lepton numbers) and these are either known to be conserved to high accuracy [2-6] or the result of unbroken local gauge invariance, new effective interactions could be looked for in processes in which the Standard Model predicts small cross sections. Cross sections predicted by the Standard Model die like $1/\hat{s}$, whilst those from effective interactions are proportional to $\hat{s}$ raised to some power that depends on the dimension of the interaction.

Hikasa [7] has suggested that effective interactions could give sizeable contributions to processes such as $q\bar{q} \rightarrow Zg$ or $gg \rightarrow \gamma g$ from operators with dimension 7 and 8 respectively. Because the cross section rises like $\hat{s}^2$ and $\hat{s}^3$ respectively these interactions favour high p_T events. It therefore seems reasonable to ask whether the "monojet" events found by UA1 [8] or the W + jet events of UA2 [9] originate from higher dimensional effective interactions with scale $\Lambda \gg 100GeV$. In this scenario the monojets occur when a high p_T Z recoiling against a coloured parton decays into two unseen neutrinos. The Standard Model contributions to boson + jet production at high p_T are shown in Figure 3. The cross sections die very steeply with increasing p_T and give far too few $Z \rightarrow \nu\bar{\nu}$ events to account for the

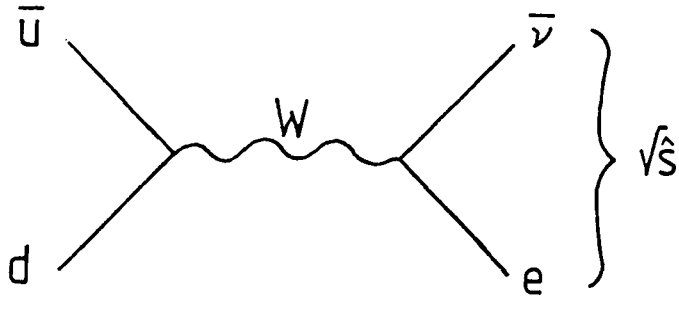

Figure 2

The intermediate vector boson interaction for the process $\bar{u}d \rightarrow e^{-}\nu$.

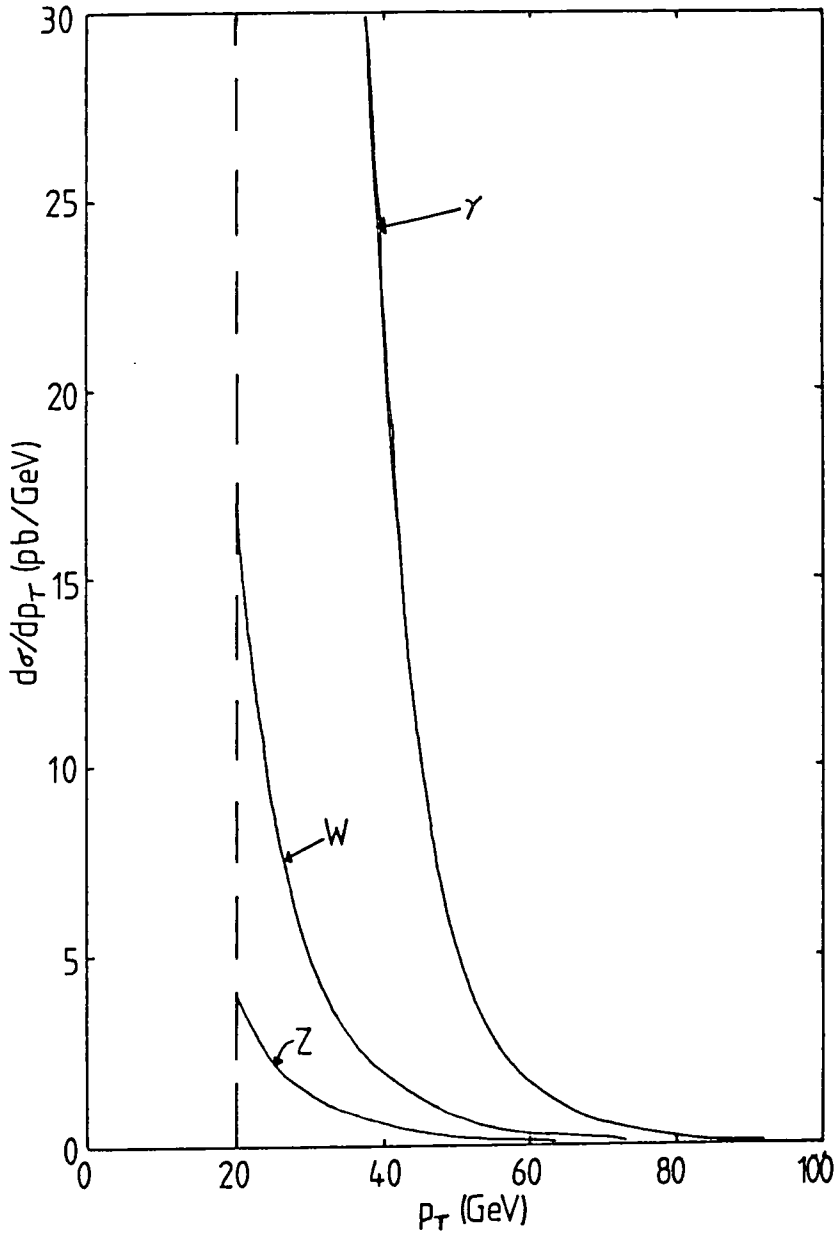

Figure 3

The p_T distribution for boson + jet production through the lowest order Standard Model process $qg \rightarrow Vq$, where V = W, Z or γ, at $\sqrt{s}$ = 540GeV. (The crossed processes are included). A p_T cut of 20GeV/c has been imposed since for low p_T, higher order processes are important.

data.

At scales larger than the weak scale, $SU(3)_C \times SU(2)_L \times U(1)_Y$ is an exact symmetry. Therefore, new interactions at scales $\Lambda \gg 100GeV$ must be gauge invariant under SU(3) x SU(2) x U(1). In the next section higher dimensional operators (dimension = 6,8), which lead to Z + jet production, are constructed which are gauge invariant under the SU(3) x SU(2) x U(1) group. The way the $SU(2)_L \times U(1)_Y$ symmetry groups are related through the symmetry breaking to $U(1)_Q$ leads to relations between W + jet, Z + jet and γ + jet production rates. By fitting the observed UA1 monojet rate to the Z + jet production cross section bounds on the couplings of the new effective interactions are found.

7.2 Effective interactions and V + jet production

New effective interactions may give rise to processes of the form,

$$q\bar{q} \rightarrow Vg, \tag{7.8}$$

$$gg \rightarrow Vg, \tag{7.9}$$

where $V = \gamma$, Z, W (γ, Z) for 7.8 (7.9). Throughout this work the assumption that such effective interactions are $SU(3)_C \times SU(2)_L \times U(1)_Y$ invariant is made.

The fields V_μ, G_μ^a describing the vector boson V, gluon have dimension 1 whereas the quark fields, q, have dimension 3/2. To describe the interaction 6.8 (6.9) the effective Lagrangian must contain operators that have dimension $\geq$ 5 (4). As well as the quark and boson fields, the operators can contain the Higgs field, φ, which

has dimension 1, the covariant derivative, D_μ, formed from all the gauge fields, also dimension 1, and the field strength tensors $V_{\mu\nu}$, $G_{\mu\nu}{}^a$ which have dimension 2. As usual $B_{\mu\nu}$ is the $U(1)_Y$ gauge field strength tensor, which decomposes into Z and γ field strength tensors, and $W_{\mu\nu}{}^i$ the triplet of $SU(2)_L$ gauge field strength tensors. T^a (colour label a =1,8) and T^i (weak isospin label i=1,3) are the SU(3) and SU(2) generators respectively.

The operator of lowest dimension that is gauge invariant has dimension 6 and is [10],

$$G_0\bar{q}\not{D}\sigma_{\mu\nu}qB^{\mu\nu} \tag{7.10}$$

where the coupling constant G_0 is of dimension Λ^{-2}. The four particle interaction, $q\bar{q}Vg$, arises when the covariant derivative is expanded in terms of the gauge fields thus allowing a gluon field to couple to the $q\bar{q}V$ part of the operator. However there is also a three particle $q\bar{q}V$ interaction that arises when the ∂_μ part of the derivative is considered and this contributes to the Z width. The matrix element for the $q\bar{q}V$ interaction is,

$$-iM = iG_0\sin\theta_W\, u(q)\not{Z}[\not{Z},\gamma^\beta]\delta_{ij}v(q)\varepsilon_\beta(Z) \tag{7.11}$$

where the $\sin\theta_W$ comes from rewriting the B field in terms of Z and A fields, δ_{ij} is the colour requirement on the quarks and the particle labels represent their four momenta. Squaring the amplitude and summing over all spins gives,

$$\Sigma|M|^2 = 48G_0{}^2\sin^2\theta_W M_Z{}^6. \tag{7.12}$$

The contribution to the Z width is thus,

$$\Gamma(Z \rightarrow q\bar{q}) = G_0{}^2\sin^2\theta_W M_Z{}^5/\pi. \tag{7.13}$$

Interference effects and the masses of final state particles have been

ignored. Assuming five flavours and requiring that the total width from this interaction be less than 6.5GeV [11], gives the bound

$$G_0^2 < 2 \times 10^{-9}\ \text{GeV}^{-4}. \tag{7.14}$$

As a consequence the contributions to $q\bar{q} \rightarrow Vg$ from this term are essentially unobservable at the CERN collider since the cross section is much too small.

Hikasa [7] gives dimension 7 operators like,

$$\bar{q}T^a q G_{\mu\nu}{}^a F^{\mu\nu}, \tag{7.15}$$

for γ + jet production which satisfy $SU(3)_C \times U(1)_Q$ invariance. In this case the effective coupling for $q\bar{q} \rightarrow \gamma g$ has dimension Λ^{-3}. However, this form of effective interaction is not SU(3) x SU(2) x U(1) invariant since the right- and left-handed quarks transform differently under the full SU(3) x SU(2) x U(1) group. Effective operators of dimension 7 are therefore ignored.

The next lowest dimension gauge invariant operator is of dimension 8. Omitting Higgs fields for the moment, the general forms of the dimension 8 operators for processes (7.8) are,

$$G_1/\cos\theta_W\ (\bar{q}T^a k_\lambda \Gamma^{\lambda\mu\nu\varrho\sigma} \gamma q)\ B_{\mu\nu} G_{\varrho\sigma}{}^a, \tag{7.16}$$

$$G_2/\sin\theta_W\ (\bar{q}T^a k_\lambda \Gamma^{\lambda\mu\nu\varrho\sigma} T^i q)\ W_{\mu\nu}{}^i G_{\varrho\sigma}{}^a, \tag{7.17}$$

where $\bar{q}\Gamma q$ are the usual bilinear covariants and where the general Lorentz structure of the dimensionless Γ ensures overall Lorentz invariance. To satisfy $SU(2)_L$ invariance the quark and antiquark fields must transform in the same manner under $SU(2)_L$. This forces Γ to be the product of an odd number of Dirac matrices since otherwise the product $\bar{q}_L \Gamma q_L$ or $\bar{q}_R \Gamma q_R$ is zero. The momentum k_λ is inserted to

absorb the extra Lorentz index.

Similarly, in the case of the subprocess,

$$gg \rightarrow Vg, \tag{7.18}$$

the lowest dimension operator is again dimension 8 and is,

$$G_3 d^{abc} C^{\kappa\lambda\mu\nu\varrho\sigma\tau\omega} G_{\kappa\lambda}{}^{a} G_{\mu\nu}{}^{b} G_{\varrho\sigma}{}^{c} B_{\tau\omega}, \tag{7.19}$$

where C is dimensionless and has the general Lorentz structure to preserve overall invariance. The couplings $G_{1,2,3}$, of the new effective interactions have dimension Λ^{-4}.

The general form of the cross section for (7.8) can be calculated from (7.16) and (7.17) by noting that the invariant amplitude squared is linear in the fermion momenta k_1, k_2, quadratic in the gluon and V momenta, k_3 and p respectively and quadratic in k of (7.16) and (7.17) which is a general linear combination of k_i. There are 17 possible combinations of these 4 momenta which, in terms of the Mandelstam variables, $\hat{s}$, $\hat{t}$, $\hat{u}$ of the $q\bar{q} \rightarrow Vg$ subprocess, simplifies to,

$$\begin{aligned} \Sigma|M|^2 = 4G_V{}^2 \, (&\alpha_1 \hat{s}(\hat{s} - M^2)^2 + \alpha_2 \hat{s}^2 \hat{t}\hat{u} + \alpha_3 \hat{t}^2 \hat{u}^2 \\ &+ \alpha_4 M^2 \hat{s}(\hat{s} - M^2)^2 + \alpha_5 M^2 \hat{s}\hat{t}\hat{u} + \alpha_6 M^4 \hat{t}\hat{u}) \end{aligned} \tag{7.20}$$

where M is the mass of the V boson and α_i are unknown coefficients. The factor of 4 comes from the trace over the colour matrices T^a. The expression for the subprocess $qg \rightarrow Vq$ is obtained by crossing $\hat{s}$ and $\hat{t}$ and multiplying by -1 on account of the interchange of fermion and boson legs. In terms of G_1 and G_2 the couplings G_V are given by,

$$\begin{aligned} G_W &= G_2/(\sqrt{2}\sin\theta_W) \\ G_Z &= \cot\theta_W \, T^3 \, G_2 - \tan\theta_W \, Y \, G_1 \\ G_\gamma &= T^3 \, G_2 + Y \, G_1, \end{aligned} \tag{7.21}$$

where $T_3 = \pm 1/2$ for q = u, d and Y is the quark hypercharge. G_1 and G_2 are arbitrary coefficients, however choosing $G_1 = G_2$ makes the coupling of the photon proportional to the fermion charge,

$$G_\gamma = G_1 Q. \tag{7.22}$$

The assumption $G_1 = G_2$ is made throughout, however other choices are possible and will change the relative (W + jet):(Z + jet):(γ + jet) rates though not the overall conclusions.

Similarly for $gg \rightarrow Vg$, with V = Z, γ, the general form for the squared matrix elements is quadratic in each of the boson momenta. The seven terms that can be formed reduce to the general form,

$$\Sigma|M|^2 = 40fG_3^2/3\ (\beta_1\hat{s}(\hat{s} - M^2)\hat{t}(\hat{t} - M^2) + \beta_2\hat{s}^2(\hat{s} - M^2)^2$$
$$+ \beta_3 M^2\hat{s}\hat{t}\hat{u} + (\hat{s} \leftrightarrow \hat{u}) + (\hat{t} \leftrightarrow \hat{u})) \tag{7.23}$$

which is symmetrical in $\hat{s}$, $\hat{t}$, $\hat{u}$ and has three unknown coefficients β_i. factor 40/3 comes from the colour trace and $f = \sin^2\theta_W, \cos^2\theta_W$ for V = Z, γ respectively.

From (7.20) and (7.23) it follows that the cross sections for the subprocess $q\bar{q} \rightarrow Vg$ and $gg \rightarrow Vg$ behave like,

$$\sigma \backsim G_i^2\,\hat{s}^3 \backsim \hat{s}^3/\Lambda^8 \tag{7.24}$$

for $M^2 \ll \hat{s} \ll \Lambda^2$. These cross sections will ultimately violate unitarity as the interactions are non-renormalisable but only at energies $\sqrt{\hat{s}} \backsim O(\Lambda)$ where the low energy form is no longer valid.

The new effective interaction allows additional weak boson decays, namely $Z,W \rightarrow q\bar{q}g$ and $Z \rightarrow ggg$. For decays to three body massless final states, the width can be expressed as an integral over two variables,

$$\Gamma = \frac{1}{256\pi^3 M^3} \int_0^{M^2} \int_0^{M^2-\hat{t}} d\hat{t}d\hat{u}\ \Sigma|M(\hat{s},\hat{t},\hat{u})|^2 \qquad (7.25)$$

where $\hat{s}$, $\hat{t}$, $\hat{u}$ are the squared combinations of final state momenta. Inserting (7.20) and (7.23) into (7.25) gives,

$$\Gamma(Z,W \to q\bar{q}g) = \frac{G_V^2 M^9}{384\pi^3}\left[\frac{\alpha_1}{15} + \frac{\alpha_2}{180} + \frac{\alpha_3}{90} + \frac{\alpha_4}{10} + \frac{\alpha_5}{60} + \frac{\alpha_6}{12}\right] \qquad (7.26)$$

$$\Gamma(Z \to ggg) = \frac{5G_3^2 M^9 \sin^2\theta_W}{576\pi^3}\left[\frac{\beta_1}{72} + \frac{\beta_2}{60} + \frac{\beta_3}{120}\right] \qquad (7.27)$$

For values of $G_i^2 \sim O(10^{-16})GeV^{-4}$ and α_i, $\beta_i \sim O(1)$ these widths are a few keV, and there is no appreciable contribution to the Z width.

The $p\bar{p} \to V$ + jet cross sections are calculated with the parton densities of Gluck et al. [12]. As an illustration of V + jet production at $\sqrt{s}$ = 540GeV resulting from the sum of $q\bar{q} \to Vg$ and $qg \to Vq$ processes two sets of the α_i coefficients of (7.20) are used,

(A) $\alpha_1 = 0$, $\alpha_2 = 1/4$, $\alpha_3 = -1/2$, $\alpha_4 = 1/8$, $\alpha_5 = -3/4$, $\alpha_6 = 1/4$ (7.28)

(B) $\alpha_2 = 1$, $\alpha_i = 0$ for $i \neq 2$. (7.29)

These choices correspond to the qg (and $\bar{q}g$) initiated reactions dominating in the case of set (A), and the $q\bar{q}$ subprocess dominating for set (B), and so span the range of possibilities. The predictions can then be compared with those resulting from the gg $\to$ Vg subprocess with the choice of the β_i coefficients of (7.23),

(C) $\beta_1 = -1$, $\beta_2 = 5/4$, $\beta_3 = 1/2$. (7.30)

In Figs. 4 and 5 the V + jet invariant mass distributions (V =

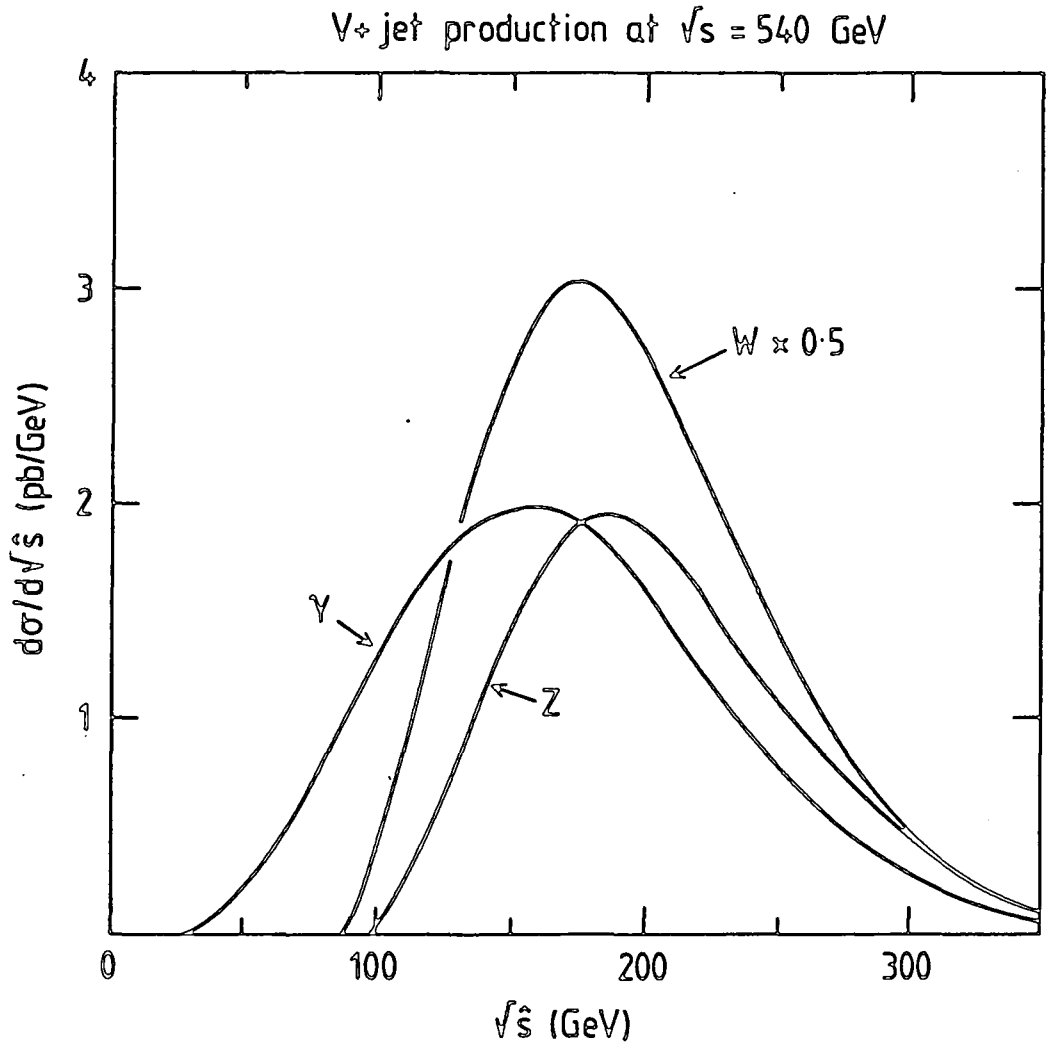

Figure 4

The V + jet invariant mass distributions at $\sqrt{s}$ = 540GeV resulting from using set (A) of the α_i coefficients of 7.28, with Z production normalised to approximately the UA1 monojet rate.

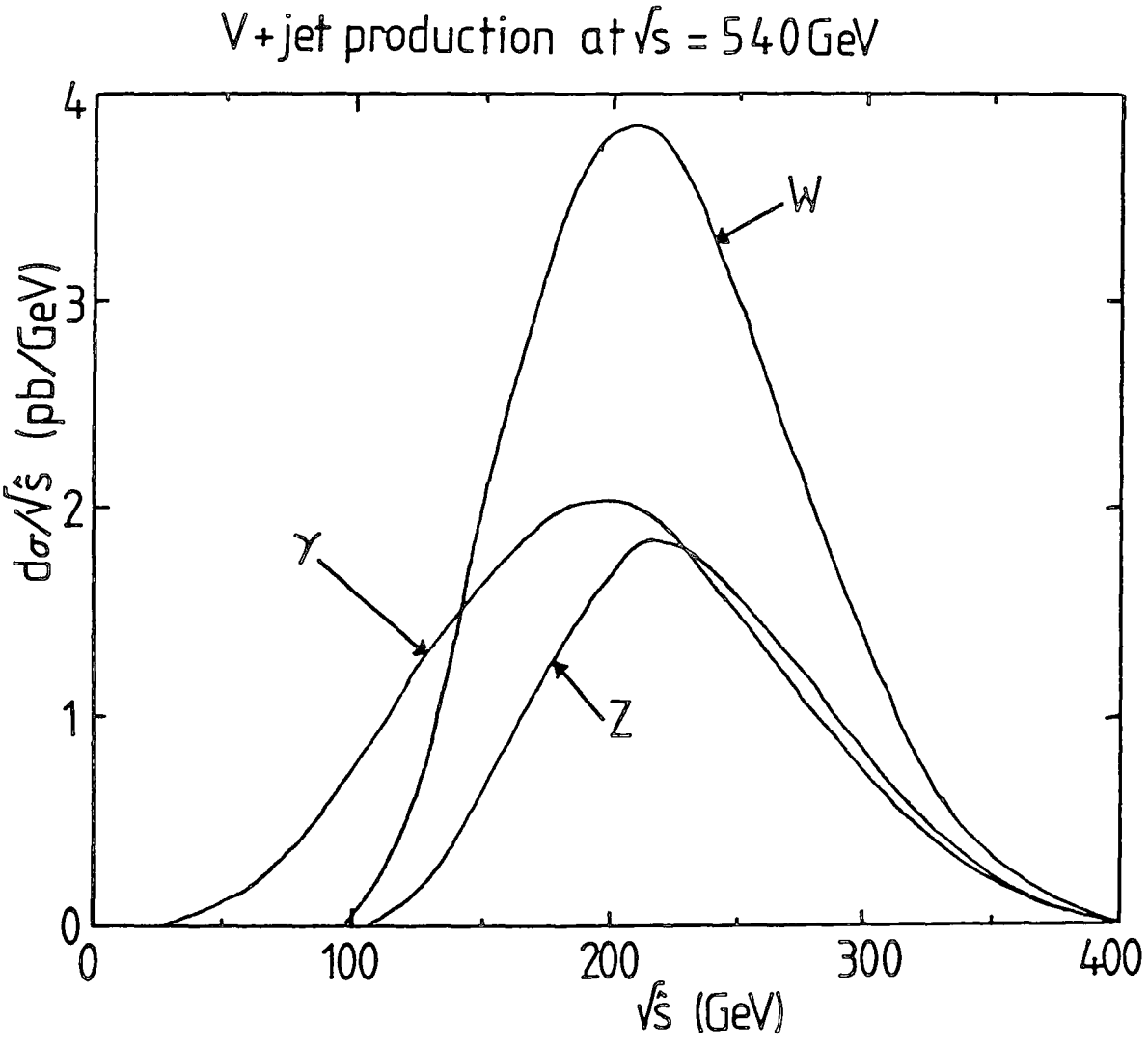

Figure 5

The V + jet invariant mass distributions at $\sqrt{s}$ = 540GeV resulting from using set (B) of the α_i coefficients of 7.29, with Z production normalised to approximately the UA1 monojet rate.

Z, W, γ) are compared for the two sets of the α_i coefficients. The general features evident from these distributions are first the broad peaks in the V + jet invariant mass around $\sqrt{\hat{s}}$ = 200GeV. This peaking arises from the convolution of the rapidly rising parton cross sections and the steeply falling parton luminosities. The V + jet invariant mass peaks for the $q\bar{q}$ dominated processes, Fig. 5, are at larger values of $\sqrt{\hat{s}}$ than in the qg dominated case, Fig. 4, as expected from the different x dependences of the quark and gluon structure functions. Correspondingly the peaks in the gg initiated process occur at even lower $\sqrt{\hat{s}}$.

Using, as an example, set (A) of the α_i coefficients the p_T distributions of the V + jet events are shown in Fig. 6. Again the distributions are broad, with peaks in the range p_T = 40 to 80 GeV. The branching ratios for the W and Z decays have been folded in. Fig. 7 compares the p_T distributions of ($Z \rightarrow \nu\bar{\nu}$ + jet) events arising from each of the $q\bar{q}$, qg and gg initiated subprocesses. The effect of the parton densities in shifting the peak is clearly visible. All these curves correspond to the choice $G_1 = G_2$ in (7.21). Although other choices of G_1/G_2 alter the relative W, Z and γ production rates, high p_T γ + jet events are an unavoidable consequence of the effective interaction. Of course, if only G_3 were non-zero, there would be no W production but only $gg \rightarrow Zg, \gamma g$. The normalisation of these contributions has been fixed so that the ($Z \rightarrow \nu\bar{\nu}$) + jet cross section is 50 pb, ie. for an integrated luminosity of around 100 nb^{-1}, about 5 such events are expected. Turning back to the dimension 6 interaction, (7.10), the bound on G_0^2 obtained from the Z width leads to contributions at least two orders of magnitude smaller than this.

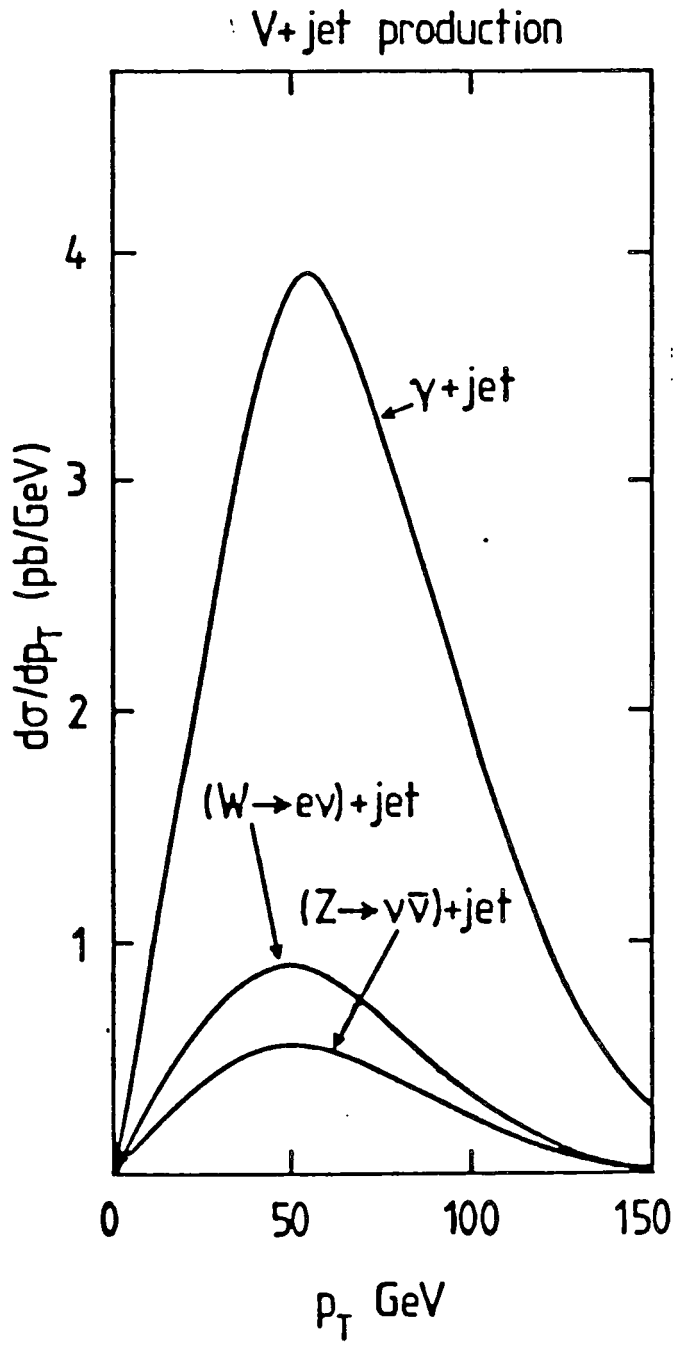

Figure 6

The V (V = W, Z, γ) boson (or jet) p_T distributions at $\sqrt{s}$ = 540GeV normalised as in Fig. 4 and multiplied by the branching ratios for the decays indicated. Set (A) of the α_i coefficients has been used corresponding to qg dominated V + jet production.

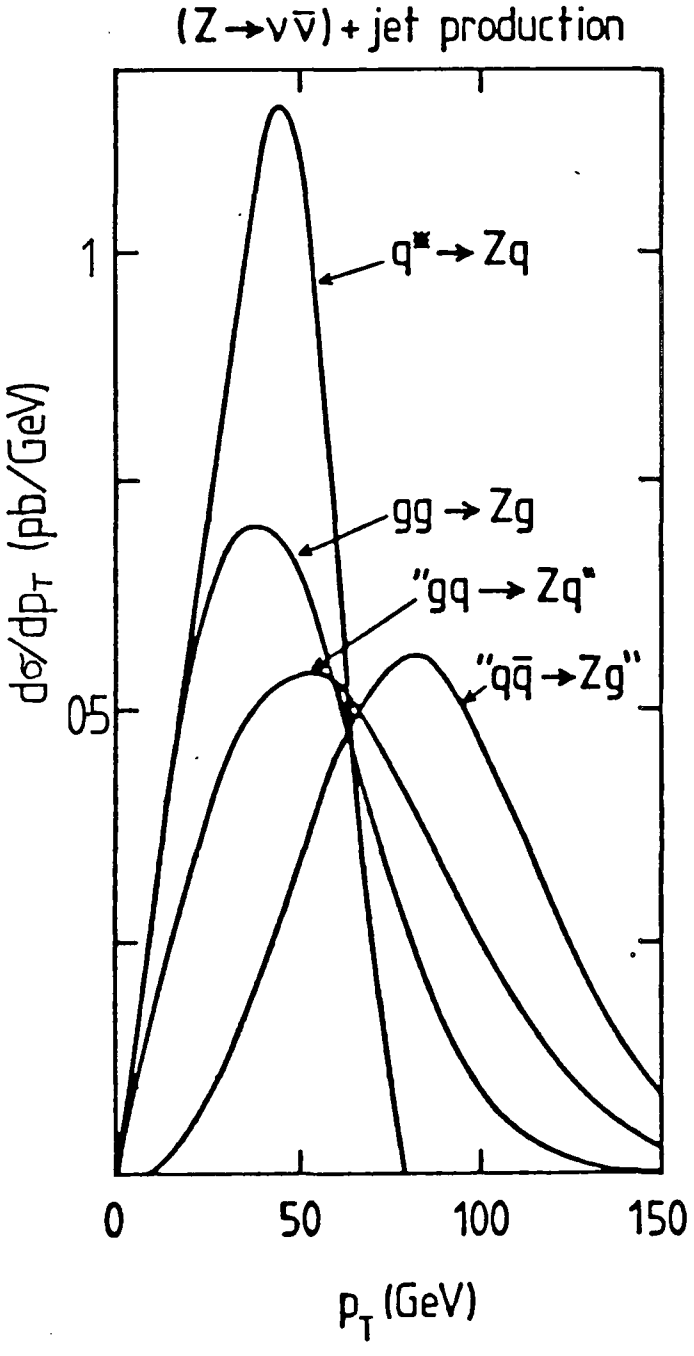

Figure 7

The Z (or jet) p_T distributions at $\sqrt{s}$ = 540GeV normalised as in Fig. 4 and multiplied by the branching ratios for the decay $Z \to \nu\bar{\nu}$ for qg (set A), $q\bar{q}$ (set B) and gg (set C) initiated reactions, together with that resulting from the decay of an excited quark of mass 160GeV, $q^* \to Zq$.

The inclusion of a Higgs doublet, φ, will allow a dimension 8 interaction of the form,

$$G_4 \bar{q}_R \varphi^+ T^a q_L G_{\mu\nu}{}^a B^{\mu\nu} \tag{7.31}$$

in addition to those of (7.16),(7.17) and (7.19). By making the replacement,

$$\varphi = v/\sqrt{2} + h, \tag{7.32}$$

where v is the vacuum expectation of the Higgs field, φ, a $q\bar{q} \rightarrow Vg$ interaction is formed. The invariant amplitude squared is thus quadratic in v and cubic in the subprocess invariants,

$$\Sigma|M|^2 = 4f(v/\sqrt{2})^2 G_4{}^2 \hat{s}(\hat{s} - M^2)^2/2, \tag{7.33}$$

where the 4 is a colour factor and $f = \sin^2\theta_W$, $\cos^2\theta_W$ for Z, γ respectively. The contribution to the Z width from this process is,

$$\Gamma(Z \rightarrow q\bar{q}g) = G_4{}^2 \sin^2\theta_W v^2 M_Z{}^7/(5120\pi^3), \tag{7.34}$$

which is small for values of G_4 that fit the monojet rate. This process is $q\bar{q}$ dominated and predicts curves very similar to those shown for the Z in Fig. 5. The relative rate of γ + jet events to $(Z \rightarrow \nu\bar{\nu})$ + jet events is approximately 30:1 for this interaction.

Although illustrated for the CERN collider, the V + jet evidence of a new interaction applies equally well to higher energies, except that the maxima in the distributions of Figs. 4 and 5 move to higher $\sqrt{\hat{s}}$ and consequently lead to higher p_T events. For instance at $\sqrt{s}$ = 2TeV the maxima would occur at $\sqrt{\hat{s}} \sim$ 600GeV.

The V + jet event rate is determined by the couplings of the effective interaction, which may be written

$$G_i \sim g^2/\Lambda^4 \tag{7.35}$$

where Λ and g are the analogues of the mass and couplings of the gauge bosons (c.f.(7.6)). For the results shown, the overall normalisations correspond to,

$$\begin{aligned} G_1 = G_2 &\sim 5 \times 10^{-8}\text{GeV}^{-4} \quad \text{for set (A); "qg} \rightarrow \text{Vq"} \\ G_1 = G_2 &\sim 3 \times 10^{-8}\text{GeV}^{-4} \quad \text{for set (B); "q}\bar{\text{q}}\text{"} \rightarrow \text{Vg"} \\ G_3 &\sim 15 \times 10^{-8}\text{GeV}^{-4} \quad \text{for set (C); "gg} \rightarrow \text{Vg"} \end{aligned} \tag{7.36}$$

while to obtain the correct rate for (7.31) requires,

$$G_4 \sim 3 \times 10^{-8}\text{GeV}^{-4}. \tag{7.37}$$

Setting $G_1 \neq G_2$ does not change the magnitude of the coupling significantly. For reasonable couplings g, i.e. O(1), all of these require Λ to be as small as 100GeV, which is contrary to the initial assumption that $\Lambda \gg M_Z$. There do, however, exist examples, where the naive coupling is dynamically enhanced, as in the case of the $\Delta I = 1/2$ rule for weak decays.

Therefore, unless there is a dynamical enhancement of the coupling, new terms in the effective Lagrangian of dimension < 9 are unable to account for the UA1 monojet data through Z + jet production. The energy regime of the new physics has already been entered and propagator effects, hitherto ignored, must be included. So if monojets are a sign of high p_T Z + jet production, they must come from the production and decay of new heavy objects, X, of mass O(150GeV), for example,

$$qg \rightarrow X \rightarrow Zq \tag{7.38}$$

$$gg,\ q\bar{q} \rightarrow X \rightarrow Zg. \tag{7.39}$$

In the next section, the production of such heavy objects is considered and section 7.4 takes a particular case, namely that of excited quarks, as an example.

7.3 Production of large mass objects

In terms of the differential luminosity (see Chapter 2) the production cross section for single massive particle (X) production in $p\bar{p}$ collisions (in the narrow width approximation) is,

$$\sigma(p\bar{p} \rightarrow X + \text{anything}) = (2J + 1)n_c \sum_{ij} \Gamma(X \rightarrow ij) \frac{4\pi^2}{M^3} C_{ij} \tau \frac{dL_{ij}}{d\tau} \qquad (7.40)$$

where $\Gamma(X \rightarrow ij)$ is the partial width for X decay to the partons i and j. C_{ij} is a colour factor depending on the colour of the initial partons, $C_{q\bar{q}} = 1/9$, $C_{qg} = 1/24$ etc. J is the X particle spin and n_c its colour degrees of freedom. M is the X particle mass and $\tau = M^2/s$. From 7.40 it can be seen that for a particular channel at fixed mass, the total cross section is proportional to $(2J + 1)n_c\Gamma(X \rightarrow ij)$. That is, the rate of X production depends on the spin and colour degrees of freedom and on the decay width (or coupling) to the partons it is produced from. Because the differential luminosities are small at large mass values (see Fig. 8 or 9 from Chapter 2) it is difficult to generate a large cross section unless the product $(2J + 1)n_c\Gamma(X \rightarrow ij)$ is large. Therefore, intermediate states of large spin, colour degrees of freedom or couplings are possible candidates for producing monojets if the branching ratio into Z + jet is significant.

Many different models have been proposed for the production of new heavy particles with mass O(160)GeV whose decays include Z + jet channels. For example,

i) Odoronia [13]

ii) coloured mesons [14]

iii) coloured W and Z bosons [15]

iv) excited quarks [16-18].

These models all make use of colour or spin enhancements to generate a large enough cross section to explain the monojet events. Furthermore, because of the two-body decay to Z + jet, there is a Jacobian peak in the Z transverse momentum and it is easier to explain events with high missing p_T than in the Standard Model.

In the next section, the excited quark model [16-18] is taken as an example of intermediate particle production (at large mass) with interactions that are invariant under $SU(3)_C$ x $SU(2)_L$ X $U(1)_Y$ transformations.

7.4 Excited quarks - an example

The existence of massive excited quarks, q^*, could lead to monojet events through the process,

$$qg \rightarrow q^* \rightarrow Zg. \qquad (7.41)$$

To give production cross section that are as large as possible two excited states with up and down flavours are considered. These excited states can couple to both the gluons and the electroweak bosons. A phenomenological analysis is possible if the excited quarks are put in SU(3) x SU(2) x U(1) multiplets and an effective Lagrangian constructed. If SU(3) x SU(2) x U(1) is an exact symmetry then the colour and electroweak currents are conserved and because of the mass difference between the excited quarks and the ordinary quarks the interactions must be of the transition magnetic moment variety.

The simplest case is for the excited quarks to be colour triplets

and weak isodoublets. In this case the mass can be generated from interactions at a preon level as in composite models. Because the mass term in the Lagrangian must be gauge invariant it is,

$$L_{mass} = Mq_L^* q_R^* + h.c. \tag{7.42}$$

and the left- and right-handed excited quarks have the same weak isospin and hypercharge. The effective Lagrangian is,

$$\begin{aligned} L_{eff} = {} & (g_s f_s/M)(\bar{q}_R^* \sigma_{\mu\nu} g^\nu T^a q_L) G^{\mu a} \\ & + (gf/M)(\bar{q}_R^* \sigma_{\mu\nu} w^\nu T^i q_L) W^{\mu i} \\ & + (g'f'/M)(\bar{q}_R^* \sigma_{\mu\nu} b^\nu Y q_L) B^\mu + h.c. \end{aligned} \tag{7.43}$$

where the boson momenta are represented by small letters, the f's are dimensionless transition magnetic moments and M is the excited quark mass. Interactions involving the left-handed quarks do not occur since they transform differently from the weak singlet q_R's. Note that the presence of an even number of Dirac matrices between the spinors forces the interaction to mix left- and right-handed states. As noted by Refs. 16,18 this is a new source of parity violation, though since large excited quark masses are involved this will be a small effect. Rewriting the W and B fields in terms of the physical gauge fields yields,

$$L_{eff} = \Sigma\, (ef_V/M)(\bar{q}_R^* \sigma_{\mu\nu} v^\nu q_L) V^\mu + \text{col. ints.} + h.c. \tag{7.44}$$

where the f_V couplings are given by,

$$\begin{aligned} f_\gamma &= T^3 f + Yf' \\ f_W &= f/(\sqrt{2}\sin\theta_W) \\ f_Z &= \cot\theta_W\, T^3 f - \tan\theta_W\, Yf'. \end{aligned} \tag{7.45}$$

where T^3 and Y are the diagonal generators of the $SU(2)_L$ and $U(1)_Y$

groups respectively.

The Feynman rules for excited quark interactons are easily extracted and the cross section for excited quark production and decay calculated. The relevant process is,

$$q(p) + g(k) \rightarrow q(p') + V(k'), \tag{7.46}$$

where V is the produced vector boson and the brackets define the particle momenta. The s channel diagram, see Fig. 8, is the dominant contribution and the matrix element is,

$$\begin{aligned} -iM = {} & \varepsilon_\mu^*(k')\bar{u}(p')_L(-i(ef_V/M)\sigma_{\mu\nu}k'^\nu) \\ & \times i(\not{k}+\not{p}+M)/(\hat{s} - M^2 + i\Gamma M) \\ & \times (-i(g_s f_s/M)\sigma_{\alpha\beta}k^\beta T^a)u(p)_L\varepsilon_\alpha(k) \end{aligned} \tag{7.47}$$

The left-handed nature of the excited quark spinors kills the M term in the numerator of the propagator. Squaring and averaging gives,

$$\Sigma|M|^2 = \frac{8\alpha\alpha_s f_V^2 f_s^2 \pi^2}{3M^4} \; \frac{\hat{s}^2(M^2\hat{t} - 2(\hat{s} - M^2)(\hat{u} - M^2))}{(\hat{s} - M^2)^2 + \Gamma^2 M^2} \tag{7.48}$$

and,

$$\frac{d\hat{\sigma}}{d\hat{t}} = \frac{\alpha\alpha_s f_V^2 f_s^2 \pi}{6M^4} \; \frac{(M^2\hat{t} - 2(\hat{s} - M^2)(\hat{u} - M^2))}{(\hat{s} - M^2)^2 + \Gamma^2 M^2} \tag{7.49}$$

If the u channel diagram is included and the $\hat{s} \ll M^2$ limit taken, then this cross section reduces to the general form (7.20) with the α_i coefficients of set (A).

Similarly the decay widths may be computed. The amplitude for excited quark decay to V + q is,

$$-iM = \bar{u}(q)_L \; (-i(ef_V/M)\sigma_{\mu\nu}V^\nu) \; u(q^*)_R\varepsilon^{\mu *}(V) \tag{7.50}$$

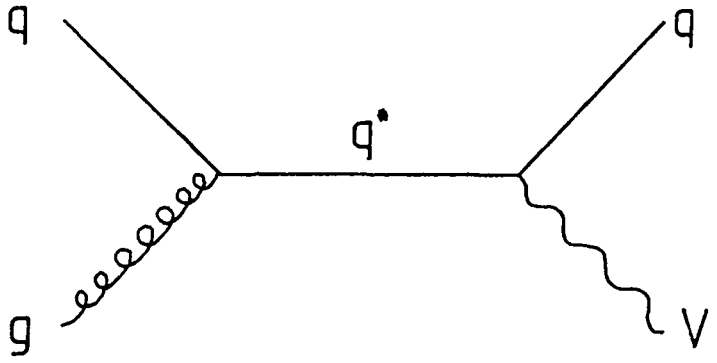

Figure 8

The $\hat{s}$ channel diagram for excited quark production and decay.

which leads to the squared matrix elements,

$$\Sigma|M|^2 = (2e^2 f_V^2/M^2)\ (4V.q\ V.q^* - m_V^2 q.q^*) \qquad (7.51)$$

where particle labels represent their 4 momenta. The resulting width is,

$$\Gamma(q_R^* \to Vq_L) = \alpha f_V^2/2\ M(1 - x)^2(1 + x/2) \qquad (7.52)$$

where $x = M_V^2/M^2$. The width for the decay to gluons is easily obtained,

$$\Gamma(q_R^* \to gq_L) = 2\alpha_s f_s^2 M/3. \qquad (7.53)$$

The left-handed excited quark widths are all zero. To obtain sufficient Z + jet production the width of the excited quark must be quite large. In fact, the couplings are taken to be,

$$f_s = 2.8,\ f = f' = 5 \qquad (7.54)$$

which are not yet excluded [19]. These lead to the excited quark decay widths, for M = 160GeV,

Γ	$q^* = u^*$	$q^* = d^*$
$q^* \to qg$	$\sim$ 40GeV	$\sim$ 40GeV
$q^* \to Wq$	4.5GeV	4.5GeV
$q^* \to Zq$	2.6GeV	3.8GeV
$q^* \to \gamma q$	3.2GeV	0.8GeV

i.e. total excited quark widths of around 50GeV. This is somewhat lower than Barger et al. [19] obtain since the branching ratio to Z + jet is lower in their calculation. The p_T spectrum of the electroweak

bosons is shown in Fig. 9. The Jacobian peak is still in evidence, though it is displaced from the naive expectation,

$$p_T(\text{peak}) = (M^2 - m_V^2)/(2M), \qquad (7.55)$$

to a lower value of p_T because of the large width of the q^*.

Figure 7 compares the missing p_T distribution from this source with the curves from the effective interactions. Clearly, for massive particles with higher spin and colour factors, the required rate can be obtained with smaller widths and will give a more striking Jacobian peak. One difference between the effective interaction approach and the intermediate particle approach is that the missing p_T peaks due to effective interactions will move as the machine energy changes whereas a new massive particle will give a peak at a given value of missing p_T independent of energy.

7.5 Summary

By introducing SU(3) x SU(2) x U(1) gauge invariant operators of higher dimensions into the Lagrangian it is possible to produce electroweak bosons of high p_T accompanied by a jet. These effective interactions are the low energy limit of some renormalisable theory with scale Λ, and are only justified if $\Lambda^2 \gg \hat{s}$. Assuming that the decay $Z \rightarrow \nu\bar{\nu}$ responsible for the missing energy and using the UA1 monojet data to determine the couplings for gauge invariant operators of dimension ≤ 8, this approach yields $\Lambda < 100$GeV unless their is a dynamical enhancement of the coupling. Since energies in the range 150-200GeV are required to reproduce the monojet p_T spectrum, this approach is clearly unjustified and propagator effects must be

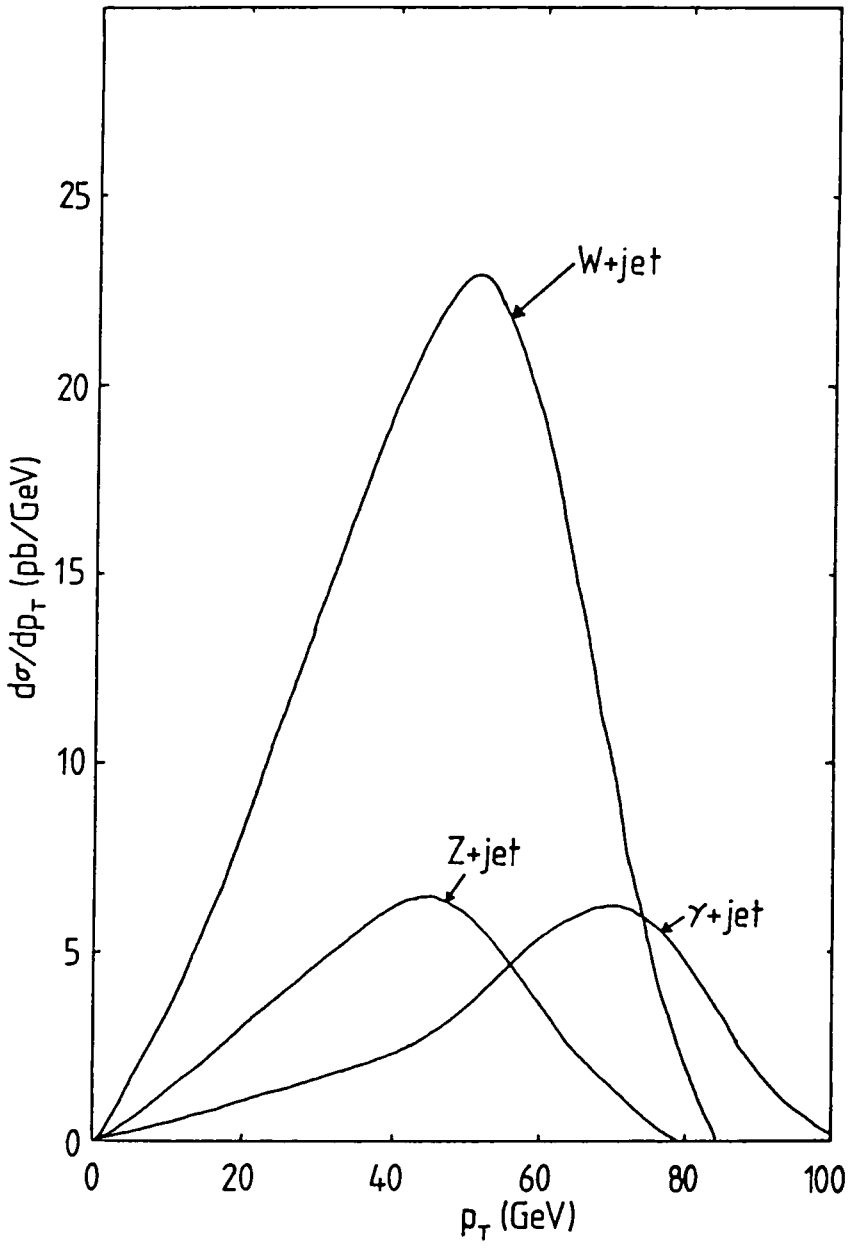

Figure 9

The V boson (V = W, Z, γ) P_T distribution from the decay $q^* \rightarrow Vq$, for excited quark production and decay at $\sqrt{s}$ = 540GeV and M_{q^*} = 160GeV.

considered.

As an example of propagator effects, a model of excited quarks is discussed. Examination of W + jet and γ + jet decay modes, which are as least as common as the Z + jet mode, will enable such models to be tested. More specifically, in a data sample containing 5 ($Z \rightarrow \nu\bar{\nu}$) + jet events the excited quark model predicts 8 ($W \rightarrow e\bar{\nu}$) + jet events and O(100) γ + jet events.

Moreover, a direct consequence of the Z + jet interpretation is that,

$$(Z \rightarrow \nu\bar{\nu})+\text{jet} : (Z \rightarrow \bar{e}e)+\text{jet} : (Z \rightarrow 2 \text{ jets})+\text{jet} \qquad (7.56)$$

$$\backsim 6 : 1 : 20$$

i.e. for every 6 monojets there should be about 20 events with 3 energetic jets (with $M^2(2\text{jets}) \backsim M_Z{}^2$). If there are more than 3 light neutrinos then this ratio will fall.

References

(1) T.Appelquist and J.Carrazone, Phys. Rev. D11, 2856, (1975)

(2) R.M.Bionta et al., Phys. Rev. Lett. 51, 27, (1983); ibid, 51, 522(E), (1983)

(3) B.G.Cortez et al., Phys. Rev. Lett. 52, 1092, (1984)

(4) W.W.Kinnison et al., Phys. Rev. D25, 2846, (1982)

(5) G.Azuelos et al., Phys. Rev. Lett. 51, 164, (1983)

(6) K.G.Hayes et al., Phys. Rev. D25, 2869, (1982)

(7) K.Hikasa, Phys. Lett. 145B, 139, (1984)

(8) G.Arnison et al., UA1 collab., Phys. Lett. 139B, 115, (1984)

(9) P.Bagnaia et al., UA2 collab., Phys. Lett. 139B, 105, (1984)

(10) K.Hikasa, private communication

(11) UA2 collab., reported by J.Schacher, Proc. 4th Topical Workshop on $p\bar{p}$ Collider Physics, Berne, (1984)

(12) M.Gluck, E.Hoffmann and E.Reya, Z.Phys. C13, 119, (1982)

(13) S.L.Glashow, Phys. Lett. 143B, 130, (1984)

(14) E.L.Berger and M.Jacob, Phys. Lett. 147B, 197, (1984)

(15) G.J.Gounaris and A.Nicolaidis, Phys. Lett. 148B, 239, (1984)

(16) A.De Rujula, L.Maiani and R.Petronzio, Phys. Lett. 148B, 239, (1984)

(17) G.Pancheri, Proc. 4th Topical Workshop on $p\bar{p}$ Collider Physics, Berne, (1984)

(18) S.S.Gershtein, G.V.Jickia and Yu.F.Pirogov, Phys. Lett. 151B, 303, (1985)

(19) V.Barger, H.Baer and K.Hagiwara, Phys. Lett. 146B, 257, (1984)

Chapter Eight

Conclusions

The CERN $p\bar{p}$ collider has provided clear evidence that the Z and W bosons predicted by the Standard Model of electroweak interactions exist with the correct masses. The production of large p_T hadronic jets gives support to the $SU(3)_C$ interpretation of the strong interaction. While the experimental confirmation of these Standard Model predictions is very satisfying it has to be noted that there are many problems left unresolved. Two relevant problems are,

(a) the masses of the fermions,

(b) the number of generations.

These questions may only be answered (at least at our present level of understanding) by actually looking for new fermions via there production and decay in high energy collisions. The $p\bar{p}$ collider offers the possibility of much higher centre-of-mass energies than currently available e^+e^- colliders and is therefore the natural place to look for new particles.

In Chapter 3, the production of heavy quarks is examined. Unlike sign dileptons give distinctive signatures from which a wealth of physics may be isolated, including the top quark. The signal involves only charged leptons and so there are not the problems associated with recognising jets or missing p_T. Methods for isolating the following processes are proposed,

(a) $t\bar{t}$ production,

(b) the Drell-Yan lepton pair production,

(c) $b\bar{b}$ production,

(d) $gg \rightarrow \chi g$.

In Chapter 4, the possibility of observing a new charged sequential lepton, L, produced from W decay is examined. Although the leptonic decay rate is always exceeded by leptonic decays of the W, the hadronic decay mode leads to a promising signature of large missing p_T accompanied by two jets. After imposing selective cuts to remove the background contributions the event rate is about a tenth of the $W \rightarrow ev$ rate for heavy lepton masses less than O(50GeV) and so such a particle, if it exists, should be readily identifiable at the $p\bar{p}$ collider.

Subsequently, the UA1 experiment found several events with extremely large missing p_T ($>$ 40GeV) accompanied by an energetic jet. These events, which are described in Chapter 5, are too energetic to originate from a heavy lepton as described in Chapter 4. The missing p_T's are so large that conventional explanations seemed unable to account for these "monojet" events.

Hadron colliders are also a natural place to look for supersymmetric particles such as squarks and gluinos (the scalar and spin-1/2 partners of quarks and gluons). Since in many supersymmetry theories the lightest sparticle is the weakly interacting photino (the spin-1/2 partner of the photon), the production and decay of coloured sparticles to photinos and partons can give rise to missing p_T + jet topologies. In Chapter 6, the production of squarks and gluinos in $p\bar{p}$ collisions is examined. Scalar quark production can account for the

monojet events if the up and down flavoured squarks have mass, $m_{\tilde{q}} \sim$ O(25GeV) and the gluino has a mass, $m_{\tilde{g}} >$ O(60GeV). On the other hand, if the monojet events do not arise from scalar quark production (and the gluino is more massive than the squarks) there is a lower bound of O(50GeV) on the squark mass.

An alternative explanation of the monojet events is attempted in Chapter 7. In this case the missing transverse energy comes from the decay of a high p_T Z boson into a $\nu\bar{\nu}$ pair. First SU(3) x SU(2) x U(1) invariant effective operators of dimension 6-8 are introduced to give four-particle point couplings, for example, $q\bar{q}Zg$, $ggg\gamma$. In the same way that the four-fermion effective interaction only describes weak interactions at scales $<< M_W$, these new effective interactions are only good approximations at energies $<< \Lambda$. The couplings are related to the scale Λ and determining the coupling (through the monojet rate) fixes Λ to be O(100GeV). This is clearly not much greater than the energy scale being probed and hence propagator effects must be introduced. Therefore, effective operators of the type considered are unable to account for monojet events.

As an example of propagator effects, the production of possible new excited quark states (q^*) is discussed. To produce a sufficiently high q^* production cross section to account for the monojet rate requires large couplings, in particular, for an excited quark of mass O(150GeV) the decay width is O(50GeV). Furthermore, the excited quarks may decay into W + jet and γ + jet topologies with rates at least as large as the decay rate into Z + jet (which gives monojets). The associated production of W + jet or γ + jet events is common to most models trying to explain monojets through the formation of

massive intermediate states. A second consequence of using Z + jet topologies to explain the monojet rate, is that the charged leptonic decays of the Z should give rise to events with two high p_T charged leptons accompanied by a jet at around a third of the monojet rate. No events of this type have so far been observed.

The theoretical origin of the 1983 monojets is therefore unclear and their present status can be summarised as follows.

(a) Supersymmetry can explain the events in many different ways - mainly due to the lack of constraints on the sparticle masses. The variety of possible scenarios tailored to fit the data naturally makes such explanations rather unsatisfying.

(b) The interpretation of the monojets as the tail of a new SU(3) x SU(2) x U(1) invariant interaction which appears as a point interaction at collider energies has been shown not to work unless there is a dynamical enhancement of the coupling.

(c) High mass intermediate states which are produced in $p\bar{p}$ collisions and then undergo two-body decay to Z + jet can explain the monojet rate if the couplings, spin and colour multiplicities are large enough. However, in most cases W + jet and γ + jet events are predicted at rates similar (or greater than) the monojet rate. Such events have not yet been seen at the appropriate rates.

In 1984 the CERN $p\bar{p}$ collider operated at a total centre-of-mass energy of 630GeV. A new dedicated trigger for events with large missing p_T was installed in the UA1 experiment. This trigger worked in the following way. The scalar sum of the transverse energy was calculated in the right-half of the detector ($|E_T|_R$) and in the left-

half of the detector ($|E_T|_L$). If the difference between $|E_T|_R$ and $|E_T|_L$ was greater than 17GeV and there was also a jet with E_T > 15GeV, the event was recorded.

Preliminary results [1] confirm the existence of monojets, but with the higher statistics the (preliminary) missing p_T distribution now appears to be more consistent with the tail of a distribution "spilt-over" from lower missing p_T values, which suggests the events may be of more conventional origin.

Clearly it is important to quantify the Standard Model expectations [2]. There are two main potential sources of monojet events.

(i) The transverse momentum distribution of convential Z production has a tail [3-5] which extends to large p_T arising dominantly from the lowest-order QCD subprocesses $q\bar{q} \rightarrow Zg$ (and $qg \rightarrow Zq$). The $(Z \rightarrow \nu\bar{\nu})$ + jet final state appears as a monojet.

(ii) The production of a W which subsequently decays,

$$W \rightarrow \tau\nu \rightarrow \text{jet} + \nu\bar{\nu},$$

gives a monojet. There appears to be a kinematic limit of $M_W/2$ on the missing p_T, however, the transverse momentum and non-zero width of the W result in a tail to the missing p_T distribution beyond this limit.

Figure 1 [2] shows the missing p_T distributions from these two processes for $p\bar{p}$ collisions at $\sqrt{s}$ = 630GeV. The cuts imposed are those described in Chapter 5 along with the missing p_T trigger described above. For events with missing p_T > 35GeV, one has [2],

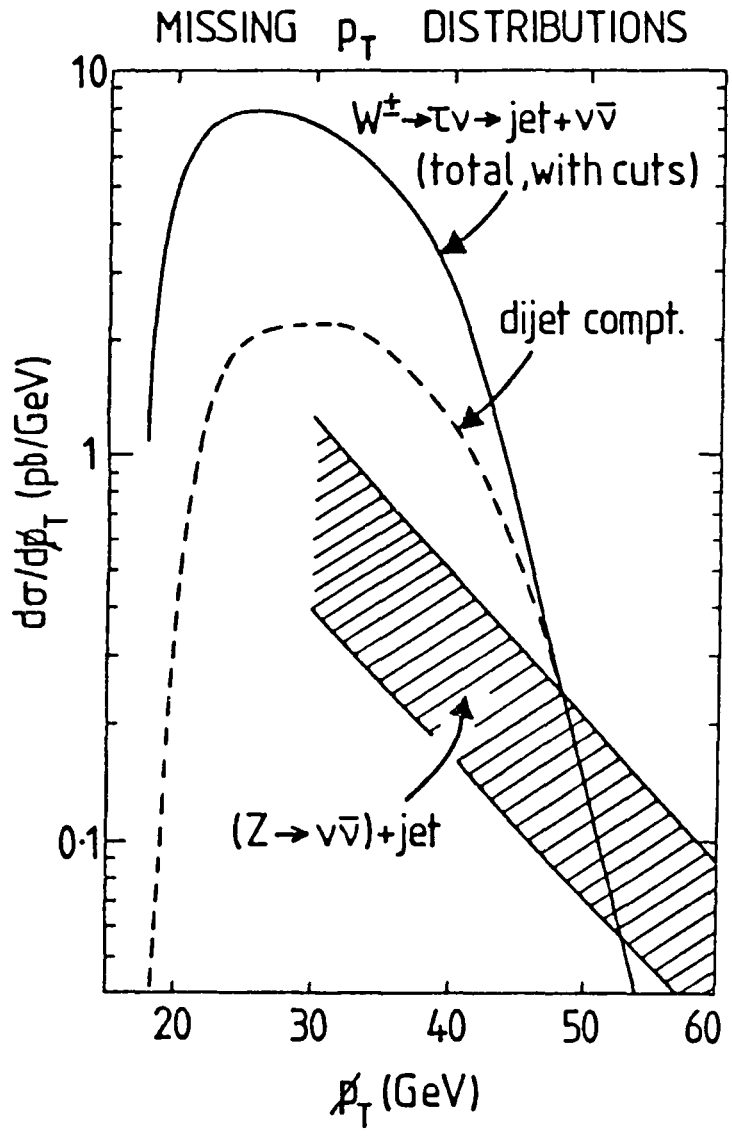

Figure 1

Missing p_T distributions from Standard Model processes in $p\bar{p}$ collisions at $\sqrt{s}$ = 630GeV; (a) $W^{\pm} \to \tau\bar{\nu} \to$ jet + $\nu\bar{\nu}$ with cuts applied (the dashed curve shows the dijet + p_T(missing) component of the total) and (b) $(Z \to \nu\bar{\nu})$ + jet taken from the QCD calculations of Ref. 4.

	$(Z \rightarrow \nu\bar{\nu})$ + jet	$W \rightarrow \tau\nu \rightarrow$ jet + $\nu\bar{\nu}$
$\sqrt{s}$ = 540GeV	4.5 ± 2 pb	19.5 pb
$\sqrt{s}$ = 630GeV	7.5 ± 2 pb	26.6 pb

That is, for an integrated luminosity of $100nb^{-1}$, around 2(3) events are expected with p_T(missing) > 35GeV at $\sqrt{s}$ = 540(630)GeV from Standard Model sources.

The Standard Model, despite its deficiencies and shortcomings (such as the origin of symmetry breaking), has received much experimental support and forms the basis of many calculations in this thesis. The monojet events, albeit with low statistics appeared to be inconsistent with the Standard Model and hinted at the possibility of observing new physics in the $p\bar{p}$ collider. However, recent preliminary data with higher statistics suggests that the monojets may, in fact, be of conventional origin. Clearly definitive new data in the 100GeV - 1000GeV range is crucial for further understanding and is eagerly awaited.

References

(1) UA1 collab., reported by C.Rubbia, 5th Topical Workshop on $p\bar{p}$ Collider Physics, Aosta, (1985)

(2) E.W.N.Glover and A.D.Martin, Durham report DTP/85/10, (1985)

(3) G.Altarelli, R.K.Ellis and G.Martinelli, Fermilab report 84/107T, (1985)

(4) J-R.Cudell, F.Halzen and K.Hikasa, Wisconsin report, MAD/PH/237,

(1985)

(5) S.D.Ellis and W.J.Stirling, 5th Topical Workshop on $p\bar{p}$ Collider Physics, Aosta, (1985)

Appendix A

Monte Carlo integration and event simulation

A.1 Introduction

Monte carlo techniques are used to calculate the multi-dimensional integrals needed in this thesis. As an illustration of the technique consider the integral I, of the function f(x) shown in Figure 1, between the limits x = a and x = b;

$$I = \int_a^b f(x)\,dx \backsim \frac{(b-a)}{N} \sum_{i=1}^{N} f(x_i) \qquad (A.1)$$

That is, the area under the curve is the average value of the function in the range multiplied by the range. In the Monte Carlo method the points x_i are picked uniformly and randomly in the range a to b. Clearly, the larger the number of random points, the closer $(1/N)\Sigma f(x_i)$ will be to the actual average of the function and the more accurate the calculated value of the integral.

As an explicit example, consider the trivial function,

$$f(x) = x^2 \text{ on } 0 < x < 1, \qquad (A.2)$$

so that,

$$I_1 = \int_0^1 f(x)\,dx = 1/3. \qquad (A.3)$$

A Monte Carlo estimate (using a BBC micro) of this integral for a set of N random x_i is given in the second column of the table,

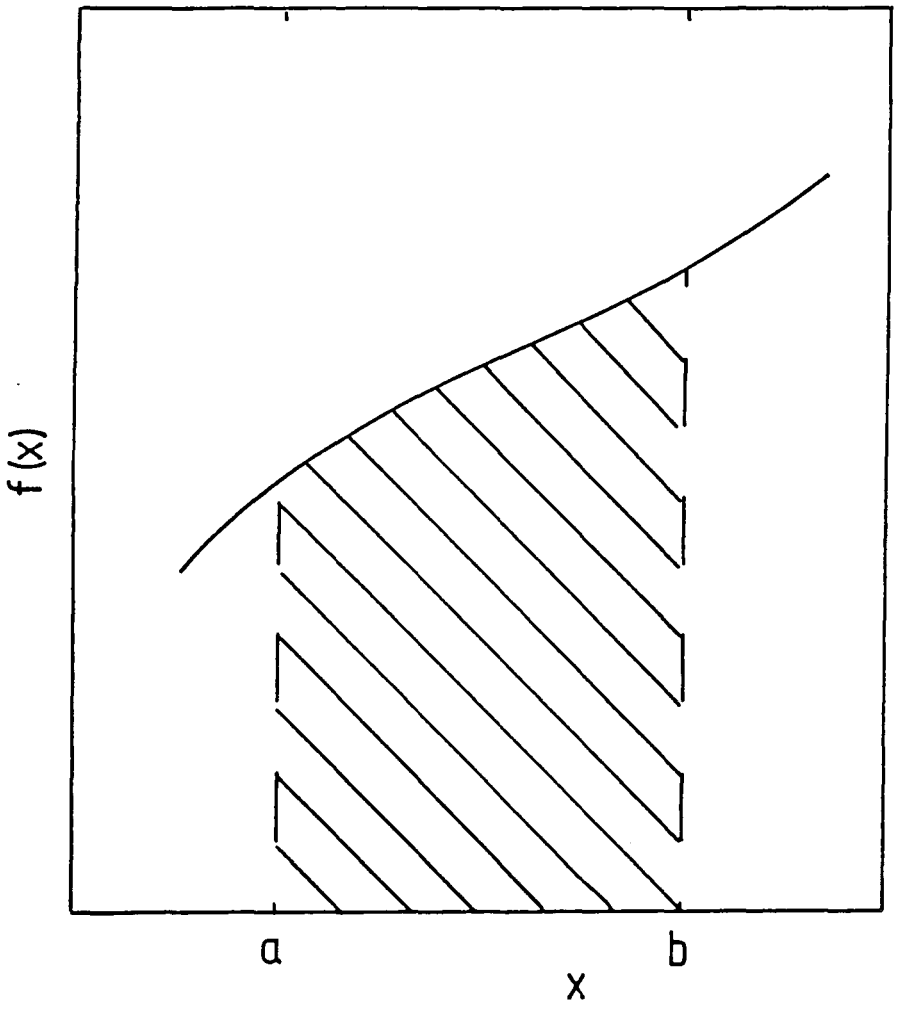

Figure 1

The function f(x) defined on the range [a,b]. The shaded area corresponds to the integral $\int f(x)\,dx$ on this range.

N	$I_1(N)$ of eq. (A.3)	$I_2(N)$ of eq. (A.9)
10	0.39541	0.26417
100	0.32282	0.32771
1000	0.34089	0.33218
10000	0.33362	0.33237
100000	0.33133	0.33340
1000000	0.33299	-

Note that since this is only an approximation based on random numbers, the actual values of the Monte Carlo integration will vary from run to run. The uncertainty in I (as represented by the standard deviation σ) is given by [1],

$$\sigma = (V(f)/N)^{1/2} \qquad (A.4)$$

where V(f) is the variance of the function f. Hence to improve the accuracy by an order of magnitude, 100 times as many function evaluations are required. This slow convergence means that for low dimension integrals there are many faster alternatives eg. Trapezoid rule. However, this changes for higher dimensional integrals and for dimension $>$ 5, the Trapezoid rule converges more slowly than the Monte Carlo method.

The variance V(f) is given by,

$$V(f) = \frac{1}{(b-a)} \int_a^b f(x)^2 \, dx - \left[\frac{1}{(b-a)} \int_a^b f(x) \, dx \right]^2 \qquad (A.5)$$

which for the example (A.2) is,

$$V(f) = \int_0^1 x^4 \, dx - \left(\int_0^1 x^2 \, dx \right)^2 \qquad (A.6)$$

$$= 4/45.$$

Since the standard deviation is proportional to $\sqrt{V(f)}$ it is possible to increase the accuracy by reducing the variance. There are many different methods for reducing the variance of a particular integral [2] of which importance sampling is probably the most useful.

A.2 Importance sampling

This approach corresponds to a change of integration variable,

$$f(x)\,dx \rightarrow f(x)\,dG(x)/g(x). \qquad (A.7)$$

Points are chosen according to G(x) instead of uniformly, and f(x) is weighted by $g(x) = dG(x)/dx$. The relevant variance is now V(f/g) which is small if f(x) and g(x) have similar shapes.

Consider the simple example (A.2) shown in Figure 2(a). The integral I_1 is formed by choosing points uniformly in x. Some points will be chosen where the function is large and some where it is small. The contribution to the integral for different x_i varies considerably. Consider now the change of variable,

$$y = x^2, \qquad (A.8)$$

so that,

$$I_2 = 0.5 \int_0^1 \sqrt{y}\,dy \sim (\Sigma\ 0.5\sqrt{y_i})/N. \qquad (A.9)$$

As shown in Fig. 2(b) the function is flatter and the contribution to the integral for different y_i varies rather less. This shows itself in the variance which is now 1/72 (as compared to 4/45). Sample results for I_2 are shown in the final column of the above table.

Making one final change of variable,

$$z = y^{3/2}, \qquad (A.10)$$

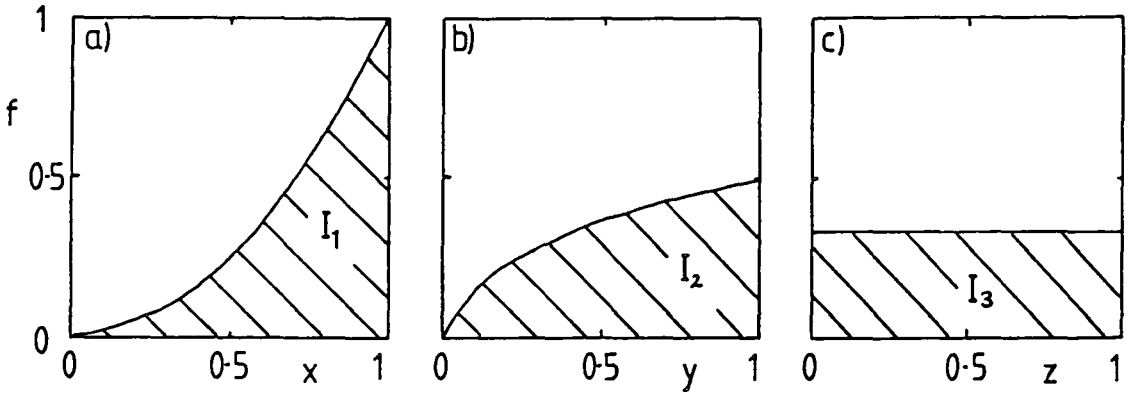

Figure 2

The integral $\int f(x)\,dx$, where the function $f(x) = x^2$ on the range [0,1] (a) as a function of x, (b) as a function of y, where $y = x^2$ and (c) as a function of z, where $z = y^{3/2}$.

so that,

$$I_3 = 1/3 \int_0^1 dz \backsim (\Sigma\ 1/3)/N = 1/3 \text{ for all } N \qquad (A.11)$$

The variance has been reduced to zero and the answer is correct for all N. Figure 2(c) shows f(z).

More generally, to apply importance sampling to a function f, a function g must be found such that,

(a) g(x) is a non-negative and is normalised so that its integral is 1,

(b) $G(x) = \int g(x)\, dx$ is known analytically,

(c) The ratio f(x)/g(x) is as nearly constant as possible, so that the variance V(f/g) < V(f).

As a second example, consider a cross section for a particle resonance,

$$\sigma \propto \int_{\hat{s}min}^{\hat{s}max} d\hat{s}/((\hat{s}-m^2)^2 + \Gamma^2 m^2), \qquad (A.12)$$

then the change of variables,

$$\hat{s} = m^2 + \Gamma m \tan\theta, \qquad (A.13)$$

with,

$$\begin{aligned} \theta_{max} &= \tan^{-1}((\hat{s}max - m^2)/(\Gamma m)), \\ \theta_{min} &= \tan^{-1}((\hat{s}min - m^2)/(\Gamma m)), \end{aligned} \qquad (A.14)$$

yields,

$$\sigma \propto \int_{\theta min}^{\theta max} d\theta/(\Gamma m), \qquad (A.15)$$

which is flat in θ.

The Monte Carlo method generalises to n dimensions,

$$I = \int f(x_1,\ldots f_n)\, d^n x \backsim \prod_{i=1}^{n} \frac{(\text{range of } x_i)}{N} \sum_{j=1}^{N} f(x_1^j,\ldots f_n^j), \qquad (A.16)$$

which again has the standard deviation given by (A.4). As noted earlier, this method is particularly good for high dimension integrals as the rate of convergence is essentially unchanged by altering n.

A.3 Monte Carlo simulation.

Simulation is a technique for conducting theoretical experiments. A theoretical model may predict some quantity J as an integral of the function F say for example,

$$J = \int F(a,b)\, da\, db. \qquad (A.17)$$

In the Monte Carlo approach, this integral will be estimated by,

$$J = \sum_{i=1}^{N} \frac{F(a_i,b_i)}{N} \times \text{range of a} \times \text{range of b}, \qquad (A.18)$$

with a_i and b_i chosen randomly so all "theoretical events" , that is particular values of a and b, are equally likely, however each event is weighted by the integrand $F(a_i,b_i)$ and the product of the ranges. (In practise the ranges may be functions of a or b.) The theoretical events with the larger weighting correspond to more likely experimental events. In an experiment, each event has equal weight however the dynamics and kinematics are such that events with particular configurations are more common.

One of the advantages in performing Monte Carlo simulations is the ease with which "cuts" may be applied. For example, if the cut

$$a + b^2 < c, \qquad (A.19)$$

is required to represent an experimental trigger say, then instead of reconfiguring the limits the function is redefined,

$$F(a_i,b_i) = 0 \text{ if } a_i + b_i^2 > c, \qquad (A.20)$$

and the restricted integral may be performed. To improve efficiency a new choice of variables or limits may be advisable, but in many cases in particle physics the cut variable is related to the integration

variables in an extremely complex manner and variable redefinition rather non-trivial.

References

(1) F.James, Rep. Prog. Phys. 43, 73, (1980)

(2) R.Y.Rubinstein, Simulation and the Monte Carlo Method, (Wiley), (1981)